2011

Western equatorial Pacific climate variability from restricted basins: Century scale changes in Kau Bay to glacial-interglacial changes in the Sulu Sea

Samantha J. Langton
University at Albany, State University of New York

Western equatorial Pacific climate variability from restricted basins: Century scale changes in Kau Bay to glacial-interglacial changes in the Sulu Sea

by

Samantha J. Langton

A Dissertation Submitted to the University at Albany, State University of New York in Partial Fulfillment of the Requirements for the Degree of Doctor of Philosophy

College of Arts and Sciences

Department of Atmospheric and Environmental Science

2011

ProQuest LLC.
789 East Eisenhower Parkway
P.O. Box 1346
Ann Arbor, MI 48106 - 1346

ABSTRACT

The surface ocean in the western equatorial Pacific contains some of the warmest water on the planet in the western Pacific warm pool (WPWP). Changes in the size and scope of the warm pool have a significant impact on global climate. With the concern of changes in the extent of this body of water as a result of anthropomorphic changes in atmospheric composition, it is vital to investigate prior changes to the WPWP, the causes of such changes, and resultant effects. For my dissertation, I used several proxies to analyze sediments from Kau Bay and the Sulu Sea in Indonesia to examine changes within the WPWP over century and glacial-interglacial time scales, respectively.

Organic matter proxies ($\delta^{15}N$, $\delta^{13}C$, C/N, relative composition and $\delta^{13}C$ of fatty acids and alkanes) were analyzed at century-scale resolution from a core from Kau Bay, Halmahera, that spanned over the last ~3,500 years. These proxies were used to decipher the flushing history of the basin and its relation to El Niño events and warm pool dynamics. Pteropod shells (*Creseis acicula*) were analyzed from the same cores from Kau Bay for $\delta^{18}O$, $\delta^{13}C$, and Sr/Ca in order to test the utility of pteropod shells in paleoclimate studies and to determine possible changes in the hydrological cycle within Kau Bay and its relation to equatorial Pacific climate. The *C. acicula* data showed that Kau Bay water and, therefore, WPWP surface water, was likely warmer 3,000yrBP than throughout the last 2,200 years. Comparisons of this data to other records from the equatorial Pacific and South China Sea revealed that zonal dynamics and the EAM may have had an effect on WPWP and global climate throughout the late Holocene and that ENSO may affect climate change at this resolution.

In the Sulu Sea, the $\delta^{18}O$ of thermocline dwelling foraminifera, *Pulleniatina obliquiloculata* and *Neogloboquadrina dutertrei*, was analyzed and compared to mixed layer foraminifera to determine that the mixed layer was probably more shallow during interglacial stages than during glacial stages over the last 800kyr, likely in response to changes in sea level and monsoon intensity.

Acknowledgements

The end of a voyage cannot be reached without the engineers who construct the road. I owe the completion of this dissertation to many people who have been my inspiration and motivation during this epic journey. My advisor, Brad Linsley, made this entire adventure possible by offering me the opportunities to pursue incredibly interesting and challenging projects. Furthermore, I am grateful to him for always having time to discuss my work and for the time and effort he spent helping me with my manuscripts.

I would like to thank Yair Rosenthal, Delia Oppo, and Tim Eglinton for their encouragement for my work and also for affording me the opportunity to work in different laboratories and learn different proxies to use in my research and I would like to thank Rebecca Robinson for her help and work with my research on Kau Bay.

I would like to acknowledge all of the laboratory technicians who have helped me achieve my goals including a very special thanks to Steve Howe, who painstakingly ran all of my stable isotope samples at SUNY Albany. I would also like to thank Daniel Montlucon for patiently training me to prepare and run samples for compound specific analyses in Dr. Eglinton's laboratory at WHOI.

Finally, I would like to thank my friends and family. My friend and dressage instructor, Jessica Riley, has kept me sane through this process by allowing me to come and ride her horses when I needed a break. Marie-Claude and Larry Stockl have been immense inspirations and warned me that great things always happen to people who work for them.

I would like to thank my parents, Ellen and John Langton, for always encouraging me to reach for the brass ring. An extra special thank you to my sister, Danielle Ellingston, who made me into an incredibly competitive individual and for giving me the motivation to fight for what I want in life no matter how daunting the battle. And finally, my greatest support came from being the lucky friend of the best dog in the world, Scooby, and also the monster dog, Rosebud.

Table of Contents

CHAPTER 1

Introduction

1. Western Pacific Warm Pool climate dynamics

Oceanographic and climatologic variability in the Western Pacific Warm Pool (WPWP) and Indo Pacific Warm Pool (IPWP) has a global impact. This region contains the warmest open ocean water on earth and changes in the spatial and temporal extent of the warm pool have an effect on global atmospheric circulation (figure 1.1). Oceanic and atmospheric circulation in this region can have an enormous impact on the heat storage and add positive and negative feedbacks to the global climate system (e.g., *Ropelewski and Halpert, 1987* and *Sun, 2003*) For example, models have shown that doubling the CO_2 concentration of the atmosphere may result in changes of oceanic and atmospheric circulation that affect climate by increasing the amplitude of El Niño Southern Oscillation (ENSO, e.g., *Merryfield, 2006*). The impact of these modifications on ocean chemistry and dynamics has not been fully realized. Looking into past variability of the WPWP will give us a better understanding of the natural range of variability of this climatically important region and may allow us to forecast future reactions to the current anthropogenic forcing that appears to be driving changes in atmospheric and oceanic chemistry and temperature.

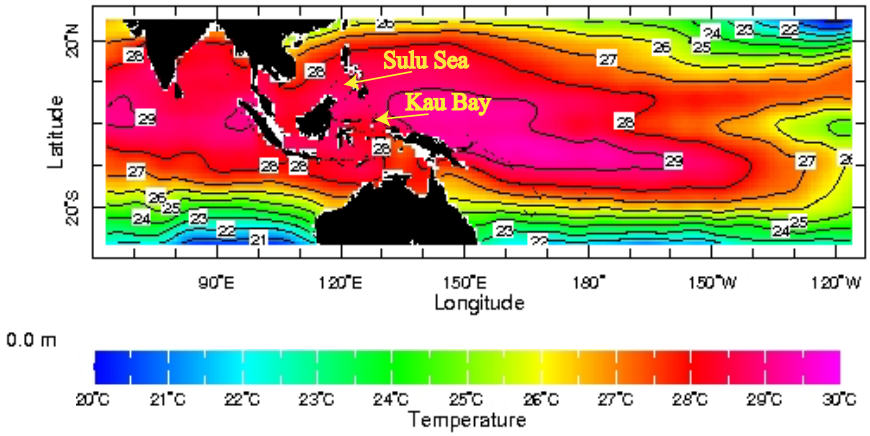

Figure 1.1. Location of the Western Pacific Warm Pool with mean annual sea surface temperatures. The WPWP is located within the ≥28˚C isotherm (*Levitus, 1994*).

The WPWP lies within the western equatorial Pacific (WEP, figure 1.1). The concentration of heat in this area results in intense convection and rainfall. The extent of the warm pool is not static and is known to vary seasonally and interannually based on instrumental data that has been acquired over the last few decades (e.g., *Yan et al., 1992; Cravatte et al., 2009*). Seasonal variations in the spatial extent of the warm pool are determined by the position of the intertropical convergence zone (ITCZ; *Waliser and Gautier, 1993*), while interannual changes in the extent of the warm pool result from changes in the phase of El Niño/Southern Oscillation (ENSO). Lower frequency changes have been tracked based on paleoclimatological studies such as marine and lacustrine fossil and sediment geochemical studies, dendrochronology records, and ice core chemistry (e.g., *Fairbanks et al., 1997; Lachniet et al., 2004; Rodriguez et al., 2005; Oppo et al., 2009*). Such records have revealed century-scale, millennial, orbital-scale, and glacial-interglacial patterns of global climate change.

While century-scale and shorter resolution records have been added to the literature in increasing numbers over the last decade, patterns of climate change on millennial to century scale appear to be the most difficult to resolve because they do not coincide with large climatic events such as calculable orbital changes or changes in land mass and geography. However, we may be able to apply current knowledge of interdecadal to seasonal climate dynamics to explain and predict future millennial and century-scale patterns. For the WPWP and IPWP, these dynamics include changes in summer and winter East Asian Monsoon (EAM) strength, the El Niño/Southern Oscillation phenomenon, and seasonal variability of the intertropical convergence zone (ITCZ).

In the following chapters, I will present data obtained from sediment cores in the western sector of the WPWP that appear to track the nature of century-scale and glacial-interglacial scale changes to this region. Chapters 2 and 3 will discuss geochemical data from a ~3,500 year sediment core from Kau Bay, Indonesia that highlights century scale changes in the WPWP, while chapter 4 will discuss glacial-interglacial changes in surface to thermocline water in the Sulu Sea probably a result of changes in monsoon strength. In this chapter, I will discuss the known factors that play a role in current WPWP variability, such as the spatial variability of the ITCZ, ENSO dynamics, and the EAM.

1.1. ITCZ variability

The mean position of the ITCZ today is located near the equator in the northern hemisphere along the rising arm of the Hadley circulation (*Waliser and Gautier, 1993*). Although the ITCZ appears as a narrow latitudinal equatorial band over most of the

globe, the ITCZ area from the western Pacific to the Indian Ocean is less latitudinally constrained. The equatorial band moves seasonally and appears to migrate on larger time scales, as well, based on paleoclimatological data (e.g., *Linsley et al., 1994*; *Koutavas and Lynch-Steiglitz, 2006; Sachs et al., 2009*). During boreal summer, the ITCZ migrates northward, and during austral summer, the ITCZ migrates equatorward. Although the ITCZ follows the position of the sun, convection and rainfall associated with the ITCZ lags about two months behind (*Waliser and Gautier, 1993*). When the location of the ITCZ is at its most northern position during the mid to late boreal summer (7-14˚N), there is increased rainfall. Meanwhile, when the ITCZ is at or near the equator during the boreal winter months, there is less convective activity (*Waliser and Gautier, 1993*).

1.2. ENSO variability in the WPWP

The variability in the WPWP related to the phase of ENSO is mostly expressed by changes in thermocline depth and the spatial extent of the warm pool. A typical ENSO cycle is 4-7 years (*Bjerknes, 1969*). The Southern Oscillation Index (SOI) is used to describe phase of ENSO by taking the difference in sea level pressure between Tahiti and Darwin, Australia. During a negative SOI phase, or El Niño conditions, equatorial trade winds slacken, upwelling is subdued in the eastern equatorial Pacific, and the warm pool in the WEP expands eastward. This causes the salinity front to migrate eastward as warmer, fresher water is brought to the central and eastern equatorial Pacific (*Picaut et al., 1996*). Convection from the WPWP is therefore shifted to the east. This action causes increased freshening in the central and eastern equatorial Pacific and more arid conditions in the WEP. In addition, the ITCZ reacts with an equatorward expansion in

the central to eastern equatorial Pacific in response to El Niño throughout the instrumental record (*Deser and Wallace, 1990*). Meanwhile, a positive SOI phase, or La Niña, is characterized by an increase in equatorial trade wind strength, deeper thermocline in the WEP, and a westward migration of the salinity front along the equator.

1.3. East Asian Monsoon

The EAM consists of the northwesterly winter component, which brings high winds and less precipitation than the northeasterly summer component. The northwest winter monsoon tends to increase surface salinity and reduce SST in the South China Sea, with less of an effect on the western WPWP region (*Wyrtki, 1961*). The East Asian summer monsoon (EASM) dominates rainfall in the western WPWP region on an annual basis (*Wyrtki, 1961*). The EASM can be intensified when El Niño peaks during mid-summer (*Zhang et al., 1996*). A strong summer monsoon tends to follow El Niño warming in the eastern Pacific by about 3 seasons (*Wang et al., 2001*).

2. Century-scale and G-I climate variability in semi-enclosed WPWP basins, Kau Bay and the Sulu Sea, Indonesia

Data from sediment cores collected from two semi-enclosed, silled basins in the WPWP are presented and with their relevance to overall WPWP and Pacific-wide paleoclimate variability is discussed. Silled and poorly ventilated basins lend an advantage to paleoclimate studies because oxygen can rapidly become depleted, leading to reduced benthic bioturbation of the sediments which results in a more detailed sediment record and enhances the preservation of various resources that can be used as

environmental proxies. While the Sulu Sea and Kau Bay records presented here consist of various proxy types over different resolutions, flushing of each basin may be significantly related to larger-scale changes in WPWP and global climate.

Kau Bay is a ~470m deep basin with a 30m deep sill that contains well-preserved organic matter due to bottom water that has varied from dysoxic to anoxic through time. A ~3,500 year $\delta^{15}N$ record of the organic matter from a sedimentary core showed variability that was probably dependent upon the flushing history of the basin. During long periods of basin stagnation, the nitrate concentration of the entire water column became depleted, thus inciting nitrogen fixation and a reduced $\delta^{15}N$ within the water column and buried in the sedimentary organic matter. Meanwhile, periods of increased flushing replenished the basin's nitrate, while productivity was generally reduced and the $\delta^{15}N$ was allowed to increase to levels congruent with those outside the basin in the WPWP waters. This record is in general agreement with other global records that appear to vary in accordance with changes in the frequency and/or intensity of ENSO.

While foraminifera $\delta^{18}O$ and Mg/Ca are often used as proxies to track past water temperature and salinity variations associated with regional climate dynamics, Kau Bay did not contain sufficient numbers of tests to perform these analyses. In contrast, the highly tolerant aragonitic pteropod, *Creseis acicula,* was found in excellent condition throughout the 3,500 year Kau Bay record. Although these organisms have not been calibrated to track changes in SST and salinity via $\delta^{18}O$ and Sr/Ca, variability of these records from Kau Bay closely resemble the variability from cores of similar resolution from the WPWP and the EEP. These records likely reflect century-scale zonal climate change in the equatorial Pacific not unlike current interannual ENSO variability.

The Sulu Sea is a ~5,580m deep basin in the western region of the WPWP. Its relatively shallow sills dissuade deep water circulation and induce dysoxia. Comparisons between the planktonic foraminifera $\delta^{18}O$ records of surface dwelling *Globigerinoides ruber* and deeper dwelling *Neogloboquadrina dutertrei* and *Pulleniatina obliquiloculata* reveal variable stratification in the upper water column. During most glacial stages over the last ~800,000 years, the $\delta^{18}O$ varied less among these three species than during interglacial stages. The mixed layer was likely deeper during glacial stages, which was possibly the result of cutting off higher salinity water from the Sulawesi Sea, while increased stratification occurred between the mixed layer and thermocline due to the intrusion of water from the Sulawesi Sea during interglacial stages.

3. Research questions to be evaluated:

3.1. Can evidence of century-scale WPWP climate variability be found from a high resolution sediment core retrieved from Kau Bay, Indonesia?

Organic and inorganic geochemical proxies will be examined from a ~3,500 year long sediment core from Kau Bay, Indonesia. Sedimentary $\delta^{15}N$ will be analyzed to determine the ventilation history of the basin since bacterial processes affected by nitrate availability, productivity, and dissolved oxygen concentration are closely linked to the isotopic concentration of nitrogen in nitrate. The C/N, $\delta^{13}C$ of organic matter, fatty acids, and alkanes, and the concentrations of fatty acids and alkanes will be measured to determine the relative source of organic matter throughout the record. $\delta^{18}O$, $\delta^{13}C$, and Sr/Ca will be measured from pteropod shells in order to determine possible changes in

water column salinity, temperature, and DIC that possibly reflect zonal equatorial Pacific climate dynamics.

3.2. How do changes in ventilation control the nitrogen cycle in Kau Bay?

The $\delta^{15}N$ of sedimentary organic matter is dependent upon the frequency and depth of flushing events within the basin through changes in bacterial processes linked to the basin's dissolved oxygen content. The main possible causes for $\delta^{15}N$ variability in ocean sediments are the bacterial processes of nitrogen fixation and denitrification. When the nitrate concentration of the water column is depleted, nitrogen fixing bacteria will fix free nitrogen from the atmosphere with a $\delta^{15}N$ of 0 into organic compounds and will result in reduced $\delta^{15}N$ within the water column (e.g., *Boyd, 2001*). Meanwhile, the $\delta^{15}N$ of the water column and sediments can be increased in anoxic conditions when denitrification is the mechanism for oxidizing organic matter (e.g., *Sigman et al., 2003*). During this process, nitrogen is converted from nitrate to N_2O and N_2 gases. The lighter isotope is preferred in this transaction, leaving residual nitrate enriched in ^{15}N. Since Kau Bay is known to have a variable history over the last century of dissolved oxygen concentration and low nitrate availability, it is likely that the sedimentary $\delta^{15}N$ record will reflect long-term changes in the basin's ventilation (*Van Aken and Verbeek, 1989*).

3.3. Can pteropod shells be used as a reliable proxy to interpret paleoenvironmental changes in Kau Bay and do these changes relate to global climate patterns?

Shells from the pteropod *Creseis acicula* will be analyzed for $\delta^{18}O$, $\delta^{13}C$, and Sr/Ca from core 102GGC at decadal to century-scale resolution. Since this pteropod has a high tolerance for salinity and low oxygen, its shell likely reflects the conditions in the

upper 30m of surface water from the WPWP because of the homogeneity within the basin and its 30m deep sill.

3.4. What are the connections between the Sulu Sea mixed layer and thermocline depths and glacial-interglacial stages?

The relative depths of the mixed layer and thermocline in the Sulu Sea will be estimated by differencing the $\delta^{18}O$ ($\Delta\delta^{18}O$) between mixed-layer and thermocline dwelling foraminifera over glacial-interglacial intervals. $\Delta\delta^{18}O$ between the mixed layer and thermocline foraminifera should be close to 0 when there is a deeper mixed layer, and larger when the mixed layer is shallower.

3.5. What are the implications of Sulu Sea mixed layer depth to WPWP climate controls?

Changes in the depth of the mixed layer within the Sulu Sea are likely related to EAM intensity and sea level. On GI timescales, sea level can be reduced to the point where water from the Sulawesi Sea is restricted from entering the Sulu Sea. Increased intensity of the East Asian winter monsoon can result in increased mixing and cooling of surface water. Meanwhile, increased intensity of the summer monsoon corresponds to increased atmospheric convection, precipitation, and decreased surface water salinity, creating a larger salinity and temperature difference between surface and thermocline waters.

Chapter 2

A 3,500 year record of centennial-scale climate variability from the Western Pacific Warm Pool

(Published in *Geology*, *2008*)

S.J. Langton

B.K. Linsley

Department of Earth and Atmospheric Sciences, University at Albany-State University of New York, Albany, New York 12222, USA

R. S. Robinson

Graduate School of Oceanography, University of Rhode Island, 103 Horn, 215 South Ferry Rd., Narragansett, Rhode Island 02882, USA

Y. Rosenthal

Institute of Marine and Coastal Sciences, Rutgers University, Piscataway, New Jersey 08854, USA

D.W. Oppo

T.I. Eglinton

Woods Hole Oceanographic Institution, 360 Woods Hole Road, Woods Hole, Massachusetts 02543-1541, USA

S.S. Howe

Department of Earth and Atmospheric Sciences, University at Albany-State University of New York, Albany, New York 12222, USA

Y.S. Djajadihardja

F. Syamsudin

BPPT, Agency for Assessment and Application of Technology, Jalam M. Thamrin No. 8, Jakarta 10340, Indonesia

ABSTRACT

We use geochemical data from a sediment core in the shallow-silled and intermittently dysoxic Kau Bay in Halmahera (Indonesia, lat 1°N, long 127.5°E), to reconstruct century-scale climate variability within the Western Pacific Warm Pool (WPWP) over the past ~3,500 yr. Down-core variations in bulk sedimentary $\delta^{15}N$ appear to reflect century-scale variability in basin ventilation, attributed to changes in oceanographic conditions related to century-scale fluctuations in El Niño Southern Oscillation (ENSO). We infer an increase in century-scale El Niño activity beginning ca. 1700 yr BP with peaks in El Niño activity at ca. 1500 yr BP, 1150 yr BP, and ca. 700 yr BP. The Kau Bay results suggest that there was diminished ENSO amplitude or frequency, or a departure from El Niño-like conditions during the Medieval Warm Period, and distinctive, but steadily decreasing, El Niño activity during and after the Little Ice Age.

1. INTRODUCTION

Kau Bay is a small (30 by 60 km), intermittently anoxic, ~470m deep basin that is semi-enclosed by the island of Halmahera (Indonesia, lat 1˚N, long 127.5˚E) and connected to the equatorial Pacific Ocean and Western Pacific Warm Pool (WPWP) by a ~30m deep, 15–20 km wide sill (figure 2.1). Because water exchange is limited to the upper 30 m, Kau Bay's deepwater temperature and salinity are nearly homogenous below the mixed layer and reflect the surface water's hydrography outside the Bay (*Van Aken and Verbeek, 1988; Van Der Weijden et al., 1989; Van Riel, 1943*) (figure 2.2A-D). The

deep basin's dissolved oxygen concentrations vary and indicate intermittent ventilation (*Van Aken and Verbeek, 1988; Middelburg, 1990*). *Middelburg (1990)* estimated that the oxygen minimum zone observed in 1985 may have developed in ~120 days and that the 150m thick anoxic layer observed in 1930 developed in fewer than 3 yr (figure 2.2E and 2.2F).

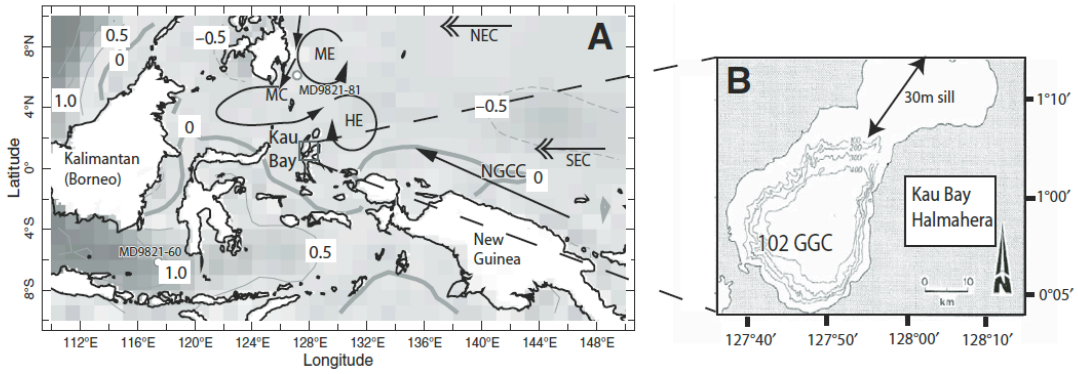

Figure 2.1. A: Location of Kau Bay in western tropical Pacific. Contours and grayscale shading are sea surface temperature anomalies during peak of very strong 1997–1998 El Niño event (*Reynolds and Smith, 1994*). Arrows represent general direction of ocean currents discussed in text. NEC—Northern Equatorial Current; SEC—Southern Equatorial Current; NGCC—New Guinea Coastal Current; MC—Mindanao Current; ME— Mindanao Eddy; HE—Halmahera Eddy. Locations of sediment cores analyzed by *Newton et al. (2006)* (MD9821–60) and *Stott et al. (2004)* (MD9821–81) are shown (see text). **B:** Kau Bay bathymetry with contours from 100 m to 400 m.

Temperature and [O_2] (figure 2.2) of the upper ~20m surface layer within Kau Bay reflect open ocean surface water values above the sill depth (figure 2.2). Freshwater input from the surrounding land reduces surface salinity within the Bay relative to outside the Bay, and stratifies the water column (figure 2.2). Ventilation of the entire water column within the basin may, however, occur when the wind- and current-driven flux of saltier and/or denser water entering the basin overcomes the salinity gradient, leading to deep mixing. *Van Aken and Verbeek* (*1988*) proposed that flushing of Kau Bay is

possible annually during September-November, when the New Guinea Coastal Current (NGCC) introduces slightly higher salinity water to the vicinity of Kau Bay (*Arruda and Nof, 2003*; *Masumoto et al., 2001; Wyrtki, 1961*). The southward flowing Mindanao Current (MC) and the seasonally northwest- and southeast-flowing NGCC collide near Halmahera to develop the cyclonic Mindanao Eddy (ME) and the anti-cyclonic Halmahera Eddy (HE). The strength of these eddies depends upon the strength of the MC and NGCC, so their presence may influence Kau Bay flushing (*Arruda and Nof, 2003; Masumoto et al., 2001; Ueki et al., 2003; Wyrtki, 1961*; figure 2.1).

There is also evidence that interannual changes in the mean climate state of the western equatorial Pacific, related to ENSO activity, exert significant control on the ventilation of Kau Bay. During modern El Niño events, the mixed-layer around Halmahera is characterized by colder and saltier water. Sea surface temperature (SST) data (*Reynolds and Smith, 1994*) for the 1 × 1 degree grid near the Kau Bay entrance reveal that SST cooled ~1 °C during all El Niño events since 1981. Mooring data collected at long 138°E and 142°E (*Ueki et al., 2003*) show that the typical seasonal variability in the flow direction of the NGCC ceased during the 1997–1998 El Niño and that instead the NGCC flowed northwestward all year, advecting cold and salty surface water toward Halmahera. Moreover, precipitation in the area of Halmahera is not significantly affected by the Asian Monsoon, but is strongly influenced by ENSO, with lower precipitation during El Niño events (*Aldrian and Susanto, 2003*). Increased primary productivity around Halmahera and Kau Bay during the very strong El Niño of 1997–1998 (*Christian et al., 2004*) is consistent with the proposed thermocline shoaling

associated with El Niño-driven changes in regional circulation (*Arruda and Nof, 2003; Ueki et al., 2003*).

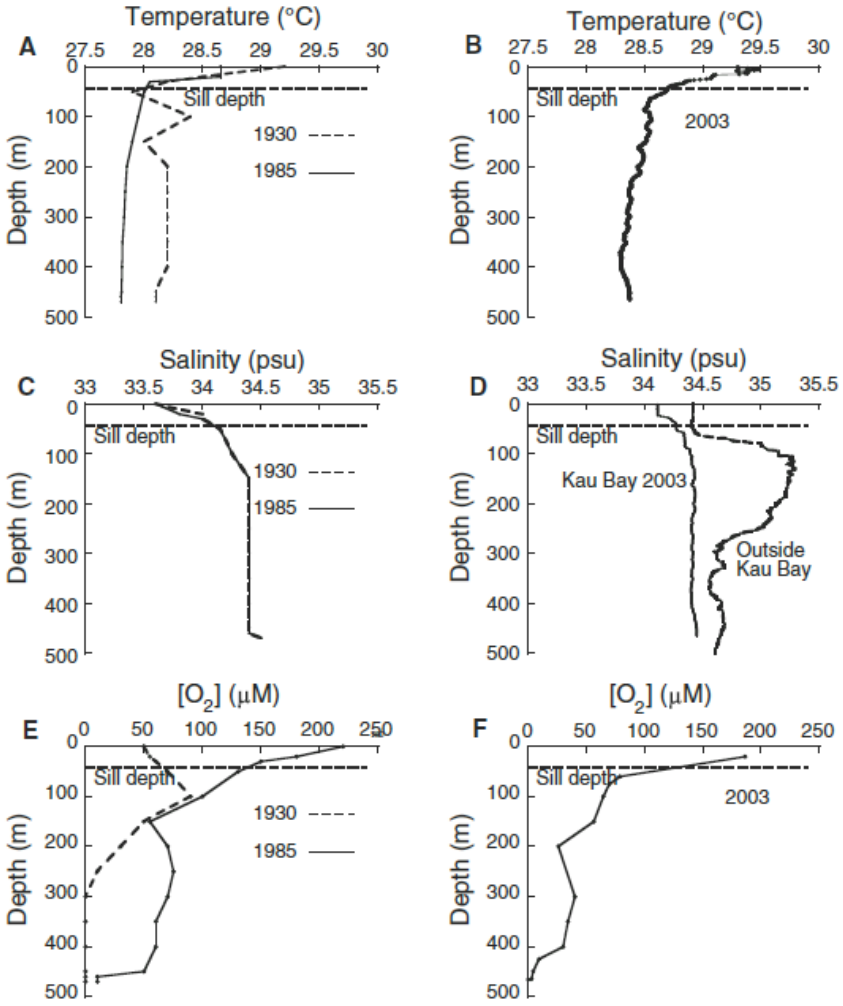

Figure 2.2. Water-column profiles of temperature (A and B), salinity (C and D), and oxygen (E and F) from 1930 (*Van Riel, 1943*), 1985 (*Van der Weijden et al., 1989*), and measurements from 2003.

2. SEDIMENTARY NITROGEN AND CARBON ISOTOPES

We measured nitrogen isotope ratios (as $\delta^{15}N$) on the <63μm fraction of bulk sediment from Kau Bay gravity core BJ8–03–102GGC at 8cm intervals (4.25m long, 377m water depth, figure 2.1). Radiocarbon dates on pteropods indicate that the $\delta^{15}N$ series has a resolution of ~1 sample per 60 yr (figure 2.3; see Supplementary Information, Table 2.2, below). Over the last 3,500 yr, sedimentary $\delta^{15}N$ varied between 2.2‰ and 5.6‰. Today, nitrate (NO_3^-) is completely consumed in Kau Bay's surface water (Fig. 4) so that sedimentary $\delta^{15}N$ records changes in the isotopic composition of subeuphotic zone nitrate. Several processes likely contribute to the $\delta^{15}N$ of nitrate in Kau Bay: 1) inputs from the open ocean; 2) inputs by N-fixation; 3) removal via denitrification in anoxic water; and 4) nitrification of ammonium fluxing out of the anoxic water and sediment. Western Pacific surface water NO_3^- has a $\delta^{15}N$ of ~5–6‰ (samples collected during the R/V *Baruna Jaya VIII* 2003 cruise). Nitrogen fixation reduces surface water NO_3^- $\delta^{15}N$ because nitrogen with a $\delta^{15}N$ of 0‰ is fixed from atmospheric N_2. In the deep basin, water column denitrifying bacteria in the absence of significant oxygen generally enrich the water column nitrate pool in $^{15}NO_3^-$through the preferential conversion of $^{14}NO_3^-$ to N_2 and N_2O gases (*Brandes et al., 1998; Liu and Kaplan, 1989; Sigman et al., 2003, 2005*). In contrast, nitrification, the oxidation of ammonium to nitrate, via nitrite, has a relatively large negative fractionation (~15‰; *Casciotti et al., 2002*) that is rarely apparent in oxic water columns because of the short turnover time for ammonium. Ammonium builds up in high concentrations in anoxic sediment, which may become a steady source of ammonium to the overlying oxic water column. The enrichment in Kau Bay bottom water $\delta^{15}N$ (figure 2.4) is not as high as expected from the observed

enrichment in bottom water $\delta^{18}O$ of NO_3. In culture they increase 1:1 (*Granger et al., 2004a & b*). In Kau Bay, $\delta^{18}O$ of NO_3 increases from 2-12‰ between 350m and the bottom, while $\delta^{15}N$ increases from 6 to 9‰. This suggests that ~7‰ of the enrichment expected from the $\delta^{18}O$ is negated by input of isotopically depleted N. The deviation in the expected relationship appears to be originating from the sediment-water interface and we infer nitrification of NH_4 to be the source.

In open ocean regions of denitrification such as the eastern tropical Pacific and Arabian Sea, sedimentary $\delta^{15}N$ is relatively high due to the effects of incomplete denitrification in the oxygen minimum zone (*Liu et al., 1989; Altabet, 2001; Ganeshram et al., 2000*). In contrast, nitrate supply to semi-enclosed basins such as Kau Bay is limited and denitrification results in the near complete removal of nitrate at depth. Moreover, extensive denitrification reduces the N/P in the water column, creating ideal conditions for nitrogen fixers (*Haug et al., 1998; Thunell et al., 2004*). Ultimately, an increase in denitrification enhances nitrogen fixation, which results in lower $\delta^{15}N$, and vice versa (*Haug et al., 1998; Thunell et al., 2004; Deutsch et al., 2007*). In Kau Bay, nearly all the nitrate below the oxycline is consumed and the proportion of denitrified nitrate bearing the $^{15}NO_3^-$-rich signature of denitrification is low relative to the overlying surface water nitrate pool (figure 2.4). An isotope effect (ε) of ~1.5‰ is calculated in Kau Bay assuming a closed system based on the Rayleigh approximation $\delta^{15}N = \delta^{15}N_{\text{mid-water column}} - \varepsilon \ln f$ (*Mariotti et al., 1981; Altabet and Francois, 1994*), where the fraction of unused nitrate, *f*, is $([NO_3^-{}_{\text{sediment water interface}}])/([NO_3^-{}_{\text{mid-water column}}])$ (~10μM). There is minimal expression of the denitrification ε of ~20-30‰ (*Thunell et al., 2004; Sigman et al., 2003*) in Kau Bay.

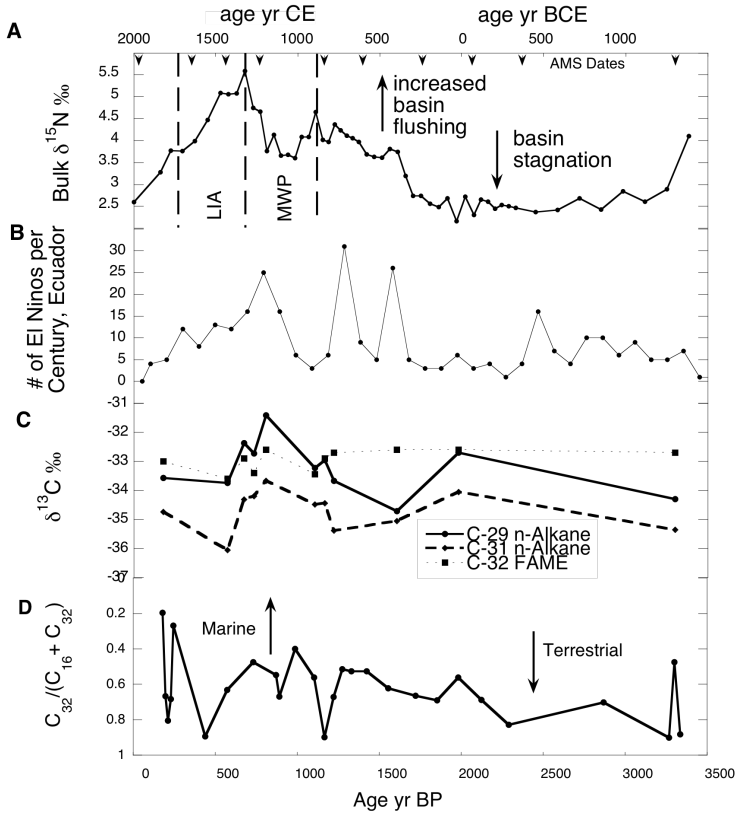

Figure 2.3. A: Bulk sediment $\delta^{15}N$. LIA—Little Ice Age; MWP—Medieval Warm Period. **B:** Total number of strong El Niño events per century interpreted from flood deposits in Laguna Pallcacocha, Ecuador (Moy et al., 2002). **C:** $\delta^{13}C$ of terrestrial plant waxes (*n*-alkanes with chain lengths of 29 and 31 carbons, fatty acids with chain lengths of 32 carbons). **D:** Ratio of terrestrial to marine fatty acids.

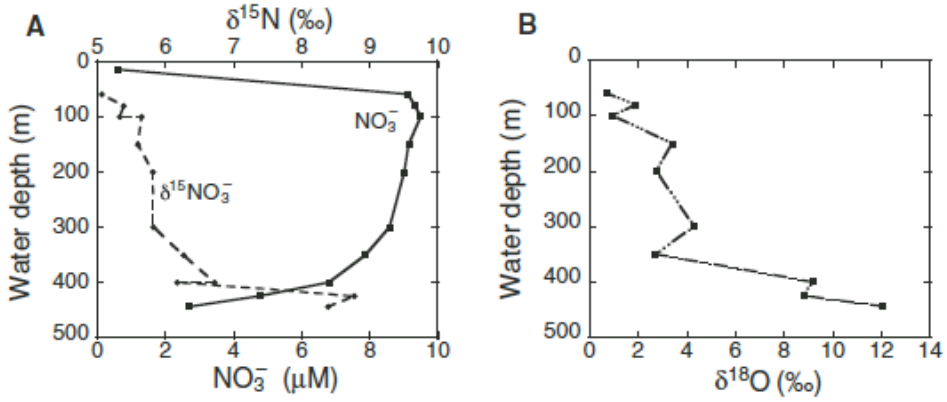

Figure 2.4. Nitrate concentrations and $\delta^{15}N$ (A) and $\delta^{18}O$ (B) of nitrate from center of Kau Bay, station 113HC; measurements taken in July 2003.

One interpretation of the downcore sedimentary $\delta^{15}N$ data in Kau Bay is that the isotopic composition of the surface nitrate pool reflects the combined effects of this nitrogen fixation-denitrification feedback and inputs from the open ocean (~5‰) (*Haug et al., 1998; Thunell et al., 2004*). Alternatively, the downcore intervals of lower sedimentary $\delta^{15}N$ may reflect periods of enhanced terrestrial inputs to Kau Bay (terrestrial organic matter has an average $\delta^{15}N$ of 0‰; *Brandes and Devol, 2002*) or enhanced inputs of isotopically light N via the nitrification pathway.

The -21 to -22 ‰ $\delta^{13}C$ values of sedimentary organic carbon (Table 2.1) indicate that there is a lack of C_4 plant influence throughout the core. The organic carbon: total nitrogen (C_{org}/N_{tot}) and $\delta^{13}C$ in the sediments (Table 2.1) indicate that marine organic carbon dominates throughout the core. The concentrations and relative abundance of terrestrial to marine fatty acids (figure 2.3D) suggest a gradual decrease in the influence of a terrestrial source for organic matter in Kau Bay concomitant with the increase in $\delta^{15}N$ from ~1,600 yr BP to 700 yr BP. The consistently low $\delta^{13}C$ values (from −36 to −31‰) of terrestrial *n*-alkanes and fatty acids clearly indicate that inputs from C_3 land plants (*Makou et al., 2007; Street-Perrott et al., 1997*) do not exert the dominant control on bulk sedimentary organic $\delta^{13}C$ values (Table 2.1) throughout the last 3,500 yr.

Table 2.1. %C (organic), %N (total), C/N, and $\delta^{13}C$ organics from core BJ8-03-102GGC, Kau Bay, Indonesia. The fraction <63um was analyzed and sub-samples for % organic carbon and $\delta^{13}C$ were acidified prior to analysis.

Age, yrBP	% Organic C	% Total N	C_{org}/N_{tot}	$\delta^{13}C$
163	4.58	0.46	11.68	-21.75
578	3.83	0.34	13.19	-22.06
1035	4.24	0.35	13.97	-22.32
1326	3.78	0.32	13.89	-21.66
2329	4.53	0.35	15.28	-22.19
3285	3.89	0.29	15.59	-21.27

Variations in the $\delta^{15}N$ and $\delta^{13}C$ therefore appear to primarily reflect water column processes (*Street-Perrott et al., 1997*). Moreover, whether the variations in $\delta^{15}N$ are related to enhanced N fixation or enhanced nitrification, low $\delta^{15}N$ corresponds to intervals of intensified stratification and anoxia in the basin and higher $\delta^{15}N$ reflects periods of increased ventilation and the input of open ocean nitrate.

The core top (modern) sample from Kau Bay multicore BJ8-03-103MC-F (companion to BJ8-03-102GGC) has a $\delta^{15}N$ of 2.6‰ while subeuphotic zone nitrate bears a $\delta^{15}N$ of ~5.5‰ (figures 2.3A and 2.4). The apparent disconnect between the modern water column nitrate pool and surface sediment $\delta^{15}N$ maybe be accomplished through intensified terrestrial inputs or a recent partial flushing of the water column (figure 2.4). Recent ventilation is consistent with the long La Niña phase from 1998-2002 and a transition to more El Niño conditions in 2003. If this is the cause, then this offset highlights the extremely dynamic nature of the Kau Bay water column.

3. DISCUSSION

We interpret downcore increases in the $\delta^{15}N$ as reflecting enhanced Kau Bay ventilation. Although we cannot unequivocally ascertain which of the proposed processes is responsible for the observed changes in sedimentary $\delta^{15}N$, it is important to note that whether acting alone or together, all generate the same response to ventilation; increased ventilation will lead to higher $\delta^{15}N$ while stagnation will reduce the $\delta^{15}N$. Increased flushing is most likely stimulated during periods of more frequent and/or intense El Niño events or a more El Niño-like mean state in the WPWP. A reduction in El Niño frequency and/or intensity or fresher and warmer mean state in the WPWP would result in basin stagnation and an overall decrease in $\delta^{15}N$. Accordingly, the $\delta^{15}N$ record (figure 2.3A) documents a less El Niño-like (neutral or La Niña-like) mean state or less frequent and/or weaker El Niño episodes from ~3,500 to ~1,700 yr BP. During this time interval, high runoff likely caused the increase in terrestrial input and may have promoted a fresh water cap at the basin's surface that resulted in basin stagnation. Ventilation improved at ~1,700 yr BP, likely due to thermocline shoaling in the WPWP in association with more El Niño-like mean surface conditions or stronger and/or more frequent El Niño events. Basin stagnation, signaling less El Niño-like conditions, occurred during the time frame of the Medieval Warm Period (MWP), from ~1000–750yrBP. This episode was followed by an increase in El Niño activity that culminated at the beginning of the Little Ice Age (LIA) at ~700yrBP. The Kau Bay record suggests that the remainder of the LIA was characterized by a steady decrease in El Niño activity with warming and freshening of the surface water that continued to the present. The surface freshening is consistent with the results of *Stott et al. (2004)* and *Newton et al. (2006).*

Within age model uncertainties, other paleoclimatic records support our interpretation of the Kau Bay geochemical records as reflecting century-scale ENSO variability. Most notably, the chronology of flood deposits in Laguna Pallcacocha, Ecuador (*Moy et al., 2002; Rodbell et al., 1999*), attributed to intense El Niño events, shows similar century-scale periods of increased El Niño frequency over the last ~1,500 yr, with diminished El Niño frequency during the past ~700 yr (figure 2.3). Decreased terrestrial input on the Peru margin and in the Cariaco Basin that began at ~1000yrBP has been attributed to drought and is also consistent with less frequent or weaker El Niño events or less El Niño-like conditions (*Haug et al., 2001; Hodell et al., 2005; Rein et al., 2004; Rein et al., 2005*). Not all climatic events recorded in the Kau Bay and Laguna Pallcacocha are evident in these other marine records, suggesting that they may be influenced by other climatic factors. By contrast, the finding of similar century-scale variability in climate archives from two El Niño-sensitive regions on opposite sides of the tropical Pacific strongly suggests that they are dominated by the low-frequency variability of ENSO or by ENSO-related changes in the mean state of the surface ocean in equatorial Pacific.

4. SUMMARY AND CONCLUSIONS

We used a record of bulk sedimentary $\delta^{15}N$ with additional complementary organic analyses from Kau Bay cores 102GGC and 103MC-F in order to determine the ventilation history of Kau Bay and its relation to WPWP climate. The $\delta^{15}N$ record remained reduced throughout much of the record, probably the result of increased nitrogen fixation and nitrification of ammonia during periods of extensive basin

stagnation. Increases in $\delta^{15}N$ were probably the result of increased basin flushing, most likely due to more frequent and/or intense El Niño events, when slackened trade winds are likely to cause the NGCC to flow northwestward towards Kau Bay throughout the entire year, bringing colder and saltier water to the vicinity of Kau Bay's sill. An increase in El Niño activity occurred at ca. 1,700yrBP followed by peaks at 1,500yrBP, 1150yrBP, and 700yrBP. According to this record, there was an overall increase in El Niño activity corresponding to the MWP and a decrease in El Niño activity during the LIA.

SUPPLEMENTARY INFORMATION

5. METHODS

5.1. C and N Stable Isotope and C/N Analyses

Gravity core 102GGC (4.25m) and companion multicore 103MC (0.7m) were collected during the BJ8-03 cruise in July 2003 from the southern portion of Kau basin at 377m water depth. Core 102GGC was split and sampled as 1-cm-thick quarter rounds from 0 to 424cm at 2-cm intervals. These samples were brought to the University at Albany, State University of New York, where they were wet-sieved into <63μm and >63μm fractions. The <63μm fractions were dried at room temperature (~25˚C). The <63μm fraction was separated from the bulk sediment sample in order to remove biogenic carbonates, coarse grained organics, inorganic carbonates, and ammonium. Samples from 8-cm intervals were analyzed for bulk $\delta^{15}N$ and 6 samples were selected for $\delta^{13}C$ measurement.

All sediment samples for $\delta^{15}N$ were combusted in tin foil capsules in a stream of helium and oxygen in a Carlo Erba NA 1500 Series II NC elemental analyzer (EA) in the Stable Isotope Ratio Mass Spectrometry (SIRMS) Laboratory at the University at Albany. Weight %C and %N of the ~12mg samples, from which C/N were calculated, were determined using the thermoconductivity detector of the EA. Reagent-grade acetanilide standards were interspersed among the samples. The $\delta^{15}N$ of ~12 mg samples was determined using a VG Instruments Optima gas-source triple-collector mass spectrometer in continuous-flow mode. All isotopic samples were analyzed in duplicate, with the average difference between replicate pairs equal to or better than ±0.25‰, and peach tree leaf standard NIST-1547 was analyzed after every 10^{th} sample. $\delta^{15}N$ is expressed as per mil deviations relative to nitrogen in air.

Carbonates were removed from the samples used for $\delta^{13}C$ of organic matter by acidification in HCl for 60-72 hours at 60-65˚C and then dried over silica gel and Drierite at 60-65˚C until the analyses were performed using a Carlo Erba 1107 Elemental Analyzer connected via a Conflo III interface to a Finnigan DeltaPlus mass spectrometer at the Woods Hole Oceanographic Institution (WHOI).

5.2. Radiocarbon AMS Dating

Radiocarbon analyses were performed on 9 samples throughout the core, shown in Table 2.2. Each sample contained ~5mg of shells of the pteropod *Creseis acicula*. These tests were cleaned with deionized H_2O and dried in an oven at ~75˚C overnight, re-weighed, and analyzed by the National Ocean Sciences Accelerated Mass Spectrometry (NOSAMS) facility at WHOI for AMS ^{14}C dating. A 300-yr reservoir correction was applied based on average reservoir ages obtained from surrounding locations (*Dang et*

al., 2004; Southon et al., 2002) and corrected using the Fairbanks radiocarbon calibration curve (*Fairbanks et al., 2005*).

Table 2.2. Radiocarbon dates on core 102GGC. The pteropod *Creseis acicula* was used for dating. Calendar ages were corrected using the *Fairbanks et al. (2005*) calibration curve following a 300-yr reservoir correction.

Core 102 GGC	Age C-14	Age Error	Calendar Ages	Sedimentation rate	NOSAMS Accession #
Depth (cm)	years	years	300 yr. Res. Corr.	(cm/100 years)	
20	690	30	333		OS-57842
40	805	35	528	10.3	OS-53225
72	1130	40	728	16.0	OS-50536
153	1520	30	1157	18.9	OS-57841
200	1790	40	1372	21.9	OS-53236
264	2120	35	1752	16.8	OS-53237
312	2400	30	2076	14.8	OS-53238
361	2600	30	2334	19.0	OS-57847
424	3460	35	3385	6.0	OS-50537
Core 103MC-F	Age C-14	Age Error	Calendar Ages	Sedimentation rate	
Depth (cm)	years	years	300 yr. Res. Corr.	(cm/100 years)	
18	165	30	-135		OS-59327
49	715	18	667	7.3	OS-59328
Core 115 GGC	Age C-14	Age Error	Calendar Ages	Sedimentation rate	
Depth (cm)	years	Years	300 yr. Res. Corr.	(cm/100years)	
37	575	30	279		OS-50567
378	1000	30	709	79.3	OS-50568

5.3. Water Column Nitrate N and O Isotope Analyses

N and O isotopes of water column nitrate were measured by the "denitrifier" method in Dr. D. Sigman's Laboratory at Princeton University. 10-20 nmol of NO_3^- is quantitively transformed to N_2O by a strain of denitrifying bacteria that lack N_2O reductase. The resulting N_2O is measured by continuous-flow isotope ratio mass spectrometry. Referencing to N_2 in air is done through parallel measurement of the IAEA-N3 standard with an accepted $\delta^{15}N$ of 4.7‰. Precision of replicate analyses was generally within 0.1‰ (1SD) (*Casciotti et al., 2002; Sigman et al., 2001*).

5.4. Fatty Acid and Alkane Analyses

Bulk samples were dried and then the total lipid extract (TLE) was obtained with a Dionex accelerated solvent extractor (ASE) 200 using 90/10 (v/v) dichloromethane (DCM)/methanol (MeOH) in 100˚C at 1,000psi pressure (Drenzek et al., 2007). Fatty acids were extracted from the TLE via fully-activated silica gel columns with 2% formic acid in DCM and were further purified by elution through aminopropyl columns with 2% formic acid in DCM. The fatty acid fractions were transesterified overnight (70˚C, 95/5 MeOH/HCl) with a methanol solution of known carbon isotopic composition. The transesterified fatty acid methyl esters (FAMEs) were recovered by extraction into hexane and further purified by elution through fully-activated silica gel columns with 5% ethyl acetate in hexane. Alkanes were separated from the TLE in fully-activated silica gel columns with 100% hexane.

n-Alkanes were separated from branched and cyclic alkanes by urea-adduction (*Ohkouchi et al., 2005*). 40g/mL urea/methanol solution was added to alkanes fractions previously dissolved in 2/1 hexane/DCM. The samples were refrigerated for 15 minutes, after which the urea clathrate containing the *n*-alkanes were rinsed twice with solvent to remove branched and cyclic compounds. Finally, elemental sulfur was removed from the alkane fraction by the addition of copper powder previously activated with 4N HCl and cleaned in distilled water (DCM extracted Milli-Q), MeOH, DCM, and hexane. The FAMEs and *n*-alkanes fractions were dissolved in hexane prior to analysis by gas chromatography using a Hewlett Packard 5890 Series II gas chromatograph (GC) equipped with flame ionization detection (60m x 0.32mm i.d. x 0.25µm film DB-5 column, H_2 carrier gas). C_{14}-C_{34} fatty acid concentrations were determined relative to an in-house FAME standard. These

samples were also submitted for $\delta^{13}C$ analysis on a ThermoFinnigan Delta^{plus} gas source mass spectrometer (*Drenzek et al., 2007; Ohkouchi et al., 2005*).

CHAPTER 3

Late Holocene climate variability recorded in pteropods from Kau Bay, Indonesia: Evidence for coordinated century-scale zonal climate change in the Pacific Basin

ABSTRACT

In order to determine long-term changes in heat storage of the Western Pacific Warm Pool (WPWP) in reference to the eastern equatorial Pacific, pteropod oxygen and carbon stable isotopes ($\delta^{18}O$, $\delta^{13}C$) and Sr/Ca were analyzed from a ~3,500-year-long sediment core record from Kau Bay, Indonesia, (0˚N, 127.5˚E). Radiocarbon dates indicate that this gravity core had an average near-linear accumulation rate of 180 to 200 cm/Kyr. Temporal variations in pteropod $\delta^{18}O$, $\delta^{13}C$, and Sr/Ca are compared to climate records of similar age and temporal resolution from the western Pacific warm pool (WPWP), China, Makassar Strait in Indonesia, and the eastern equatorial Pacific (EEP). The Kau Bay pteropod $\delta^{18}O_{sw}$ record correlates with East Asian Monsoon records on glacial-interglacial timescales, while large segments of the pteropod Sr/Ca record are remarkably similar to several records from the EEP. The pteropod Sr/Ca record correlates to the El Junco % sand (*Conroy et al., 2008*) with congruity to the Laguna Pallcacocha record of flood events from intense El Niño events (*Moy et al., 2002*). This indicates that: 1) Kau Bay pteropod shell $\delta^{18}O$, $\delta^{13}C$, and Sr/Ca do contain significant paleoclimate information, 2) based on Kau Bay pteropod $\delta^{18}O$, $\delta^{13}C$, and Sr/Ca, the surface water in Kau Bay was warmer ~3,000-2,500 years ago than during the last 2,200 years, 3) century-scale changes in late Holocene zonal dynamics may have had a strong effect on the WPWP and,

therefore, global climate, and 4) varying strength of the East Asian Summer Monsoon (EASM) in addition to zonal dynamics and variable positioning of the ITCZ have had a strong influence on Kau Bay climate. This may suggest that ENSO-like variability, or the mean state of ENSO in the Pacific, occurs in the equatorial Pacific on century-scale frequencies.

1. INTRODUCTION

The Western Pacific Warm Pool (WPWP; part of the Indo-Pacific Warm Pool, IPWP) has a significant influence over global climate by storing large quantities of heat (e.g., *Clement et al., 1999; Klein et al., 1999; Wang and Fu, 2000)*. Today, changes in the heat distribution from the WPWP cause major global shifts in climate that can, in turn, have a large effect on all ecosystems (as discussed in *Qu et al., 2005, and Cane, 2005*). Cross-basin oceanic and atmospheric dynamics play a tremendous role in the storage of energy within the WPWP, affecting inter-annual climate phenomena such as El Niño Southern Oscillation (ENSO) and the East Asian Monsoon (EAM). There is a need to examine lower resolution changes in the WPWP in order to determine if there were any previous large-scale shifts or recurring temporal patterns in WPWP heat distribution due to changes in Walker circulation or other unknown phenomena.

1.1. Century-Scale Zonal Climate Variability in the WPWP

Today, zonal climate variability in the equatorial Pacific is typically characterized by interannual ENSO variability. ENSO is a climate phenomenon during which changes of equatorial trade wind strength redistributes heat across the Pacific Ocean. This

phenomenon is fed by sea surface temperature (SST) gradient changes across the Pacific and affects global distributions of heat and convection (e.g., *Cane, 2005*). Based on the instrumental record, this phenomenon appears to vary with a periodicity of 3-7 years. Paleoclimate data suggest that processes similar to ENSO may occur in cycles over greater periods of time. For example, changes in the mean state of the Pacific during the late Holocene that would induce longer durations of more frequent and/or intense El Niño and La Niña episodes and are unrelated to other known forcings, such as solar or orbital forcings, may be related to the interannual ENSO phenomenon (e.g*., Stott et al., 2002; Conroy et al., 2008; Moy et al.,2002; Oppo et al., 2009; Koutavas and Lynch-Steiglitz, 2004; Mitsuguchi et al., 2008*). However, the connection between lower resolution patterns and interannual ENSO remains unclear despite paleo-records from both the eastern and western equatorial Pacific that appear to portray decades, centuries, or millennia over which ENSO was diminished in frequency and/or strengthened (e.g., *Moy et al., 2002; Stott et al., 2002; Lachniet et al., 2004; Controy et al., 2008*).

High resolution records that extend back across millennia, like those presented here, are valuable because they potentially can document past environmental variability taking place in a region currently dominated by ENSO. Many other sediment-based paleoclimate records from ENSO-sensitive regions do not specifically record interannual changes in ENSO. Records that reach back several thousands of years and show possible millennial-scale changes in ENSO include temperature and salinity records derived from $\delta^{18}O$ and Mg/Ca of planktonic foraminifera from the western equatorial Pacific (*Stott et al., 2002*) and % grain size varying alongside storm intensity likely stemming from variability in ENSO frequency and/or intensity from Laguna Pallcacocha in Ecuador

(*Moy et al., 2002*) and El Junco Lake in the Galapagos islands (*Conroy et al., 2002*). More recent Holocene data sets that appear to demonstrate century-scale or shorter-term ENSO variability include planktonic foraminifera $\delta^{18}O$ and Mg/Ca records from Makassar Strait, Indonesia (*Newton et al., 2006; Oppo et al., 2009*). Meanwhile, a δD record from Makassar Strait reflects century-scale hydrological shifts possibly associated with ENSO (*Tierney et al., 2010)*. Therefore, although ENSO variability is described as an interannual phenomenon, century-scale and millennial-scale trends in the frequency and/or intensity of ENSO appear to exist and need to be reconciled within records from the equatorial Pacific region.

1.2. Kau Bay Hydrography

Kau Bay is a 470m deep, silled basin located in Halmahera, Indonesia within the western sector of the WPWP (figures 3.1 and 3.2). Surface water between the basin and the WPWP can be exchanged on the northern end of Kau Bay, where there is a restrictive sill that is 30m deep (*Van Aken and Verbeek, 1988*). Temperature and salinity profiles of the Kau Bay water column measured in 1930, 1985, and 2003 show that the basin is commonly well-mixed and that temperature and salinity throughout the basin reflect those properties of the uppermost surface water entering from across the sill (figure 3.3). Regional surface oceanographic conditions near Halmahera appear to control mixing with external water (*Van Aken and Verbeek, 1988*). These conditions are influenced by the interaction of the southward flowing Mindanao Current (MC) and by the variable northwestward flowing New Guinea Coastal Current (NGCC; figure 3.2). The

interaction of these two currents near the equator leads to the seasonally alternating development of the cyclonic Mindanao Eddy (ME) and the anti-cyclonic Halmahera Eddy (HE) (e.g., *Wyrtki, 1961; Masumoto et al., 2001; Arruda and Nof, 2003*). The NGCC seasonally changes direction, but generates a net equator-ward movement. *Van Aken and Verbeek* (1988) proposed that flushing of Kau Bay was possible annually during September-November, when the NGCC introduces slightly higher salinity water to the vicinity of Kau Bay and recurves into the North Equatorial Countercurrent (NECC; figure 3.2). This is also the time of year that the HE is fully developed (*Masumoto et al., 2001*). During the northeast monsoon, the ME develops and the HE dissipates (*Masumoto et al., 2001; Arruda and Nof, 2003*).

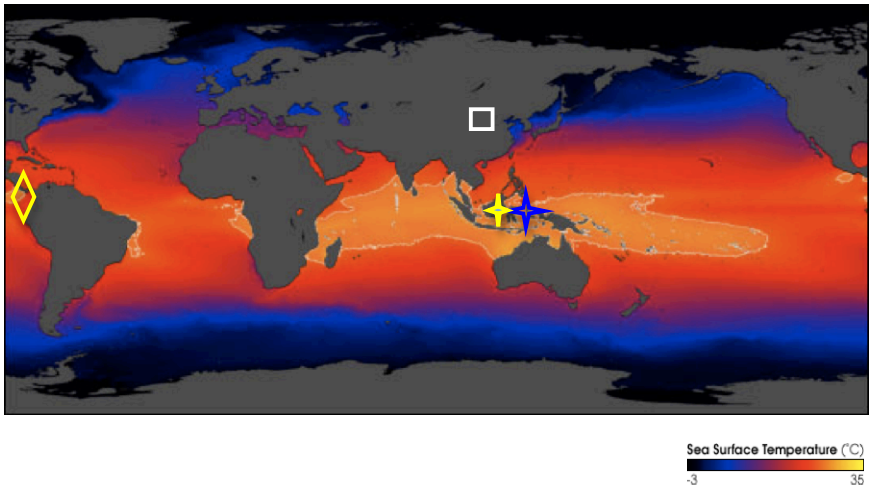

Figure 3.1: Extent of the IPWP and WPWP, and location of Kau Bay (blue star), Makassar Strait (yellow star), Panama and the Galapagos Islands (yellow diamond), and the Heshang and Dongge caves (white square) (http://earthobservatory.nasa.gov/Features/WarmPool/).

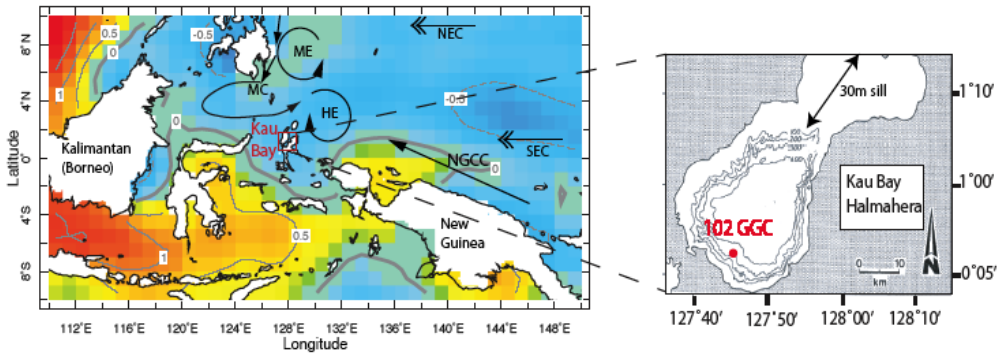

Figure 3.2. Map of SST anomalies (left) during January 1998 (peak El Niño conditions) in the western Pacific region (*Reynolds and Smith, 1994*) with the New Guinea Coastal Current (NGCC), South Equatorial Current (SEC), North Equatorial Current (NEC), and the Mindanao and Halmahera Eddies shown. The location of core 102GGC in Kau Bay is shown in the right panel (*Van Aken and Verbeek, 1989*).

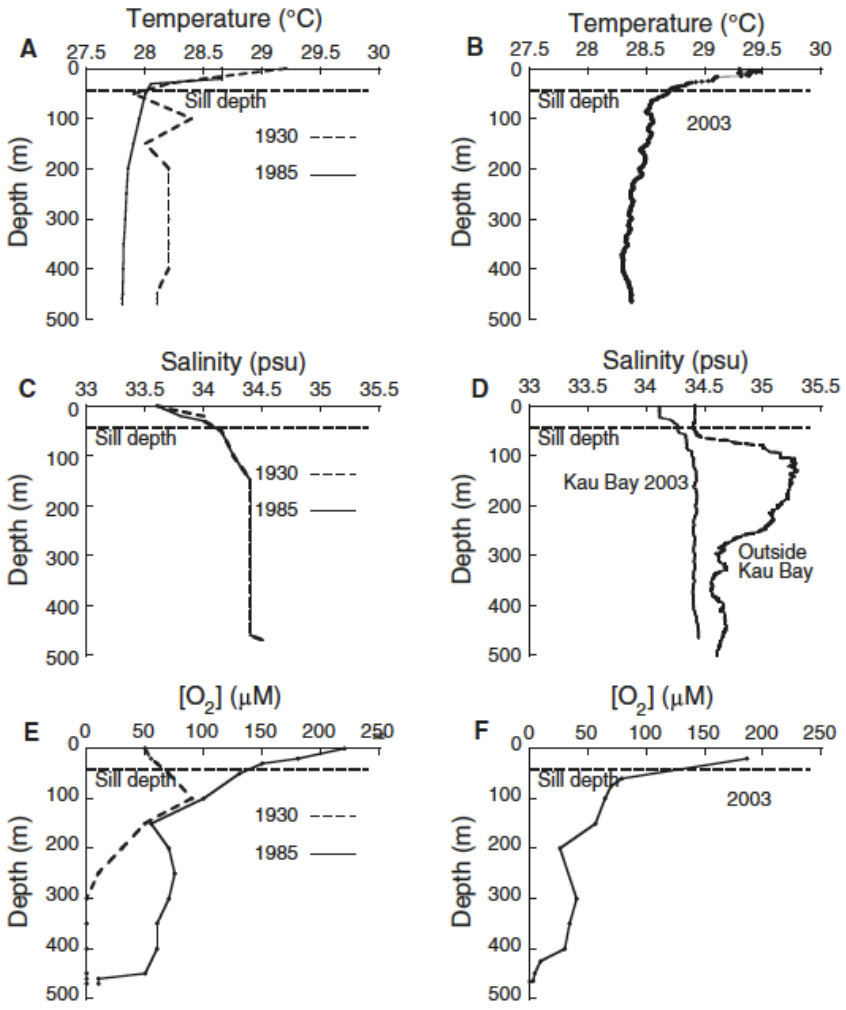

Figure 3.3. Temperature, salinity, and oxygen depth profiles from Kau Bay. A and B: temperature; C and D: salinity; E and F: oxygen. Adapted from *Langton et al., 2008*.

Since the 1970s, El Niño events have brought colder and saltier water to the surface ocean mixed layer around Halmahera (figure 3.2). During strong El Niño events, such as during the 1982-1983 and 1997-1998 El Niños, the WPWP was ~1-1.5˚ cooler than average in the area of Halmahera. Meanwhile, Halmahera was up to 2˚ warmer than average during strong La Niña events, e.g., 1988-1989, 1998-1999, 2000-2001, and 2010-2011. Increased rainfall persists during these strong periods of La Niña, while decreased

rainfall and increased salinity is typical of strong El Niño episodes in the vicinity of Kau Bay. SST data (*Reynolds and Smith, 1994*) for the 1 x 1 degree grid near the Kau Bay entrance reveal that SST cooled ~1°C during all El Niño events since 1981, apparently in response to regional thermocline shoaling. Salinity data from *Levitus et al. (1994)* show that the NGCC brings colder, saltier water towards Halmahera during the northwest monsoon (figure 3.4). Mooring data collected at longitudes 138°E and 142°E showed that the typical seasonal variability in the flow direction of the NGCC ceased during the 1997-1998 El Niño and, instead, flowed northwestward all year. This advected cold, salty surface water to the area of Halmahera (*Ueki et al., 2003*). Meanwhile, *Aldrian and Susanto* (*2003*) formulated a double correlation model that showed that precipitation in the area of Halmahera is strongly influenced by interannual variations in ENSO. This region exhibits strong negative precipitation anomalies during the already dry months of June through November during El Niño episodes, while increased rainfall is present during these months in a La Niña episode (*Aldrian and Susanto, 2003*). This evidence suggests that the most significant changes in salinity and temperature within Kau Bay are linked to ENSO variability.

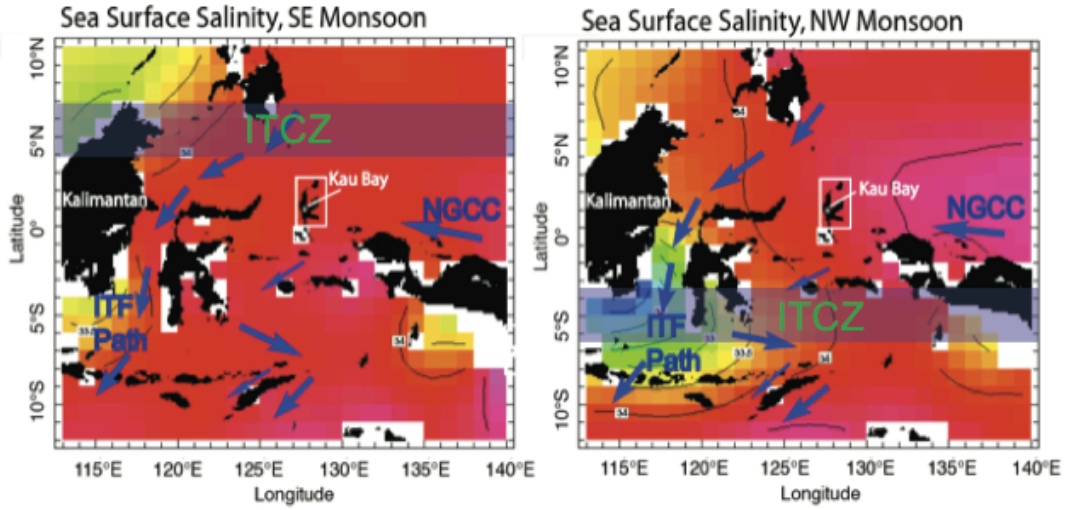

Figure 3.4. Maps of surface salinity during the southeast monsoon (July-Sept) (left) and northwest monsoon (January-March) (right) in the western Pacific region. Halmahera and Kau Bay are indicated by the white box. Note the slightly more saline water in the NGCC region and Kau Bay during the boreal winter monsoon. Salinity data are from *Levitus et al. (1994)*. Blue arrows denote the flow of the ITF, of which ~ 80% flows through the Makassar Strait, between Kalimantan and Sulawesi. The general latitudinal range of the ITCZ convection belt for summer and winter in the Western Pacific based on *Waliser and Gautier (1993)* are shown.

1.3. Rainfall in Kau Bay

The Kau Bay-Halmahera region receives ~4,000mm of rain on average each year (*Suparan et al., 2001*). The largest river is the Kau River and it empties into Kau Bay on its northwestern shore. There is little seasonal climate variability, but the months of July through September are typically drier. Prior to the twentieth century and into the WWII era, explorers described the lowlands surrounding Kau Bay to be comprised of evergreen lowland forest. The coastal belt along Kau Bay was comprised of secondary forest and scrub and natural grasslands, and the interior plain contained large open grassland to herbaceous swamps, sago palm swamps, swamp forests, and mangrove stands within the Kau River delta (*Suparan et al., 2001*).

In the Kau Bay watershed, precipitation is mainly affected by ENSO variability and the mean position of the ITCZ (*Aldrian and Susanto, 2003*). The ITCZ enhances equatorial upwelling during the peak of the northern hemisphere summer (Aug.-Sept.), when southeast trade winds are strongest. Equatorial upwelling reduces SSTs and creates a shallow thermocline. During the peak of the northern hemisphere winter (Feb.-Mar.), the ITCZ migrates to its southernmost point, winds subside, equatorial upwelling is diminished, and equatorial SSTs may increase (*Chelton et al., 2001*). At present, the ITCZ has a northern bias and a southern migration of the ITCZ was apparent during the last glacial maximum (LGM; e.g., *Koutavas and Lynch-Stieglitz, 2004*).

The position of the ITCZ is affected by ENSO on interannual time periods most clearly in the eastern Pacific. During El Niño, the ITCZ shifts toward the equator in the eastern Pacific and migrates north during La Niña. La Niña peaks during the boreal summer while the ITCZ is in its more northern position and this phase of ENSO intensifies equatorial upwelling. Weakened trade winds during El Niño episodes add to the diminished upwelling and increased SSTs across the equatorial Pacific that normally peak when the ITCZ is in its southernmost position from January to February (*Waliser and Gautier, 1993*).

Records from the tropical Pacific within the ITCZ show a southward migration of the ITCZ from the Medieval Warm Period (~700yrBP) to the Little Ice Age (~200yrBP), followed by a return to a more northern position after 200yrBP (e.g., *Newton et al., 2006; Moy et al., 2002; Sachs et al., 2009*). For example, a δD lipid record from El Junco Lake in the Galápagos (1˚S; *Sachs et al., 2009*) and foraminiferal Mg/Ca records from Makassar Strait, Indonesia (2˚S; *Newton et al., 2006; Oppo et al., 2009*), both display

evidence for wet climates during the LIA, which suggests a more southerly location of the ITCZ. Currently, these areas are on the southern edge of the seasonal ITCZ and are more arid now than they were during the LIA. Meanwhile, areas that currently are located at the northern extreme of the seasonal ITCZ, e.g., Palau (7˚N, 134˚E, *Sachs et al., 2009*); Washington Island (5˚N, 160˚W, *Sachs et al., 2009*); Panamá, (8˚N, 82˚W, *Linsley et al., 1994)*; and the Cariaco Basin (11˚N, 72˚W; *Haug et al., 2001*) were drier during the LIA than at present. The more southerly position of the ITCZ during the LIA was likely the result of, or led to, a period of decreased ENSO activity. This is demonstrated by ENSO records such as the grain size distribution records from El Junco Lake, Galápagos, and Laguna Pallcacocha, Ecuador, which show significantly increased ENSO activity 1,500-2,000yrBP and during the MWP followed by a decrease in ENSO activity during the LIA (*Conroy et al., 2008; Moy et al., 2002*).

1.4. Basin Sediments:

Gravity and multi-cores were collected in Kau Bay in 2003. This unique setting has resulted in an intermittently dysoxic water column in the basin with high sedimentation rates in excess of 180 cm/kyr in many parts of the basin and minimal bioturbation. The Kau Bay cores were essentially devoid of benthic and planktonic foraminifera. As a result, other proxies were explored to determine if paleo-environmental signals existed in sediments from Kau Bay. Organic matter proxies, including $\delta^{15}N$, C/N, $\delta^{13}C$, and compound specific C and O isotopes were examined in *Langton et al., 2008*.

In addition, unbroken and unaltered pristine aragonitic pteropod shells of the species *Creseis acicula* were abundant throughout the cores. Although it is known that

these organisms will migrate to various depths throughout a large temperature range, Kau Bay does not display temperature stratification below the shallow thermocline at 50m. Although most pteropod species cannot tolerate salinities greater than 34‰ (*Rottman, 1979*), which is characteristic of most of Kau Bay's water column (figure 3.3), *C. acicula* is able to thrive in high salinity environments (*Winter et al., 1983*). Pteropod shells were analyzed for $\delta^{18}O$, $\delta^{13}C$, and Sr/Ca. $\delta^{18}O$ typically reflects temperature and salinity change in other biogenic aragonites (e.g., *Grossman and Ku, 1986*), while Sr/Ca in gastropods often varies in response to water temperature (e.g., *Sosdian et al., 2006; Smith et al., 1979; Beck et al., 1992)*, although in pteropods these tracers are very poorly calibrated. We compared our pteropod $\delta^{18}O$ and Sr/Ca records to other records from the Makassar Strait and eastern equatorial Pacific (EEP). These include a leaf wax δD record from cores 31MC and 34GGC from Makassar Strait (*Tierney et al., 2010*), a grain size record from El Junco Lake in the Galápagos (*Conroy et al., 2008*) and a $\delta^{18}O$ record of a speleothem from Chilibrillo Cave, Panamá (*Lachniet et al., 2004*). These comparisons lead to two new findings: 1) pteropod shells in this setting can be used to generate detailed paleoclimate reconstructions, and 2) there is a correlation between century-scale cross-basin variability in the WPWP and EEP.

1.5. Pteropod Analyses

The $\delta^{18}O$ and $\delta^{13}C$ of calcium carbonate precipitated by marine microorganisms can vary with temperature, salinity, and changes of the DIC content of the water (*Broecker and Peng, 1983; Epstein and Mayeda, 1953; Juranek et al., 2003*). The co-precipitation of Sr varies in inorganically precipitated aragonite with respect to water

temperature (*Elsdon and Gillanders, 2005*). Pteropod shell $\delta^{18}O$, $\delta^{13}C$, and Sr have not been used for paleoclimate reconstructions in part because accurate calibration has not been possible due to the difficulties of studying live specimens. Pteropods are often poorly preserved in the fossil record due to a shallow or variable aragonite lysocline depth (*Fabry and Deuser, 1992; Sijinkumar et al., 2010*). However, their ubiquitously large populations in many marine environments in addition to their comparatively large size would make them potentially useful for paleoclimate and paleoenvironmental reconstructions, especially as an accompaniment to foraminifera-based records. In Kau Bay, the abundance of pteropods and scarcity of foraminifera gave us the opportunity to more closely examine pteropod shell chemistry as possible proxies for paleoclimate reconstructions.

One of the hindrances of using pteropods for paleothermometry or paleo-environmental studies is that their calcification depths are poorly known. *Fabry and Deuser* (*1992*) initially determined that several species of pteropods calcify their shells within the upper 75m of the water column in the Sargasso Sea. In this study, *C. acicula* (the pteropod present in Kau Bay) appeared to calcify its shell only within the upper 25m of the surface water. However, *Juranek et al. (2003*) found that *C. acicula* has a diel migration down to 250m in order to follow food sources that vary from day to night and seasonal vertical migration may be in excess of 1000m, which clearly affected the shell $\delta^{18}O$ and apparently contradicted the previously estimated shallow calcification depths. Although more research is necessary to determine the correct calcification depths for *C. acicula*, the calcification depth of *C. acicula* probably does not affect their shell $\delta^{18}O$ stable isotope geochemistry in Kau Bay for several reasons: 1) Kau Bay does not exhibit

significant temperature and salinity stratification (1°C and ~0.5 p.s.u. difference between top and bottom of thermocline and halocline respectively); 2) Kau Bay is dysoxic and the low dissolved oxygen levels should discourage deeper calcification of pteropods; and 3) the water column in the basin reflects conditions of only the Pacific Ocean surface water directly over the bay's sill, down to ~30m depth (figure 3.3).

There are several advantages of using pteropod shells for paleoclimate reconstruction in Kau Bay. Since Kau Bay temperature and salinity are well mixed and the basin water is only fed by surface water from the upper 30m across the sill connecting it with the open Pacific and WPWP, pteropod shells should approximate temperature and salinity variability in the WPWP assuming they calcify in the mixed layer. A previous study (Chapter 2 and *Langton et al., 2008*) showed that Kau Bay is periodically flushed by water from the WPWP. This study evaluated the ventilation history of Kau Bay via changes in nitrogen isotope composition of sedimentary organic matter. Significant changes in nitrogen isotope variability occurred when the basin bottom waters were flushed with water from the WPWP, but this record did not record subtle changes in water composition due to partial mixing with water from over the sill. The pteropod shell records possibly show greater variability in relation to partial mixing with surface water from the WPWP in addition to rainfall because this variability is not dependent on complete flushing of the basin's bottom water.

1.5.1. Pteropod Oxygen and Carbon Isotopes

According to *Grossman and Ku* (*1986*) and *Juranek et al.* (*2003*), pteropods appear to build their aragonitic shells at or near aragonite-water equilibrium so that their

shell $^{18}O/^{16}O$ is controlled by a combination of ambient temperature and the precipitation/evaporation cycle. The entire water column in Kau Bay is above the aragonite lysocline and alkalinity throughout the entire 470m depth reflects the alkalinity of the upper 50m of surface water from over the sill just to the northeast of the basin (table 3.1), so there is no reason to suspect alteration of oxygen or carbon isotopes from dissolution. This is supported by the pristine preservation of pteropods in the Kau Bay cores we collected. The ratio of $^{18}O/^{16}O$ in biogenic carbonates often bears an inverse relationship with sea surface temperature (SST). However, since marine biogenic carbonate $^{18}O/^{16}O$ is also a function of $^{18}O/^{16}O$ in seawater (linear relationship with salinity), calcium carbonate can preserve a record of absolute SST and surface water salinity from the time of calcification.

Table 3.1. Alkalinity within Kau Bay and to the east of Kau Bay measured during the BJ8-03 expedition in 2003.

Kau Bay (0˚N, 127˚E) Depth, m	Alkalinity (µmol/eq)	East of Kau Bay Sill (1˚N, 128˚E) Depth, m	Alkalinity (µmol/eq)
14.67	2255.84	25.58	2269.25
59.55	2258.68	50.38	2257.73
80.44	2258.31	100.00	2313.46
99.67	2259.06	150.12	2331.64
150.25	2259.17	199.92	2332.72
300.00	2260.23	400.31	2312.35
350.36	2272.95	500.75	2328.52
400.28	2283.15	749.93	2350.51
424.94	2282.11	1000.04	2364.25
		1399.89	2381.33
		1849.52	2404.08

Records of $\delta^{18}O$ in calcitic and aragonitic foraminifera tests from ocean sediments have been extensively utilized as paleotemperature and paleosalinity tracers because of their widespread abundance in ocean sediments. Mollusk shell $\delta^{18}O$ has been shown to correlate well with the aragonitic foraminifera *Hoeglundina elegans* (*Grossman and Ku,*

1986). In addition, the $\delta^{18}O$ in coral aragonite is often analyzed to determine temperature and salinity variations on monthly to interannual timescales in tropical regions for shorter periods of time. While the use of pteropods in geochemistry is limited by inadequate numbers of calibrated datasets and the inability to preserve and to culture living specimens for calibration studies, there is great potential to expand their use to other basins with parameters like Kau Bay (*Fabry and Deuser, 1992; Juranek et al., 2003*). Finally, pteropods have the potential to expand paleoclimate studies in such basins because of their robust size that encourages easier analytical procedures, ubiquitous range, salinity tolerance, and year-round life spans.

While the effect growth rate and other biological factors on pteropod aragonite $\delta^{18}O$ is not defined, their shells are developed close to equilibrium with seawater less a possible enrichment of $\delta^{18}O$ by ~0.8‰ compared to calcite, which is equal to the amount of offset from inorganic precipitates (*Grossman and Ku, 1986*; *Tarutani et al., 1969*). Since the extent and magnitude of this offset is thought to be constant, relative changes in the timing and amplitude of downcore pteropod $\delta^{18}O$ remains unaffected. *Fabry and Deuser (1992)* determined that the magnitude of the non-equilibrium $\delta^{18}O$ fractionation for *C. acicula* was 0.3‰. These pteropods appear to have faster growth rates with a total developmental time of only a few months compared to a rate that extends up to a year in other species (*Fabry and Deuser, 1992*). Pteropods in the Sargasso Sea calcify their shells at different depths and water temperatures seasonally (*Juranek et al., 2003*). In addition, *C. acicula* does not show a seasonal preference for calcification, so $\delta^{18}O$ from a group of specimens likely reflects annual averages.

The $\delta^{13}C$ of pteropods is affected by a combination of salinity, DIC content, and $[CO_3^{2-}]$ (*Grossman and Ku, 1986; Juranek et al., 2003*). Pteropod $\delta^{13}C$ appears to vary inversely with DIC and $[CO_3^{2-}]$ (*Fabry and Deuser, 1992; Grossman and Ku, 1986; Juranek et al., 2003*). The amount of the carbonate ion effect (CIE) is similar in at least two species of pteropod (*Juranek et al., 2003*) and the foraminifer *Globigerina bulloides (Spero et al., 1997)*. $[CO_3^{2-}]$ and alkalinity vary with water depth and temperature, so the variability of pteropod $\delta^{13}C$ has previously been shown to reflect variability in water temperature (*Juranek et al., 2003; Grossman and Ku, 1986*). Although many of the same parameters affect $\delta^{13}C$ and $\delta^{18}O$, unknown metabolic and microhabitat controls can affect $\delta^{13}C$, adding to the difficulty and uncertainty of the interpretation.

1.5.2. Variability of Strontium in Pteropod Shells

Trace metals with long residence times (~100,000 years) that are incorporated into the calcite and aragonite of marine organisms and act in a conservative manner in the oceans may be used as paleoclimate and paleoenvironment tracers if the Metal:Ca ratio (Me/Ca) in the organism is in equilibrium or at a constant offset with ratios in seawater (*Allison, 1996; Russell et al., 2004; Elsdon and Gillanders, 2005a*). Trace metals may form a solid solution in $CaCO_3$ by the following processes: 1. aqueous speciation and diffusion, 2. adsorption and desorption onto mineral surfaces, 3. ligand exchange reactions, 4. rearrangement of ligand coordination, and 5. coordination changes and diffusion within the solid (*Meece and Benninger, 1993; Russell et al., 2004*). All of these processes combined will affect the total co-precipitation of trace metals in biogenic precipitation of calcium carbonate. Environmental parameters affect each of these

processes and thus influence the incorporation of trace metals into shell calcium carbonate, which is why calibration experiments are important to paleoclimate records using trace metal abundances.

While Sr/Ca in biogenic calcite tends to increase with temperature (*Lea et al., 1999*), there have been discrepancies in the water temperature effects on Sr/Ca in aragonite. In corals, Sr is incorporated into the aragonite lattice in an inverse relationship with temperature change (e.g., *Kinsman and Holland, 1969*; *Smith et al., 1979; Beck et al., 1992; deVilliers et al., 1994, 1995*). Inorganically precipitated aragonite also displays an inverse relationship between Sr incorporation and water temperature (*Elsdon and Gillanders, 2005b*). Sr incorporation into some gastropods covaries with growth rate (*Sosdian et al., 2006; Zacherl et al., 2003*). *Sosdian et al. (2006)* found a positive correlation between water temperature and Sr/Ca in aragonitic shells from the gastropod *Conus ermineus*. Meanwhile, the growth rate dependency on Sr incorporation may only exert an effect on aragonite that has a relatively large growth rate as shown by a study on larval gastropods—more quickly precipitated aragonite (protoconchs) had a positive Sr/Ca and temperature relationship, while more slowly deposited aragonite within the same larvae (statoliths) resembled the inorganic inverse relationship between Sr incorporation and temperature (*Zacherl et al., 2003*).

Gastropods and bivalves typically live for up to several years, while pteropods generally live and grow their shells over a period of less than one year. The rate of pteropod shell development and the influence of extrapallial fluid in growth is poorly known, which makes it difficult to determine whether the Sr precipitated in their shells covaries more closely as a result of changes in growth rate or directly in response to

water temperature. In order to attempt to resolve the dependence of Sr incorporation on pteropod shells as a direct function of temperature change or growth rate, we compared the paleo-records of pteropod Sr/Ca to other paleo-records from the WPWP that display temperature change in the region at the same temporal scale.

2. METHODS

Gravity core 102 GGC, multi core 103 MC, and hydrocast HC113 were collected from Kau Bay as part of the Baruna Jaya 8-03 Cruise to Indonesia in July 2003 (BJ8-03). Core 102 GGC is 4.25m in length and 103 MC-F is 0.56m in length. 102 GGC was stored in ~1.5 m sections and later cut in half lengthwise to store as the working and archived halves at WHOI. Quarter rounds at 1cm intervals were sampled and brought to the Stable Isotope Laboratory at the University at Albany. 103 MC-F was slabbed on the cruise and 1cm thick samples were refrigerated and stored in plastic bags. These samples were soaked in deionized water overnight and then shaken in Erlenmyer flasks for 1 hour. Samples were transferred to sieves where they were sieved into <63µm and >63µm sections and stored in separate beakers. These samples were dried in a low temperature oven (50˚C) and then dry sieved into 63-150µm and >150µm sections and stored in glass vials.

2.1. Age Model

A total of 11 AMS radiocarbon dates were acquired to produce age models for sediment cores 102GGC and 103MC, 9 samples from 102GGC and 2 samples from 103MC (see table 3.2 and figure 3.5). Each sample contained ~5mg of shells of the

pteropod *Creseis acicula*. These shells were cleaned with deionized H_2O and dried in an oven at ~50˚C overnight, re-weighed, and analyzed by the National Ocean Sciences Accelerated Mass Spectrometry (NOSAMS) facility at WHOI for AMS ^{14}C dating. A 200-yr reservoir correction was applied based on correlation of pteropod data to shallow marine records showing similar variability from Makassar Strait (*Tierney et al., 2010*). Reservoir correction dates from other parts of the western Pacific show an average reservoir correction of ~318 years (*Reimer and Reimer, 2001).* The reservoir correction for Kau Bay is likely less than that for other open ocean areas in the region because water from below the surface layer is completely restricted from entering and interacting with the water within the basin. Furthermore, young carbon may be introduced from prominent rivers on Halmahera, in particular, the Kau River, that drains into Kau Bay. In addition, records from Makassar Strait cores used ^{210}Pb in addition to radiocarbon dating to more accurately determine the reservoir age of Indonesian surface water (*Tierney et al., 2010; Oppo et al., 2009*). This data suggests that a much younger reservoir correction should be applied in Kau Bay.

Table 3.2. Radiocarbon AMS data from NOSAMS for 102GGC and 103MC-F. The pteropod *Creseis acicula* was used for dating. Calendar ages were corrected using the Fairbanks0107 calibration curve following a 200-year reservoir correction (*Fairbanks et al., 2005).*

Core 102 GGC Depth (cm)	Age C-14 years	Age Error years	Calendar Ages 200 yr. Res. Corr.	Sedimentation rate (cm/100 years)	NOSAMS Accession #
20	690	30	519		OS-57842
40	805	35	594	26.67	OS-53225
72	1130	40	837	13.17	OS-50536
153	1520	30	1266	20.23	OS-57841
200	1790	40	1477	22.27	OS-53236
264	2120	35	1864	16.54	OS-53237
312	2400	30	2218	13.56	OS-53238
361	2600	30	2397	27.37	OS-57847
424	3460	35	3474	5.85	OS-50537
Core 103MC-F Depth (cm)	Age C-14 years	Age Error years	Calendar Ages 200 yr. Res. Corr.	Sedimentation rate (cm/100 years)	
18	165	30	-35		OS-59327
49	715	18	529	9.26	OS-59328

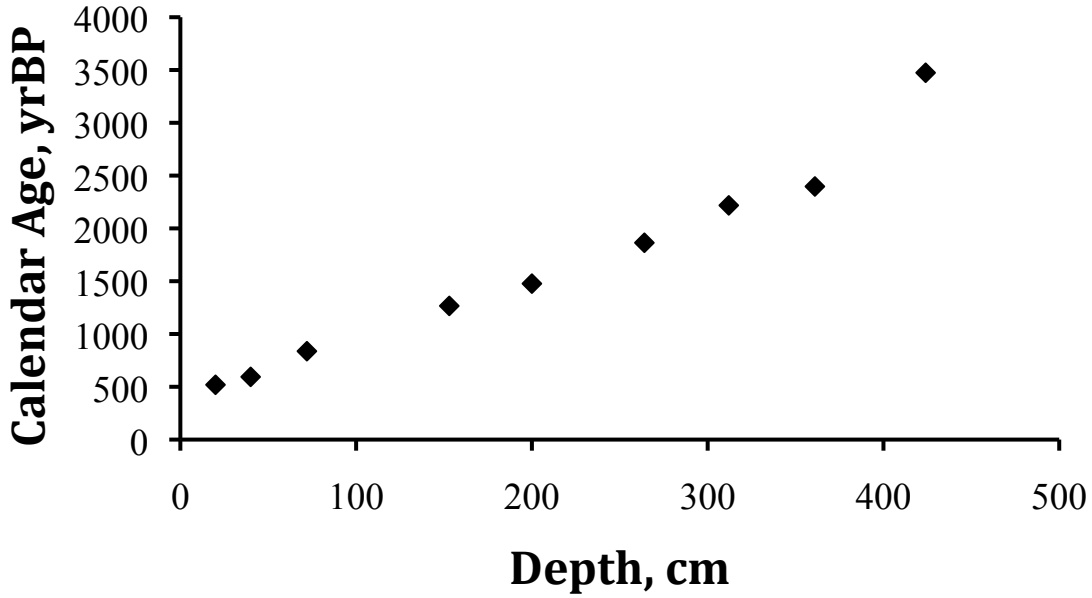

Figure 3.5. Depth vs. age plot for core 102GGC including a 200-year reservoir correction and ^{14}C calibration using Fairbanks0107 calibration curve (*Fairbanks et al., 2005)*.

The downcore dates in 102GGC revealed approximately linear sedimentation rates above 3.6m in the core near 200 cm/kyr with lower rates of 59cm/kyr from 3.6m to the core bottom at 4.2m. This depth-age relationship was applied to the depth-data using the Arand Ager software (*Howell et al., 2006*) and interpolating ages between depths with AMS ^{14}C dates. The top 17cm of 103MC-F did not contain enough whole pteropod shells for AMS radiocarbon dating, so the uppermost date was obtained from a depth of 18cm down core and contained bomb carbon.

2.2. $\delta^{18}O$ and $\delta^{13}C$ Isotope Ratio Mass Spectrometry

Sediment samples were collected as 1-cm-thick quarter rounds at 2cm intervals from core 102GGC and at ~3cm intervals from its companion on-ship slabbed multicore, 103MC-F. The average sampling resolution was ~17 years based on the current age

model. Whole pteropods were picked from the >150μm fraction of each sample and then each pteropod was individually cleaned with deionized water from a garden sprayer and dried in aluminum trays. Cleaned pteropods were analyzed on a VG Instruments Optima gas-source triple collecting mass spectrometer at the University at Albany. A total of 190 samples were analyzed from 102GGC, 25 samples were replicated, and 43 samples of the NBS-19 standard were interspersed. The average difference between replicates for $\delta^{13}C$ was 0.07‰ and the average difference between replicates for $\delta^{18}O$ was 0.058‰. The standard deviation for NBS-19 $\delta^{13}C$ was 0.019 and for $\delta^{18}O$ the standard deviation was 0.035. 16 samples were analyzed from 103MC-F at a resolution of ~3cm with a total of 2 replicates. The average replicate difference for $\delta^{13}C$ was 0.016‰ and the average difference for $\delta^{18}O$ was 0.113‰ (one sample had an error of 0.153‰ and the other had a difference of 0.072‰).

The $\delta^{18}O_{sw}$ record was generated from relating WPWP surface water temperatures determined from 50yr binned averages of Mg/Ca of G. ruber from cores 31MC and 34GGC from the Makassar Strait (*Oppo et al., 2009*) to 50yr binned averages of the 102GGC $\delta^{18}O$ of pteropod aragonite spanning the last 2,300yr. The following equation to relate the total aragonite $\delta^{18}O$ ($\delta^{18}O_a$) to temperature and the $\delta^{18}O$ of seawater ($\delta^{18}O_{sw}$) was determined in *Bohm et al., 2000:*

$$T = 20.0 - 4.42 * (\delta^{18}O_a - \delta^{18}O_{sw}) \quad (1)$$

$$\delta^{18}O_{sw} = -[(T - 20.0)/-4.42 - \delta^{18}O_a] \quad (2)$$

2.3. Sr/Ca ICP-MS

Inductively coupled plasma mass spectrometry (Element XR, ICP-MS) at Rutgers University was used to analyze Sr variability in pteropods from 102 GGC and its

companion multicore, 103MC-F, at 2cm intervals. ~500µg of deionized water-cleaned pteropods (~2-6 individual tests) from every 2cm of the gravity core and at about every 3cm from the multicore (see Age Model section under METHODS above) were broken into visible pieces. These samples were transferred into 5mL polypropylene microcentrifuge tubes that were acid washed in 20% reagent grade nitric acid.

Fine clay particles were removed by adding ~1mL of distilled H_2O into each tube and ultrasonicating for 1-2 minutes. More water was added to agitate the sample and mix the clay particles, then allowed to resettle. Nearly all of the water was siphoned off with a 1000µL Eppendorf pipet tip. This step was repeated three times with distilled H_2O and two times with methanol.

Metal oxides were removed through a reducing procedure. 100µL of 3.75% anhydrous hydrazine in a solution of half NH_4OH and half 5% citric acid in NH_3 solution were added to each sample vial. The vials were placed into a hot bath of distilled H_2O at 80-90˚C for 30 minutes and then briefly ultrasonicated every 2 minutes. The reagent was then siphoned off from the samples and the samples were once again rinsed with deionized H_2O three times.

Organic matter was removed from the samples using an oxidizing procedure. 250µL of 33% H_2O_2 in 0.1N NaOH solution was added to each sample, which were then heated in a bath of distilled water at ~80-90˚C for 5 minutes, followed by briefly ultrasonicating the samples. This step was repeated once more and the samples were transferred into clean, acid-leached microcentrifuge vials.

A weak acid leach followed the oxidation by adding 100µL 0.001 HNO_3 to each sample. The samples were ultrasonicated for 30 seconds and then allowed to settle for ~1

minute. The nitric acid was siphoned off and this step was repeated 4 times. The entire samples were then dissolved in 300µL of 0.5 HNO3 and ultrasonicated for about 5 minutes. These samples were then centrifuged for 5 minutes before being analyzed in the ICP-MS.

3. RESULTS AND DISCUSSION

3.1. *Creseis acicula* $\delta^{18}O$, $\delta^{13}C$, and Sr/Ca variability in Kau Bay

The *C. acicula* $\delta^{13}C$, $\delta^{18}O$, $\delta^{18}O_{sw}$, and Sr/Ca data are shown in figure 3.6. These records were compared to various records of similar resolution from different Pacific Basin and East Asian locations in order evaluate the regional climatic significance of the results. Records with similar resolution were available from the EEP and the EAM regions, which allowed comparisons between Kau Bay pteropod chemistry and paleo-records thought to reflect changes in the EAM and ENSO.

Below the thermocline in Kau Bay, temperature and salinity are relatively constant reflecting the ~30m sill depth (figure 3.3). The salinity and temperature profiles measured in Kau Bay's water column in 1930, 1985, and 2003 do not vary significantly as the oxygen profiles do. Temperature and salinity vary from around 28-28.5˚C and 33.5-34.5p.s.u., respectively (figure 3.3). Changes in temperature and salinity appear to affect only the mixed layer, which reaches down to ~150m depth. This suggests that flushing of the basin with water from the Pacific does not have a lasting effect on the water column temperature and salinity like it does with oxygen. Salinity is increased and temperature is diminished when cold and salty water is able to break the threshold over Kau Bay's shallow sill, for instance, during the northwest monsoon, when saltier water

may be brought to the area of Halmahera by the NGCC (figure 3.4). In turn, salinity decreases and temperature may increase when the WPWP is warmer and there is increased precipitation.

Increased rainfall reduces the $\delta^{18}O$ of precipitation through Rayleigh fractionation and also lowers surface water salinity and $\delta^{18}O$. Near the equator the relationship between salinity and $\delta^{18}O_{sw}$ is approximately is ~0.27‰ per 1.0 p.s.u. (e.g., *Fairbanks et al., 1997*), Kau Bay rainfall is currently affected by interannual ENSO-related variability (*Aldrian and Susanto, 2003*). It is unclear what forces rainfall variability at decadal-scale frequency and less in this region, the reconstruction of which is one of the goals of analyzing the sediment record in Kay Bay.

In an enclosed basin, such as Kau Bay, surrounded on three sides by mountainous tropical jungle, surface water $\delta^{18}O$ could be tightly coupled to regional hydrology and river discharge. Meanwhile, Kau Bay SSTs are currently >28˚C. If we assume that SST in Kau Bay has remained relatively constant near ~28˚C, then the $\delta^{18}O$ variability recorded by the pteropod shells should predominantly reflect changes in the hydrology of Kau Bay and the WPWP. Support for this conclusion comes from the magnitude of downcore pteropod $\delta^{18}O$ and $\delta^{18}O_{sw}$ variability in 102GGC. From BC 500 to AD 500, pteropod $\delta^{18}O$ became more enriched in ^{18}O by ~0.8‰ (figure 3.6). If this were all due to water temperature, it would indicate that the mixed layer in Kau Bay cooled ~3˚ since BC 500. Put another way, the water column, which is now 28.5˚C below the thermocline to the bottom, would be unrealistically warmer (~32˚C) 2,500 years ago. Meanwhile, Kau Bay $\delta^{18}O_{sw}$ calculated using SST derived from Mg/Ca of *G. ruber* from Makassar

Strait in the WPWP for the last 2,500yr shows a 9‰ increase in $\delta^{18}O_{sw}$ (*Oppo et al., 2009*), which suggests an overall decrease in rainfall.

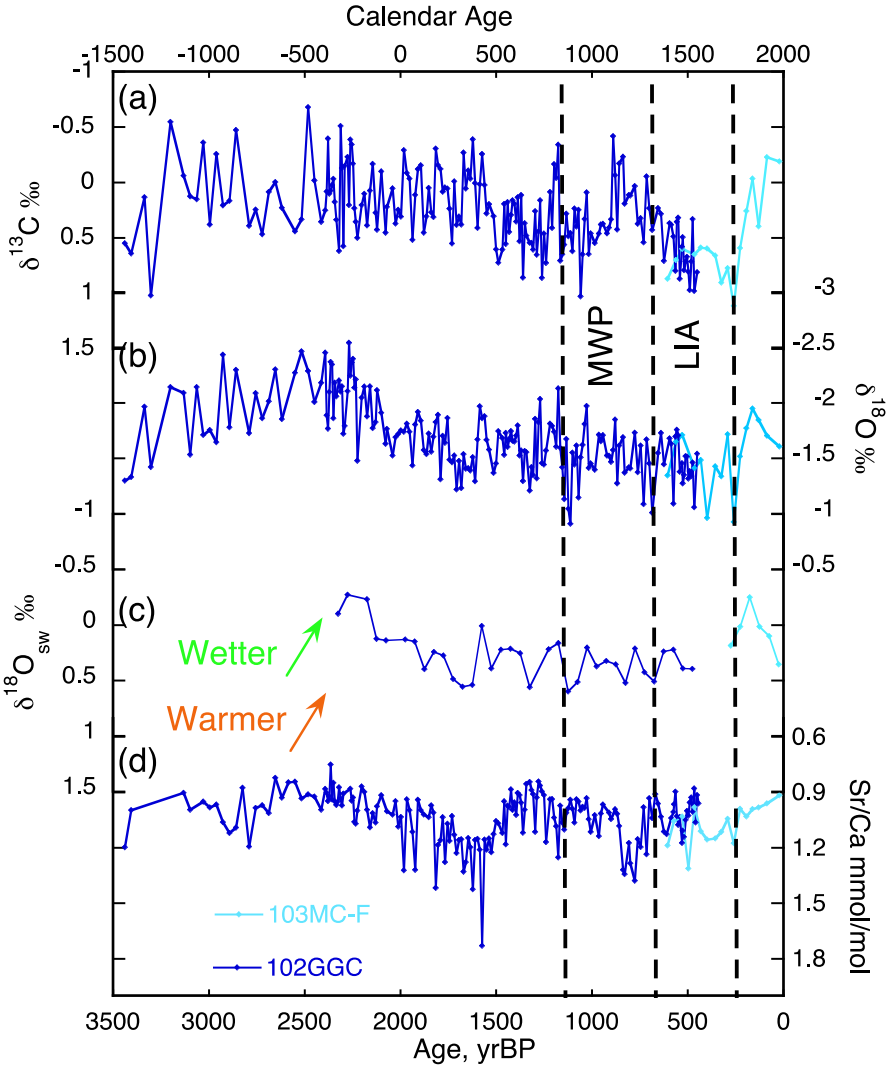

Figure 3.6. Data from Kau Bay cores 103MC-F and 102GGC. (a) *C. acicula* $\delta^{13}C$; (b) *C. acicula* $\delta^{18}O$, (c) $\delta^{18}O_{sw}$ generated from 50yr binned averages of SST from 31MC and 34GGC (*Oppo et al., 2009*) and *C. acicula* $\delta^{18}O$ (d) *C. acicula* Sr/Ca.

$\delta^{13}C$ of pteropods has been correlated to the carbonate ion concentration in water, which is related to changes in alkalinity within the surface water (*Juranek et al., 2003; Chou et al., 2007*). Alkalinity is affected by surface water salinity, pH, and DIC, so pteropod $\delta^{13}C$ must reflect these parameters to some extent since it inversely correlates to water column DIC (*Juranek et al., 2003; Bates et al., 1996*). Although pteropods can calcify their shells vertically throughout the water column, Kau Bay's entire water column salinity and temperature is homogenous and also reflects the salinity and temperature of the surface water outside the basin, above the ~30m sill depth. Both the $\delta^{13}C$ and $\delta^{18}O$ reached minima at BC 500 and have steadily become more enriched since that time, reflecting a trend towards dryer conditions (figure 3.6). Kau Bay water temperature generally reflects surface water in the WPWP, which has been shown to not vary more than 1˚C during the last 3,500yr based on foraminifera Mg/Ca results (*Oppo et al., 2009; Linsley et al., 2010*). The variability seen in Kau Bay pteropod $\delta^{13}C$ and $\delta^{18}O$ records has a distinct positive correlation throughout much of the record. Since the pteropod $\delta^{13}C$ is controlled mainly by alkalinity in Kau Bay, which is directly related to salinity, the generally positive correlations between pteropod $\delta^{13}C$ and $\delta^{18}O$ throughout the record may reflect changes in salinity.

Overall, *C. acicula* $\delta^{18}O$ varied as much as 1.2 to 1.5‰ from BC 500 until AD 1850 (figure 3.6). This would suggest an overall temperature decrease of ~5 to 6˚C (*Grossman and Ku, 1986*). Since such a large surface water temperature change is highly implausible over this time period (see Figure 3.3 and WPWP lateral SST gradients), there must have been significant changes in the salinity of Kau Bay assuming that only temperature and $\delta^{18}O_{sw}$ control *C. acicula* $\delta^{18}O$ in Kau Bay. The *C. acicula* $\delta^{18}O$ is most

depleted from BC 500 to AD 0. During this period of time, it is possible that there was an increase in precipitation in the central WPWP, however, this change is not reflected in the *C. acicula* $\delta^{13}C$ record. Algal and plant wax compound-specific abundances showed that Kau Bay experienced a decrease in terrestrial influence after AD 0 (*Langton et al., 2008*), which would have led to a DIC source change.

Although we lack a *C. acicula* Sr/Ca- SST calibration, the fact that the *C. acicula* Sr/Ca record correlates with the *C. acicula* $\delta^{18}O$ from BC 500 to AD 400 may indicate that pteropod $\delta^{18}O$ was affected by changes in temperature during this time. If downcore *C. acicula* Sr/Ca variability is due to water temperature, then there was a maximum temperature in Kau Bay near BC 400, which was also during a period of maximum precipitation according to the *C. acicula* $\delta^{18}O$ and the $\delta^{18}O_{sw}$ records. The Sr/Ca record possibly reflects a reduction in surface water temperature from BC 500 to AD 400, concordant with an increase in salinity according to the *C. acicula* $\delta^{18}O$ record. The Sr/Ca rapidly dropped from 1.8mmol/mol at AD 400 to 0.8mmol/mol at AD 600. Lower Sr/Ca, and possibly elevated surface water temperature at AD 700, matches minima in both the $\delta^{18}O$ and $\delta^{13}C$ records, which relay periods of increased surface water temperature and precipitation. Overall, the $\delta^{18}O$ and Sr/Ca records convey a trend of increasing surface water temperature from AD 1700 to present.

3.2. Kau Bay and the East Asian Summer Monsoon

The relative strength of the East Asian Summer Monsoon (EASM) over the last ~9ka has been interpreted from Dongge Cave stalagmite DA (*Wang et al., 2005*). Overall, speleothem records from the EASM region in China show that the EASM has

gotten progressively weaker over the last ~3,000yr (*Hu et al., 2008*). In order to more clearly evaluate the general multi-decadal influence of the EASM on the Kau Bay *C. acicula* records, the $\delta^{18}O$ record of stalagmite DA averaged at 50 yr intervals was compared to the Kau Bay $\delta^{18}O_{sw}$ record and $\delta^{18}O_{sw}$ records from Makassar Strait, derived from $\delta^{18}O$ and Mg/Ca from the foraminifer *Globigerinoides ruber* from cores MD9821-60 (*Newton et al., 2006*), BJ8-03 31MC and 34GGC. The Makassar Strait $\delta^{18}O_{sw}$ records are highly correlated to EASM variability (*Oppo et al., 2009*).

At this resolution, the Dongge Cave $\delta^{18}O$ record correlates in some intervals with Kau d18O. The enrichment in our estimated $\delta^{18}O_{sw}$ from Kau Bay (using paleo-SST data from the Makassar St.) corresponds to an enrichment in $\delta^{18}O$ from the Dongge Cave from BC 500 to AD 500, a time period interpreted to have had a weakened EASM. The Dongge Cave record also showed a strengthening of the EASM towards the conclusion of the LIA, which corresponds to reductions in $\delta^{18}O_{sw}$ from Kau Bay, or increased aridity from a weakened IM. Peaks in precipitation seen in both the Kau Bay and the Makassar Strait records from AD 500-1000, reflecting increased IM precipitation, occurred simultaneously when the Dongge Cave record reflected a period of reduced EASM. The MWP in both the Makassar Strait and Kau Bay records were characterized by relatively enriched $\delta^{18}O_{sw}$ presumably due to decreased mean annual precipitation. The most recent segment of these records suggests increased aridity and a reduction in the EASM similar to levels experienced during the MWP. Overall, the comparison of the Kau Bay $\delta^{18}O_{sw}$ to other EASM records shows that the EASM does exert some control over the hydrology of Kau Bay and this is reflected in pteropod shell $\delta^{18}O$.

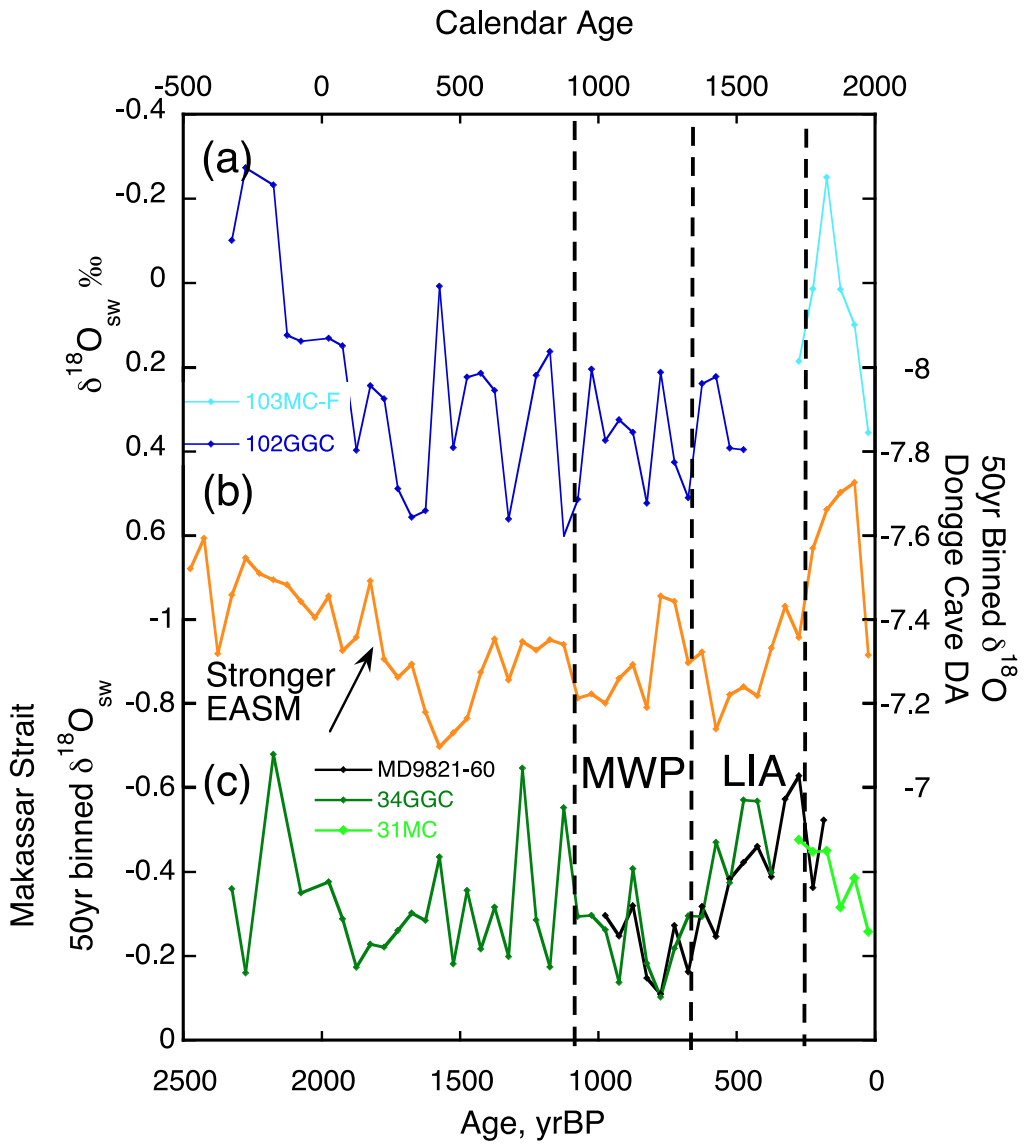

Figure 3.7. (a) Kau Bay cores 102GGC and 103MC-F $\delta^{18}O_{sw}$, (b) 50yr binned averages from $\delta^{18}O$ of Dongge Cave speleothem DA (*Wang et al., 2005*), and (c) 50yr binned averages of $\delta^{18}O_{sw}$ from Makassar Strait cores MD9821-60, 34GGC and 31MC (*Newton et al., 2006; Oppo et al., 2009*). Approximate timing of the MWP and LIA are shown.

3.3. Comparison to Eastern Equatorial Pacific

In order to determine the zonal relevance of the records from Kau Bay, comparisons were made to climate records from the EEP. Interestingly, the Kau Bay pteropod Sr/Ca record shows similarities to records that have been interpreted to reflect ENSO variability such as the El Junco Lake (Galápagos islands) down-core % sand (>63μm) fraction (*Conroy et al., 2008*), and a record of flood events from Laguna Pallcacocha, Ecuador (*Moy et al., 2002*; figure 3.8). Distinct maxima in the Kau Bay pteropod Sr/Ca record occur at AD 1500, 1100, 750, 500, and BC 800. These increases in pteropod Sr/Ca, probably due to cooling of Kau Bay, correspond to increases in % sand size fraction in El Junco (figure 3.8). Minima in the Sr/Ca record occur from BC 750 to 300 and AD 600 and 1000. These periods were possibly warmer in Kau Bay and more La Niña-like as they correspond to periods of less frequent or intense flooding in both El Junco and Laguna Pallcacocha. El Junco is in the Niño 1.2 region and elevated grain size deposition occurs during times of increased precipitation as periodically occur during El Niño events today.

The record of grain size variability from El Junco Lake over the last 3,000 years suggests that century-scale changes in rainfall have occurred in the Galápagos possibly related to El Niño recurrence interval. Meanwhile, red color intensity units from Laguna Pallcacocha, Ecuador, represent clastic sediment laminae deposited during periods of intense flooding during intense El Niño episodes (*Moy et al., 2002*). Kau Bay is located in the western Pacific region that experiences the opposite effects during El Niño with cooler and dryer conditions (figure 3.9). We previously asserted that Kau Bay water temperature can be reduced when colder water from the NGCC is able to flush the basin,

which is more likely to occur during strong El Niño events, when the NGCC flows in a northwestern direction throughout the year due to slackened trade winds and a shallow thermocline in the WPWP (*Langton et al., 2008*). If pteropod Sr/Ca is inversely correlated with temperature (as in corals, and as also discussed above), then it is possible that the changes in Sr/Ca indicate century-scale changes in Kau Bay temperatures over the last 3,000 years. The noted similarities between our Kau Bay results and ENSO related proxy records in the EEP indicates that these changes were potentially driven by El Niño activity per century. It is also possible that changes in the mean WPWP SST state are responsible for Kau Bay upper thermocline and mixed layer temperature variability and/or that changes in El Niño frequency influenced mean upper water column temperatures in Kau Bay.

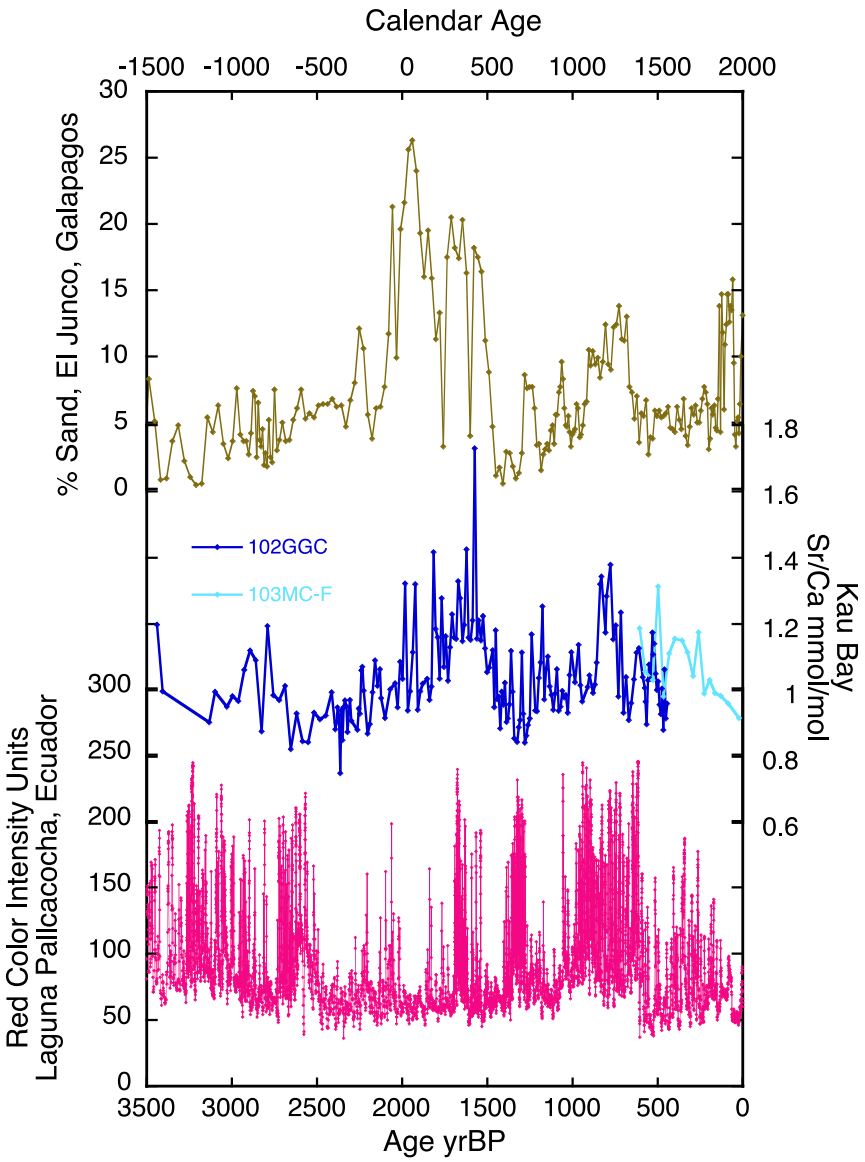

Figure 3.8. % sand from El Junco Lake, Galápagos (top, *Conroy et al., 2008*), Kau Bay *C. acicula* Sr/Ca (center), and the red color intensity bands from Laguna Pallcacocha, Ecuador (bottom, *Moy et al., 2002*).

Whereas the Kau Bay nitrogen isotope record in *Langton et al. (2008)* was interpreted to reflect changes in basin flushing, the higher temporal resolution Kau Bay pteropod $\delta^{18}O$ and Sr/Ca records likely display more subtle and higher resolution changes (figure 3.7). This is apparently because larger, basin-wide changes are necessary in order

to either establish or prohibit the biological processes that would result in a great enough shift in the nitrogen isotope record to become stored in the sediments. Meanwhile, pteropods probably live throughout the water column and the isotopic changes within their shells are more directly a result of hydrological and temperature changes.

The nitrogen isotope record from Kau Bay presented by *Langton et al. (2008)* suggests that down-core variations in bulk sedimentary $\delta^{15}N$ reflect century-scale alternations between basin ventilation and stagnation during this period. *Langton et al. (2008)* interpreted downcore increases in $\delta^{15}N$ as a consequence of increased basin flushing during periods of more frequent/intense El Niño events or a more El Niño-like mean state in the WPWP. Increased basin flushing during El Niño events, or times of more frequent El Niño activity, results from a shallower thermocline in the WPWP bringing water with higher $\delta^{15}N$ into the basin. Lower $\delta^{15}N$ reflects basin stagnation and reduced flushing during periods of fewer/weaker El Niño events or less El Niño-like conditions, when denitrification removes most of the nitrate pool, prompting intensified nitrogen fixation and an overall reduction in $\delta^{15}N$.

In Kau Bay, a broad $\delta^{15}N$ maximum occurred between AD 300 and 700, and then again between AD 1200 and 1400 (figure 3.9). These intervals of relatively enriched ^{15}N are similar in timing to distinct maxima in the Kau Bay pteropod Sr/Ca record and probably reflect increased basin flushing. These intervals of inferred Kau Bay flushing are also times of maxima δD (in the organic fraction) in Makassar Strait cores 31MC and 34GGC (*Tierney et al., 2010*) and % sand maxima in El Junco Lake (figure 3.9, *Conroy et al., 2008*). These geochemical records on opposite sides of the Pacific may indicate

similar variability in the state of the equatorial Pacific over the last 2,000 years and suggest a coherent zonal response in the Pacific basin.

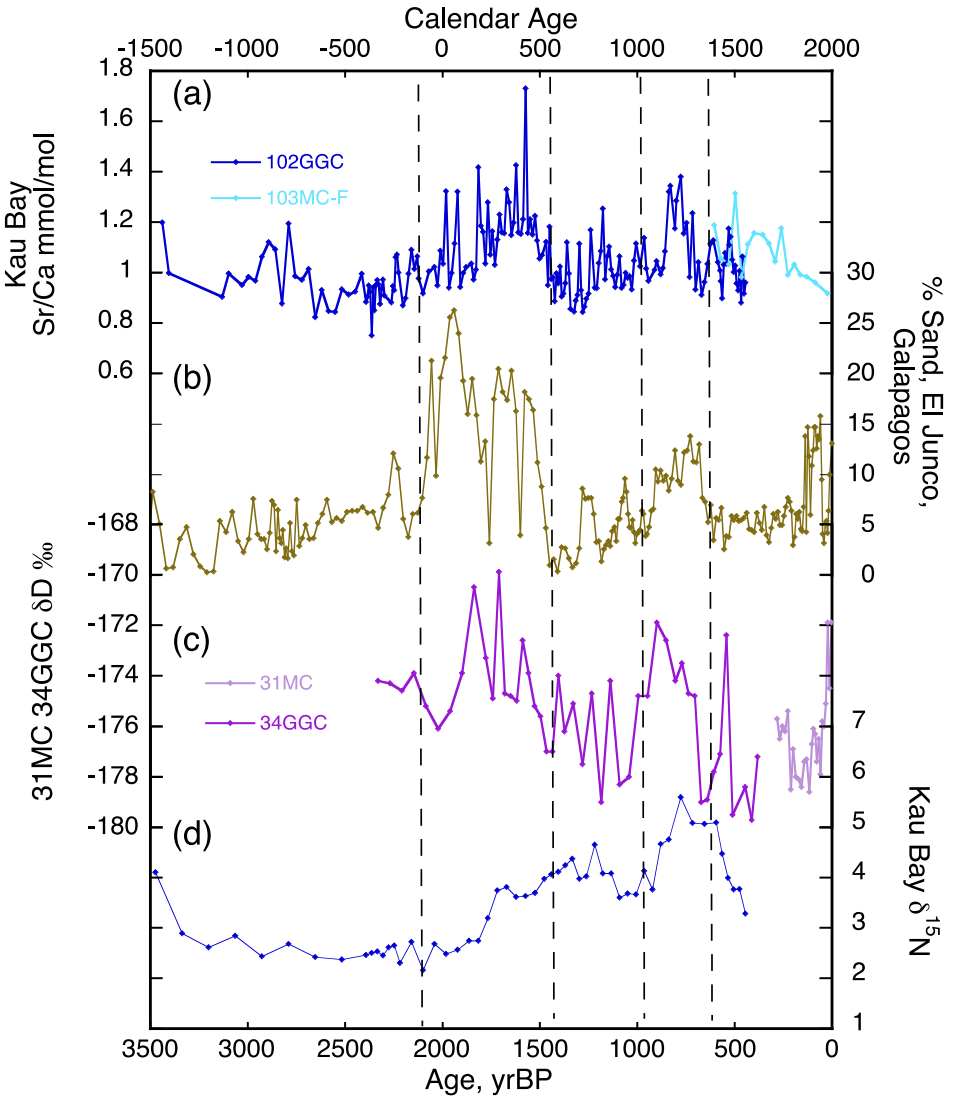

Figure 3.9. (a) Kau Bay *C. acicula* Sr/Ca, (b) El Junco % sand record (*Conroy et al., 2008*), (c) Makassar Strait δD (*Tierney et al., 2010*), and (d) Kau Bay $\delta^{15}N$ (*Langton et al., 2008*). Dashed lines outline similarities between the records.

4. CONCLUSIONS

The following conclusions were made from the analysis of down-core variability of $\delta^{18}O$, $\delta^{13}C$, and Sr/Ca in the pteropod *Creseis acicula* from Kau Bay sediments:

1) The pteropod, *C. acicula*, may be used in paleoclimate reconstructions within Kau Bay. Kau Bay's unique setting accommodates the use of pteropod shells as markers for the surface water from the WPWP because of its homogenous water column that reflect properties of the upper 30m of surface water from the WPWP. Therefore, regardless of where the pteropods reside within the water column, in Kau Bay their shells will reflect the properties of the upper WPWP surface water. Pteropod $\delta^{13}C$, $\delta^{18}O$, and Sr/Ca clearly reflect similar parameters, particularly during the last 1,600yr, and are likely reflecting temperature and salinity change in the surface water of the central WPWP after that time.

In addition, this study implicates that pteropods may have an extended use in global basins that display similar hydrography to Kau Bay, for instance, in basins that are characteristically homogeneous in temperature and salinity. Pteropod shells may be used in paleoclimate studies in order to decipher past change in $\delta^{18}O_{sw}$ and possibly to show variability in basin alkalinity and temperature through time.

2) The EASM probably affects Kau Bay $\delta^{18}O_{sw}$ by modulating precipitation in the WPWP as seen through the relationship between various records that display hydrologic variability throughout the late Holocene in the WPWP. This rainfall signal appears to be amplified by the hydrologic configuration of the Halmahera drainages feeding fresh water into Kau Bay.

3) The Kau Bay pteropod records suggest that century-scale changes in late Holocene zonal dynamics may have a strong effect on the WPWP and, therefore, global climate. The zonal dynamics may have been caused by low-resolution patterns in ENSO, long-term shifts in the mean position of the ITCZ, or a combination of the two.

Chapter 4

Glacial-Interglacial changes in stratification of the Sulu Sea mixed layer and upper thermocline

ABSTRACT

The Sulu Sea is a deep and poorly ventilated silled basin located in the western region of the Western Pacific Warm Pool. The basin is ~5,580m deep with main ventilating sills ranging in depth from 340m to 570m. Today, East Asian monsoon strength affects oceanographic conditions that, in part, control changes in the mixed layer depth in the Sulu Sea. On glacial-interglacial time scales, ventilation into the basin would have been controlled by changes in sea level and density differences between water from the intruding South China Sea and the Sulawesi Sea. In order to assess these changes on glacial-interglacial time scales, the $\delta^{18}O$ of two upper thermocline dwelling foraminifera, *Neogloboquadrina dutertrei* and *Pulleniatina obliquiloculata*, were analyzed and compared to previous analyses of *Globigerinoides ruber* from core site ODP 769 over the past ~800,000 years. The difference between the shallow and deeper dwelling planktonic foraminifera $\delta^{18}O$ were calculated to assess the stratification of the mixed layer to the upper thermocline on glacial-interglacial timescales. Most of the interglacial stages over this time period were characterized by significant differences (>1‰) between the $\delta^{18}O$ of the shallow and deeper dwelling foraminifera, which we interpret as evidence of a shallower mixed layer and thermocline, while glacial stages had reduced differences indicative of a deeper mixed layer. The deep mixing of the Sulu Sea during glacial stages confirms the increased intensity of the winter monsoon (*Beaufort et al., 2003*), which

brings cold northeasterly winds towards the WPWP, while the freshening of the mixed layer and shallower thermocline during interglacial stages argues for extremely intensified atmospheric convection as a result of increased summer monsoon with a concomitant decrease in winter monsoonal strength.

1. INTRODUCTION

1.1. Geographic and Oceanographic Setting

The Sulu Sea is a poorly ventilated, 5,580m deep basin (*Wang, 1999*) located within the WPWP (Figure 4.1). The average depth of the mixed layer is currently ~30m (*Wyrtki, 1961*). This basin is surrounded by very shallow shelves and contains ventilation passageways from the South China Sea and the Sulawesi Sea, through the Mindoro Strait [sill depth = 570 (*Gordon, unpublished data*, measurements from off the coast of Panay) or 420m according to *Wyrtki, 1961*] and the Sibutu Strait (sill depth = 340m), respectively (*Wyrtki, 1961*). The ventilation of this basin throughout geologic history is not entirely understood. However, there are clues that link the Sulu Sea's ventilation to regional climate change.

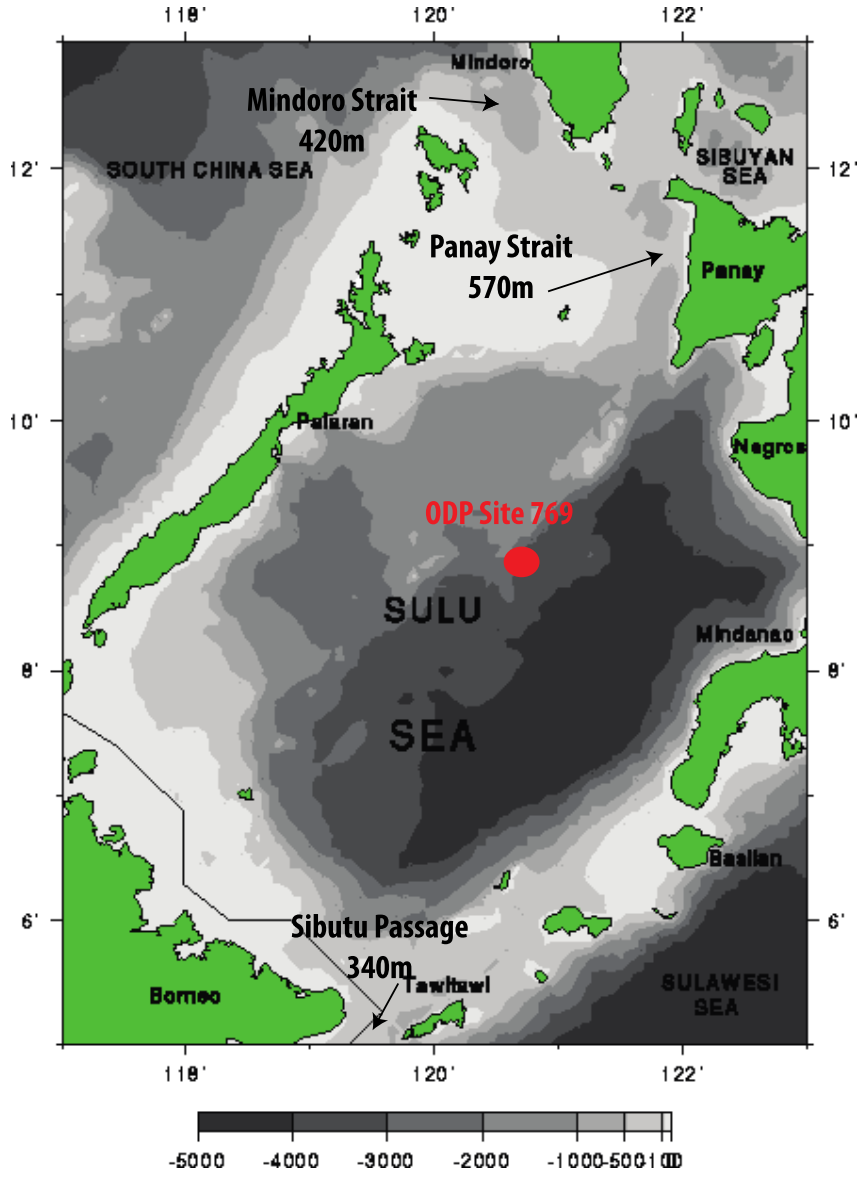

Figure 4.1. Map of the Sulu Sea with bathymetry contours (http://stommel.tamu.edu/~baum/paleo/seamaps/sulu-sea-c.gif). ODP Site 769, 8° 47'N, 121° 17'E, is shown.

In the Sulu Sea, water ventilation depends on its interaction with bordering bodies of water (*Frische and Quadfasel*, *1990*; *Quadfasel et al., 1990; Gamo et al., 2007*). In this respect, the Sulu Sea does not form its own bottom water and relies upon lower thermocline water from surrounding basins for ventilation. If bottom water dissolved

oxygen within a basin is not replenished at a rate greater than the rate of oxygen consumption, it will become anoxic. Although the Sulu Sea is hypoxic today, it remains unclear as to whether the basin was completely anoxic at any depth over the last ~2.4Ma (*Gamo et al., 2007; Wyrtki, 1961*).

The ventilation of the Sulu Sea is greatly affected by the East Asian Monsoon (EAM) and possibly ENSO because of the effect these systems have on rainfall and salinity within the basin (figure 4.2). The summer monsoon occurs from May to November (figure 4.3). Precipitation in the Sulu Sea is greatest during this time and salinity is lowest. The ITCZ is in its southernmost location by November. During this time, the East Asian monsoon merges with Pacific trade winds over the South China Sea (*Beaufort et al., 2003*). Sulu Sea salinity is reduced because of southerly winds that force the flow of fresher water from the South China Sea (*Wyrtki, 1961; Oppo et al., 2003*). Surface salinity reaches its maximum during June, when the summer monsoon causes the water to flow from the Sulawesi Sea located to the southeast. Overall, the change in the intensity of the precipitation during the winter EAM as well as changes in the mean state of ENSO may have appreciable affects on the ventilation, salinity, and temperature of the Sulu Sea and this is likely reflected in various geochemical proxies. The stratification of the surface water and thermocline may be affected by the EAM and the mean state of ENSO by changes in wind stress that might affect the source of surface water into the Sulu Sea and by moderating the amount of precipitation in the WEP. For example, diminished summer monsoon strength in combination with increased winter monsoon strength may result in a deeper mixed layer due to increased wind stress and mixing,

whereas increased summer monsoon intensity may result in more stratified surface waters due to increased precipitation in the upper mixed layer and reduced mixing.

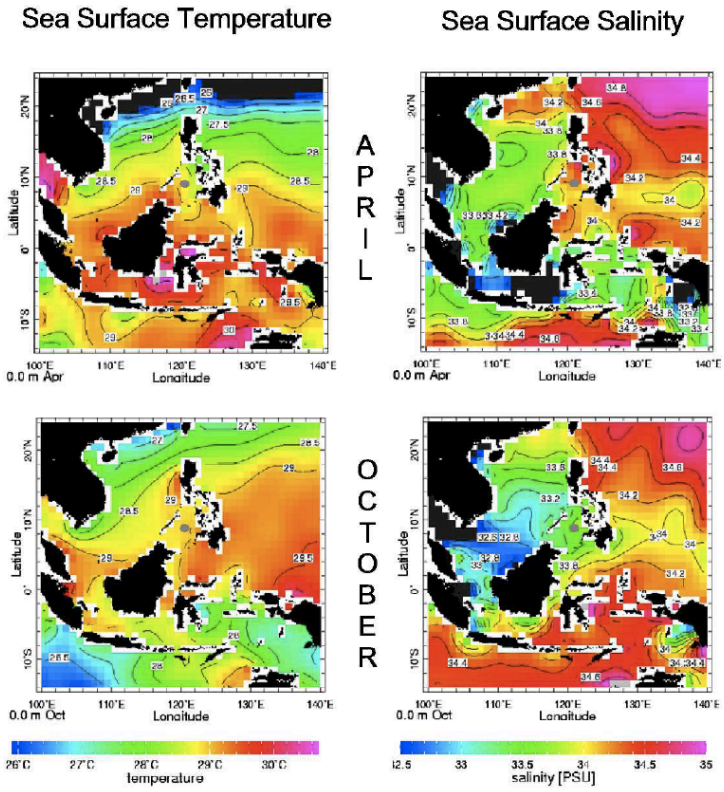

Figure 4.2. Average surface temperature and salinity from the Indo-Pacific during the end of the winter monsoon (top panels) and the end of the summer monsoon (lower panels) (modified from *Dannenmann et al., 2003*).

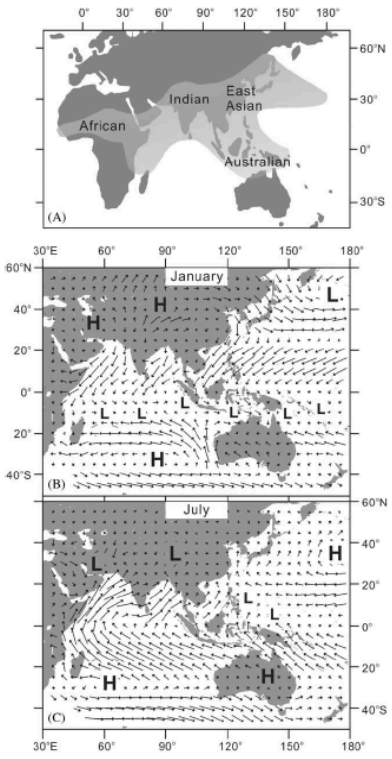

Figure 4.3. (A) Monsoonal regions in East Asia, India, Africa, and Australia. (B) Surface wind pressure during winter. (C) Surface wind pressure during summer (*Wang et al., 2005*).

1.2. Previous Research in the Sulu Sea

The Sulu Sea contains well-preserved carbonate sediments due to its isolation, relatively warm bottom water and deep carbonate lysocline (*Wyrtki, 1961; Linsley et al., 1985; Linsley and Thunell, 1990*). Long and undisturbed records have been recovered from the Sulu Sea, which have provided insight into WPWP climate variability. Previous paleoclimate research in the Sulu Sea has focused on SST and salinity variability of the surface water (*Linsley and Thunell, 1990; Linsley and von Breymann 1991; Linsley, 1996; Oppo et al., 2003; Rosenthal et al., 2003, Dannenmann et al., 2003*).

ODP Site 769 was previously dated by radiocarbon, oxygen isotope stratigraphy, and paleomagnetic reversal methods and extends back to ~4 m.y. (*Linsley and von Breymann 1991, Linsley 1991; Linsley, 1996*). The entire Pliocene record of the core is devoid of carbonates, which first appear at ~2.47Ma, at the Gauss-Matuyama

paleomagnetic boundary. This is concomitant with the onset of the Pleistocene Glaciation (*Linsley, 1991*). It is apparent that glacial-interglacial climate variability affects primary productivity and the deposition of calcium carbonate in the Sulu Sea (*Beaufort et al., 2003; Garidel-Thoron et al., 2001; Linsley, 1991*). *Linsley* (*1996*) presented a record of surface water $\delta^{18}O$ from planktonic foraminifera (*Globeriginoides ruber*) at millennial resolution for the last 150kyr. This record correlates with the glacial-interglacial changes in climate resolved from the GRIP and Antarctic ice cores. In addition, primary productivity in the Sulu Sea was measured using coccolithophorid assemblages to assess East Asian winter monsoon strength, which appears to control winter monsoon dynamics on orbital-sale cycles (*Beaufort et al., 2003*). Higher frequency (20kyr-10kyr) cycles appear to be in the inverse phase to records from the eastern Pacific, which convey an ENSO-like mechanism controlling the East Asian summer monsoon dynamics.

While the $\delta^{18}O_{G.ruber}$ record alone did not fully explain what was causing the variability of the $\delta^{18}O$ in the Sulu Sea, the addition of high-resolution records of *G. ruber* $\delta^{18}O$ with Mg/Ca SST from Sulu Sea core MD97-2141 revealed a possible explanation (*Rosenthal et al., 2003*). The Mg/Ca record showed that Sulu Sea SST was ~2.3˚ C cooler and the mixed layer fresher during the LGM than at present. The freshening of the Sulu Sea during the LGM corresponded to a freshening of the South China Sea that resulted in depleted foraminifera $\delta^{18}O$ in the Sulu Sea even as the surface temperature was reduced (*Oppo et al., 2003*; *Rosenthal et al., 2003; Pelejero et al., 1999*). Meanwhile, other WEP records displayed increasing salinity and diminished SST during the LGM, which construes decreased precipitation alongside a decrease in the total zonal

gradient of SST in the region, for example, along the Ontong Java Plateau and in the central equatorial Pacific (*Lea et al., 2000*; *Lyle et al., 1992*). The surface water $\delta^{18}O$ records from the Sulu Sea were probably influenced primarily by hydraulic controls and that the source of surface water was in the South China Sea, which had an identical $\delta^{18}O$ signature (*Rosenthal et al., 2003*).

On glacial-interglacial time scales, lower sea level during the LGM in addition to decreased summer monsoon intensity led to a greater proportion of inflow from the South China Sea to the Sulu Sea (*Oppo et al., 2003; Dannenmann et al., 2003*). *Shintani et al. (2008*) used alkenone-derived SSTs to determine that the SST difference between the Sulu Sea and the South China Sea was diminished during the LGM, which suggests that the Sulu Sea follows a similar SST trend to the South China Sea during interglacials than during glacials due to the increased strength of the winter monsoon during glacials. Holocene $\delta^{18}O_{G.\ ruber}$ values from the Sulu Sea reflect a greater influence from the Sulawesi Sea as compared to glacial values, which are closest in value to those of the South China Sea (*Oppo et al., 2003; Rosenthal et al., 2003; Wang et al., 2001; Lea et al., 2000*). On suborbital timescales of ~4-10kyr, the Sulu Sea is fresher during warmer periods, as ice volume does not exert as much influence (*Oppo et al., 2003*). It is uncertain whether ENSO or high-latitude climate may affect the Sulu Sea at this resolution.

Changes in thermocline depth and circulation of surface water between the Sulu Sea, the Sulawesi Sea, and the South China Sea remains unresolved on glacial-interglacial timescales. To attempt to directly address these questions, this study focused on the determination of glacial/interglacial changes in the mixed layer and thermocline

depth in the Sulu Sea by comparing $\delta^{18}O$ of mixed layer- and thermocline-dwelling foraminifera. The contrast in $\delta^{18}O$ between shallow- and deep-dwelling foraminifera reflects sharp temperature and/or salinity differences between the mixed layer and upper thermocline (*Lin et al., 2007*). This study will discuss how this depth is related to changes in the strength of the EAM and the flow of surface and mixed layer water between the Sulu Sea and neighboring seas through the Mindoro Strait, the Sibutu Strait, and other shallow openings.

2. METHODS

The initial sampling procedures for $\delta^{18}O$ of *Globigerinoides ruber* and age model determinations for site ODP 769 were explained in *Linsley and Dunbar, 1994*. Samples were previously obtained from the top 65m of this core at 20cm intervals. Each sample was wet-sieved to remove the fine (<63μm) fraction. *G. ruber* was initially picked from the coarse fraction of these samples within the size range of 150-350μm for $\delta^{18}O$ and $\delta^{13}C$ analyses. *N. dutertrei* was occasionally used in place of *G. ruber* at intervals where *G. ruber* tests were insufficient for stable isotope analyses (see *Linsley and Dunbar 1994*). These samples were normalized to estimate *G. ruber* $\delta^{18}O$ values given an average *N. dutertrei* enrichment of ~1.09‰ (+/- 0.21‰) (*Linsley and Dunbar 1994*).

For this current study, *Pulleniatina obliquiloculata* and *Neogloboquadrina dutertrei* were picked from the >150μm size fraction. No additional cleaning procedures were performed as these foraminifera were visibly free of clay and/or organic material. $\delta^{18}O$ from *P. obliquiloculata* and *N. dutertrei* were analyzed at a resolution of ~0.3-0.4m at glacial-interglacial (G-I) time scales from ODP 769A at the SUNY Albany isotope

ratio mass spectrometer laboratory on a Micromass Optima triple collecting mass spectrometer with replicates run every 5-10 samples. Approximately 10 tests were analyzed for each sample. 62 analyses of standard NBS-19 were run in between samples with a standard deviation of 0.014‰ for $\delta^{13}C$ and 0.029‰ for $\delta^{18}O$. The average difference of $\delta^{18}O$ replicates was 0.21‰ for *P. obliquiloculata* (n=21) and 0.17‰ for *N. dutertrei* (n=19).

3. RESULTS AND DISCUSSION

The depth habitats of planktonic foraminifera may cover a large vertical scope, but calcification takes place over a much more narrow range for many species (e.g., *Ravelo and Fairbanks, 1982; Lin et al., 2011*). The $\delta^{18}O$ of a mixed-layer dwelling foraminifera in the South China Sea, such as *G. ruber*, is clearly more depleted than that of thermocline dwellers, such as *N. dutertrei* and *P. obliquiloculata* (*Lin et al., 2011*). Therefore, the difference between the $\delta^{18}O$ of these foraminifera over periods of time has the potential to show changes in the depth of the mixed layer. *P. obliquiloculata* appears to preferentially follow the temperature range of ~24-25˚C within the lower mixed layer to the upper thermocline (*Lin and Hsieh, 2007; Pflaumann and Jian, 1999*). Given the $\delta^{18}O$ range of *N. dutertrei* from this and other studies, this foraminifer calicifies at a similar depth as *P. obliquiloculata* (*Lin and Hsieh, 2007*). In the South China Sea, *G. ruber* demonstrated the most narrow depth migration range of these three foraminifera and globally calcifies within the upper 30-60m of surface water (*Lin et al., 2011; Hemleben et al., 1989*).

The $\delta^{18}O$ data of the thermocline dwelling species of foraminifera, *P. obliquiloculata,* and *N. dutertrei,* from ODP 769 is compared to the previously measured $\delta^{18}O$ data of mixed layer dwelling *Globigerinoides ruber* (figure 4.3). The difference between the $\delta^{18}O$ of each of these species is shown as $\Delta\delta^{18}O$ (figure 4.4). The average difference between $\delta^{18}O$ of *G. ruber* and both *P. obliquiloculata* and *N. dutertrei* was ~0.90‰. We interpret more negative values to represent periods of greater stratification between the upper mixed and thermocline layers due to diminished surface mixing with increased surface precipitation or changes in surface temperature. Values that were closer to 0 indicate that there was less difference between the three species and, therefore, less stratification and possibly increased mixing between the mixed and thermocline layers.

The $\Delta\delta^{18}O$ between *G. ruber* and the thermocline foraminifera represent the general depth between the mixed layer and the thermocline, while the $\Delta\delta^{18}O$ between the two thermocline species may portray variations of the depth habitats of these species at different times and possible stratification within the thermocline layer in the Sulu Sea. While each marine isotope stage (MIS) has characteristic differences within the records shown here, there are general similarities between interglacials and glacial cycles that may be related to broader changes in climate and surface ocean dynamics.

Thermocline depth in the Sulu Sea over the last 400kyr was previously inferred by determing the percentage of the coccolithophorid species, *Florisphaera profunda* (%Fp) in piston core IMAGES MD97-2141 (*Beaufort et al., 2003*). However, the %Fp also reflects changes in productivity so that greater productivity occurs during times when the thermocline is shallower. Although greater percentages of *F. profunda* were

associated with a deeper thermocline in the Sulu Sea, this record did not appear to correlate with the $\Delta\delta^{18}O$ records presented here. Whereas the productivity rate in the Sulu Sea is probably increased by upwelling and a shallower thermocline, factors other than thermocline depth may affect productivity. Meanwhile, the foraminifera $\Delta\delta^{18}O$ records here are not a direct reflection of productivity, but the difference between the $\delta^{18}O$ of the mixed layer and upper thermocline, which may also reflect parameters other than thermocline depth such as micro-thermal structures in the water column, changes in source water, and salinity variability due to precipitation and global ice volume.

These $\delta^{18}O$ records display glacial-interglacial (G-I) variability (see Figure 4.3). The average G-I $\delta^{18}O$ amplitude of *N. dutertrei* and *P. obliquiloculata* is 1.4-1.5‰, and 1.2‰ for *G. ruber* (*Linsley and Dunbar, 1994; Linsley et al., 1996*). The amount of $\delta^{18}O$ change due to ice volume is ~1-1.2‰ (*Fairbanks, 1989*). As expected, the $\delta^{18}O$ of *G. ruber* was always more depleted than that of the deeper-dwelling foramifera. The $\delta^{18}O$ of *N. dutertrei* and *P. obliquiloculata* are within the same range of 0 to -1.5‰. Interestingly, these foraminifera do not always display equal amounts of variability. For example, during the interglacial-glacial transition from marine isotope stage (MIS) 11 to 10, the G. ruber $\delta^{18}O$ became enriched by nearly 1.5‰ (figure 4.3). During the same transition, the $\delta^{18}O$ change of both *P. obliquiloculata* and *N. dutertrei* was half that amount.

In order to estimate the timing of possible shifts in the source of the thermocline and upper mixed layer water in the Sulu Sea, the differences between *N. dutertrei* and *P. obliquiloculata* $\delta^{18}O$ ($\Delta\delta^{18}O_{N\text{-}P}$), *G. ruber* and *N. dutertrei* ($\Delta\delta^{18}O_{G\text{-}N}$), and *G. ruber* and *P. obliquiloculata* ($\Delta\delta^{18}O_{G\text{-}P}$) were determined and are shown below in figure 4 as a representation of changes in thermocline depth. The $\Delta\delta^{18}O$ was calculated based on

shallow – deep planktonic foraminifera. Table 1 can be used as a guide to show general differences between the average values and ranges of $\Delta\delta^{18}O_{G\text{-}N}$ and $\Delta\delta^{18}O_{G\text{-}P}$ for each MIS in the Sulu Sea. The total average glacial stage difference for $\Delta\delta^{18}O_{G\text{-}P}$ was -0.80‰ and for $\Delta\delta^{18}O_{G\text{-}N}$ was -0.85‰. The total average interglacial stage difference for $\Delta\delta^{18}O_{G\text{-}P}$ was -1.02‰ and for $\Delta\delta^{18}O_{G\text{-}N}$ was -1.05‰. These differences may reflect the level of stratification of the water column with greater isotopic differences indicating more pronounced stratification in the upper water column.

A visual comparison between $\Delta\delta^{18}O_{N\text{-}P}$, $\Delta\delta^{18}O_{G\text{-}P}$ and $\Delta\delta^{18}O_{G\text{-}N}$ helps to distinguish between periods when stratification was the result of increased salinity in the mixed layer or shoaling of the thermocline. The greatest variances in $\Delta\delta^{18}O_{N\text{-}P}$ can possibly reflect periods when one of these two thermocline dwelling foraminifera was calcifying at a different depth and that there may have been greater stratification within the thermocline. Since both *N. dutertrei* and *P. obliquiloculata* appear to calcifiy within a narrow temperature range and vary in their depths accordingly, it is unlikely that one would go far above or below the other in calcification depth range, so changes in $\Delta\delta^{18}O_{N\text{-}P}$ from 0 may be due to biologic differences between the species (*Lin et al., 2011*). Meanwhile, there was increased salinity stratification or varying thermal structure between the mixed layer and upper thermocline when the $\Delta\delta^{18}O_{G\text{-}P}$ and $\Delta\delta^{18}O_{G\text{-}N}$ displayed the greatest differences.

The mean $\Delta\delta^{18}O_{N\text{-}P}$ is -0.04‰ with significant excursions from 0‰ occurring at interglacial stages and values closer to 0‰ or within error occurring during glacial stages. This demonstrates that, in general, *P. obliquiloculata* and *N. dutertrei* were calcifying at

the same general depth, but also that the thermocline in the Sulu Sea was possibly more stratified during some interglacial stages and less stratified during glacial stages.

Table 4.1. Average and range of $\Delta\delta^{18}O_{G\text{-}P}$ and $\Delta\delta^{18}O_{G\text{-}N}$ for MIS 1-18 from ODP 769A.

MIS Stage	Average $\Delta\delta^{18}O_{G\text{-}P}$	Average $\Delta\delta^{18}O_{G\text{-}N}$	Range of $\Delta\delta^{18}O_{G\text{-}P}$	Range of $\Delta\delta^{18}O_{G\text{-}N}$
1	-0.95	-1.21	-0.71 -1.29	-1.017 -1.51
2	-0.94	-0.94	-0.87 -1.01	-0.62 -1.27
3	-1.15	-1.08	-1.00 -1.28	-1.05 -1.26
4	-0.94	-1.07	-0.90 -0.99	-1.03 -1.11
5	-0.77	-0.91	-0.59 -1.05	-0.74 -1.17
6	-0.9	-0.85	-0.61 -1.17	-0.53 -1.24
7	-1.01	-1.01	-0.85 -1.22	-0.65 -1.23
8	-0.66	-0.77	-0.19 -1.06	-0.32 -1.22
9	-0.78	-0.76	-0.5 -1.06	-0.58 -1.10
10	-0.62	-0.86	-0.04 -1.10	-0.15 -1.33
11	-1.35	-1.29	-0.83 -1.72	-0.88 -1.71
12	-0.8	-0.84	-0.69 -0.99	-0.64 -1.05
13	-1.1	-1.08	-0.34 -1.51	-0.57 -1.59
14	-1.08	-0.98	-0.69 -1.57	-0.37 -1.52
15	-1.1	-1.13	-0.69 -2.05	-0.55 -2.00
16	-0.66	-0.65	-0.53 -0.92	-0.33 -1.21
17	-1.05	-1	-0.38 -1.59	-0.44 -1.65
18	-0.66	-0.77	-0.43 -0.88	-0.41 -1.14

Total Average Glacial Values: $\Delta\delta^{18}O_{G\text{-}P}$ = -0.80‰; $\Delta\delta^{18}O_{G\text{-}N}$ = -0.85‰
Total Average Interglacial Values: $\Delta\delta^{18}O_{G\text{-}P}$ = -1.02‰; $\Delta\delta^{18}O_{G\text{-}N}$ = -1.05‰.

The $\Delta\delta^{18}O_{G\text{-}P}$ and $\Delta\delta^{18}O_{G\text{-}N}$ records display differences between the mixed layer and the upper thermocline in the Sulu Sea. The similarity between these two records are due to the greater similarities of the calcification depth and $\delta^{18}O$ of *P. obliquiloculata* and *N. dutertrei* in comparison to the relatively larger $\delta^{18}O$ and calcification depth difference between these two foraminifera and *G. ruber*. The average of all $\Delta\delta^{18}O_{G\text{-}P}$ and $\Delta\delta^{18}O_{G\text{-}N}$ values are -0.90‰ for $\Delta\delta^{18}O_{G\text{-}P}$ and -0.95‰ for $\Delta\delta^{18}O_{G\text{-}N}$ (table 4.1). The lowest value of these records was ~-2.00‰. The average values for all of the interglacial stages with the exception of MIS 5 and MIS 9 were ~-1.00‰ or more negative. These more negative

values were likely caused by larger differences in temperature and salinity between the upper mixed and thermocline layers. The greatest extent of change in these records occurred at G-I boundaries (figure 4.4). In the $\Delta\delta^{18}O_{G\text{-}P}$ and $\Delta\delta^{18}O_{G\text{-}N}$ shown here, MIS 9 resembles the glacial stages more than other interglacials, possibly denoting a period that was characterized by a deeper mixed layer within the Sulu Sea.

Throughout many of the glacial stages, the $\Delta\delta^{18}O_{G\text{-}P}$ and $\Delta\delta^{18}O_{G\text{-}N}$ average values were more enriched than -1.00‰ and the ranges were, in general, less than 1.00‰ and more reduced as compared to ranges from interglacial stages. During these glacial stages, the Sulu Sea appeared to have a deeper mixed layer and thermocline than during interglacials based on the greater difference between $\delta^{18}O$ from mixed to thermocline foraminifera. $\delta^{18}O$ enrichment of *G. ruber, P. obliquiloculata*, and *N. dutertrei* was probably the result of increased influence from the South China Sea lower salinity water and restricted input from the Sulawesi Sea, which was cut off from interaction with the Sulu Sea by the exposed Sunda shelf (*Oppo et al., 2003*). Meanwhile, my results support other studies that have concluded that EASM intensity was greatly reduced during glacials with an increased winter monsoon (*Wang et al., 1999; Oppo et al., 2003*), which led to increasing monsoon winds during the winter season, while the ITCZ was in its most southern position. These additional factors added to the freshening and deepening of the mixed layer in the Sulu Sea (*Wang et al., 2009; Wang et al., 2008*; *Wang et al., 2005)*.

During the transition of MIS 11 to 10 and then again during MIS 8, $\Delta\delta^{18}O_{G\text{-}P}$ was reduced to almost 0, while $\Delta\delta^{18}O_{N\text{-}P}$ became very negative. *P. obliquiloculata* was much more depleted in ^{18}O than *N. dutertrei* and closer in value to *G. ruber*. *G. ruber* $\delta^{18}O$

ranged from ~-1.7 to -2.2‰, which implies warmer or fresher surface water. The wide gap between the two thermocline species and the narrow gap between *P. obliquiloculata* and *G. ruber* implies 1.) *P. obliquiloculata* may have migrated up in the water column and 2.) the thermocline was more shallow, but with steeper temperature gradations. In this respect, glacial stages 8 and 10 were very different from other glacial stages within this record.

Throughout many interglacials, sea level rose to allow surface water from the Sulawesi Sea with higher salinity into the Sulu Sea. The mixed layer was shallower probably due to decreased mixing from a diminished winter monsoon as recognized from GI records from the neighboring South China Sea (*Steinke et al., 2010*; *Wang et al., 1999; Wang et al., 2008*; *Wang et al., 2005*). Meanwhile, the increased intensity of the summer monsoon attributed to the increase in freshening of the upper surface water within the Sulu Sea. Altogether, these factors led to a fresher surface layer and a shallower thermocline during most of the interglacial stages in this record.

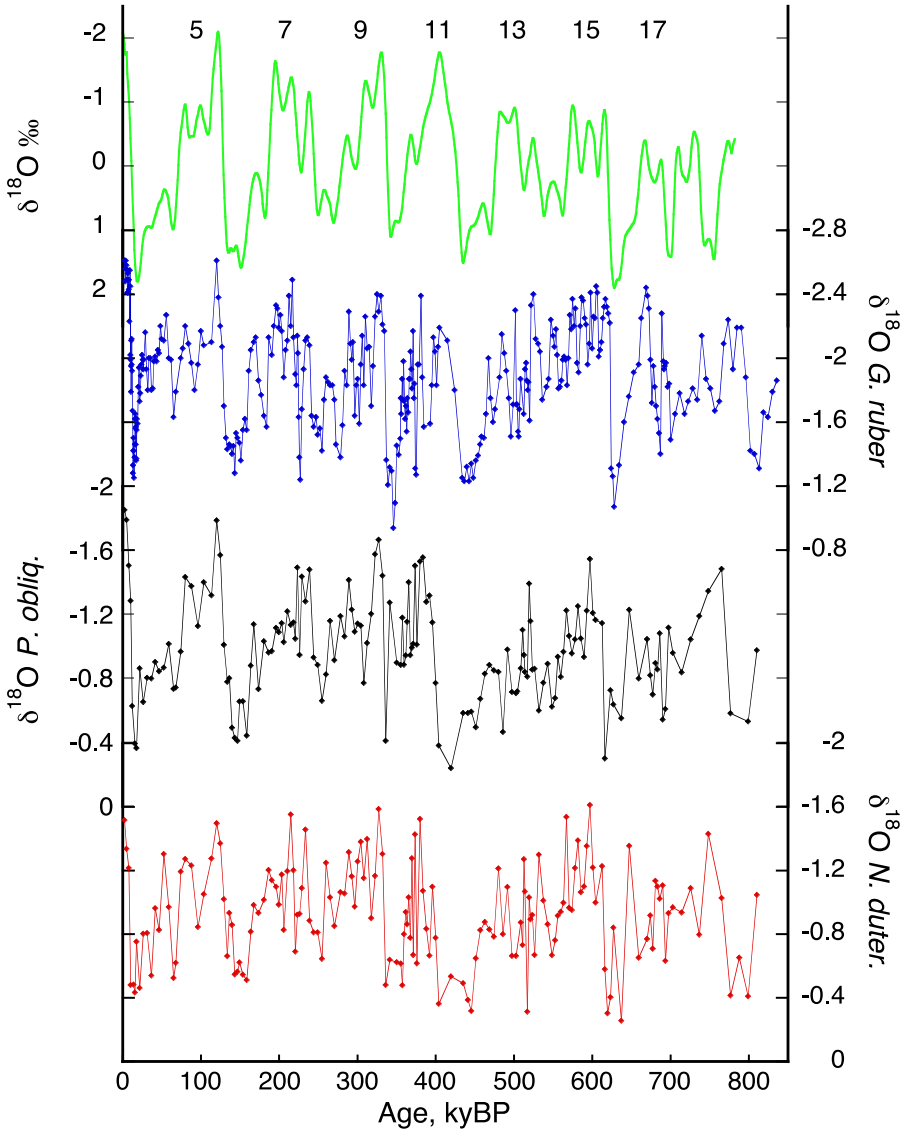

Figure 4.3. $\delta^{18}O$ of *G. ruber* (*Linsley and Dunbar, 1994*), *P. obliquiloculata,* and *N. dutertrei* from ODP 769. The SPECMAP $\delta^{18}O$ time series and marine isotope interglacial stages shown above (*Imbrie and McIntyre, 2006;* $\delta^{13}C$ data for *P. obliquiloculata,* and *N. dutertrei* listed in Appendix C1 and C2).

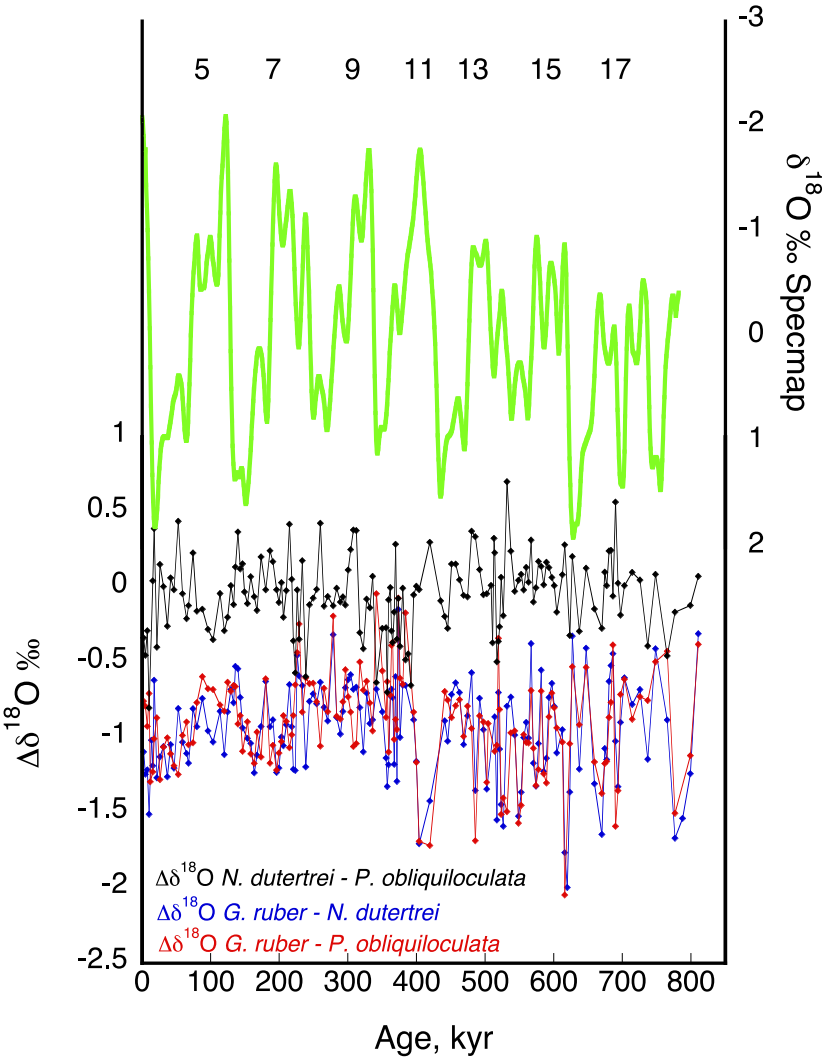

Figure 4.4. $\Delta\delta^{18}O$ of *P. obliquiloculata – N. dutertrei* (black), *G. ruber – P. obliquiloculata* (red), and *G. ruber – N. dutertrei* (blue). Numbers above the SPECMAP curve represent interglacial marine isotope stages (*Imbrie and McIntyre, 2006*).

4. CONCLUSIONS

The $\delta^{18}O$ of thermocline dwelling foraminifera, *P. obliquiloculata* and *N. dutertrei,* were analyzed and compared to a previous record of $\delta^{18}O$ of *G. ruber* from the Sulu Sea core ODP 769. The difference between the $\delta^{18}O$ of these species was calculated as $\Delta\delta^{18}O$ in order to determine the stratification of the Sulu Sea upper water column over G-I timescales. Changes in the intensity of the summer and winter EAM in addition to sea level likely played important roles in the stratification of the upper water column (*Wang et al., 1999; Oppo et al., 2003; Tian et al., 2005; Wang et al., 2008*; *Wang et al., 2005*). Tracking the $\delta^{18}O$ of mixed layer and thermocline dwelling species of foraminifera can be used to determine the degree of stratification and hence the strength of the EAM and source water variability between G-I stages. Mixed-layer and thermocline dwelling foraminifera $\delta^{18}O$ signatures relay information in reference to the salinity and temperature of different source waters driven by monsoon strength or changes in sea level, while a deeper mixed layer may pertain to increased monsoon intensity. Therefore, determining the similarities or disparities between the $\delta^{18}O$ of different water depths at GI intervals may lead to the determination of flow between the Sulu Sea and its neighboring bodies of water.

Interglacial stages were primarily expressed by higher values of $\Delta\delta^{18}O_{N\text{-}P}$, $\Delta\delta^{18}O_{G\text{-}N}$ and $\Delta\delta^{18}O_{G\text{-}P}$. This conveyed that the mixed layer was more shallow, while the thermocline may have been more sharply stratified. The $\Delta\delta^{18}O_{G\text{-}P}$ and $\Delta\delta^{18}O_{G\text{-}N}$ from MIS 5 and 9 were uncharacteristically higher than during other interglacials and showed greater resemblance to glacial stages. Meanwhile, for most interglacials, greater salinity contrast between the mixed layer and thermocline may have existed in the Sulu Sea due

to increased freshening of the mixed layer because of strengthened summer EAM that brought higher salinity water from the Sulawesi Sea and weakened winter EAM that would have reversed the current and added fresher water from the South China Sea. Glacial stages were characterized by overall $\Delta\delta^{18}O_{G\text{-}N}$ and $\Delta\delta^{18}O_{G\text{-}P}$ higher than -1.00‰. This conveys a deeper mixed layer and thermocline. The deeper mixed layer is probably the result of intensified winter EAM in addition to a diminished summer monsoon, which reduced the influence of higher salinity water into the Sulu Sea.

These findings are in general agreement with previous conclusions that 1.Winter monsoon caused increased glacial surface water mixing in the WPWP, 2. Increased summer monsoon intensity powered freshening in the Sulu Sea mixed layer, and 3. Sea level controlled the source of surface water entering the Sulu Sea by restricting salty water from the Sulawesi Sea from entering during glacial stages (*Oppo et al., 2003; Wang et al., 2008*; *Wang et al., 2005*). Interglacial stages 7, 9, and 11 experienced anomalous cooling and freshening of the mixed layer that contrasted the salinity and temperature of the thermocline.

REFERENCES CITED

Aldrian, E., and R. Dwi Susanto, 2003, Identification of three dominant rainfall regions within Indonesia and their relationship to sea surface temperature, *International Journal of Climatology, v. 23*, 1435-1452, doi: 10.1002/joc.950

Allison, N., 1996, Geochemical anomalies in coral skeletons and their possible implications for palaeoenvironmental analyses, *Marine Chemistry, v. 55*, 367-379.

Altabet, M.A., 2001, Nitrogen isotopic evidence for micronutrient control of fractional NO3 utilization in the equatorial Pacific, *Limnology and Oceanography, v. 46,* 368-380.

Arruda, W. Z., and D. Nof, 2003, The Mindanao and Halmahera Eddies – Twin eddies induced by non-linearities, *J. Phys. Ocean*, *v. 33*, 1815-2830.

Bates, N.R., Michaels, A.F., Knap, A.H., 1996, Seasonal and interannual variability of oceanic carbon dioxide species at the US JGOFS Bermuda Atlantic Time Series Study (BATS) site, *Deep-Sea Research II v. 43,* 347–383.

Beaufort, L., T. de Garidel-Thoron, B.K. Linsley, D.W. Oppo, and N. Buchet, 2003, Biomass burning and oceanic primary production estimates in the Sulu Sea area over the last 380 kyr and the East Asian monsoon dynamics, *Marine Geology, v. 201*, 53-65.

Beck, J.W., R.L. Edwards, I. Emi, F.W. Taylor, J. Recey, F. Rougerie, P. Joannot, and C. Henin, 1992, Sea-surface temperature from coral skeletal strontium/calcium ratios, *Science, v. 257*, 644-647.

Bjerknes, J., 1969, Atmospheric teleconnections from the equatorial Pacific, *Mon. Weather Rev.*, *v. 97*, 163.

Boyd, R.S., 2001, Nitrogen in future biosphere studies, *Chemical Geology, v. 176*, 1-30.

Bohm, F., M.M. Joachimski, W.C. Dullo, A. Eisenhauer, H. Lehnert, J. Reitner, and G. Worheide, 2000, Oxygen isotope fractionation in marine aragonite of coralline sponges, *Geochimica et Cosmochimica Acta v. 64*, 1695-1703.

Brandes, J.A., and Devol, A.H., 2002, A global marine-fixed nitrogen isotopic budget: Implications for Holocene nitrogen cycling, *Global Biogeochemical Cycles, v. 16*, doi:101029/2001GB001856.

Brandes, J.A., Devol, A.H., Yoshinare, T., Jayakumar, D.A., and Naqvi, S.W.A., 1998, Isotopic composition of nitrate in the central Arabian Sea and eastern tropical North Pacific: A tracer for mixing and nitrogen cycles, *Limnology and Oceanography, v. 43*, p. 1680-1689.

Broecker, W.S., and T. H. Peng, 1982, Tracers in the Sea, Eds. *Eldigio Press Lamont Doherty Geological Observatory*, 690 pp.

Cane, M.A., 2005, The evolution of El Niño, past and future, *Earth and Planetary Science Letters, v. 230,* 227-240.

Casciotti, K.L., Sigman, D.M., Hastings, G.M., Bohlke, J.K., and Hilkert., A., 2002, Measurement of the oxygen isotopic composition of nitrate in seawater and freshwater using the denitrifier method, *Analytical Chemistry, v. 74*, 4905-4912.

Chelton, D. B., S. K. Esbensen, M. G. Schlax, N. Thum, M. H. Freilich, F. J. Wentz, C.L. Gentemann, M. J. McPhaden, and P. S. Schopf, 2001, Observations of coupling between surface wind stress and sea surface temperature in the eastern tropical Pacific, *J. Climate*, *v. 14*, 1479-1498.

Chou, W.C., D.D. Sheu, B.S. Lee, C.M. Tseng, C.T.A. Chen, S.L. Wang and G.T.F. Wong, 2007, Depth distributions of alkalinity, TCO_2 and $\delta^{13}C_{TCO2}$ at SEATS time-series site in the northern South China Sea, *Deep-Sea Research II v. 54*, 1469-1485, doi:10.1016/j.dsr2.2007.05.002.

Christian, J.R.m C.R. McClain, R. Murtugudde, and J. Ballabrera-Poy, 2004, A ribbon of dark water: Phytoplankton blooms in the meanders of the Pacific North Equatorial Countercurrent, *Deep-Sea Research. Part II, Topical Studies in Oceanography, v. 51*, 209-228, doi: 10.1016/j.dsr2.2003.06.002.

Clement, A.C., R. Seager, and M.A. Cane, 1999, Orbital controls on El Nino/Southern Oscillation and the tropical climate, *Paleoceanography, v. 14*, 441-456.

Conroy, J.L.; J.T. Overpeck, J.E. Cole, T.M. Shanahan, and M. Steinitz-Kannan, 2008, Holocene changes in eastern tropical Pacific climate inferred from a Galapagos lake sediment record, *Quat. Sci. Rev*., *v. 27*, 1166-1180.

Cravette, S., T. Delcroix, D. Zhang, M. McPhaden, J. Leloup, 2009, Observed freshening and warming of the western Pacific Warm Pool, *Climate Dynamics, v. 33*, 565-589.

Dang, P.X., T. Kobayashi, T. Mitsuguchi, H. Kitagawa, and Y. Shibata, 2004, Marine reservoir correction in the south of Vietnam estimated from an annually-banded coral, *Radiocarbon, v. 46*, 657-660.

Dannenmann, S., B.K. Linsley, D. W. Oppo, Y. Rosenthal, and L. Beaufort, 2003, East Asian monsoon forcing of suborbital variability in the Sulu Sea during Marine Isotope Stage 3: Link to northern Hemisphere climate, *Geophys. Geochem. Geosys., v. 4*, 1001, doi: 10.1029/2002GC00390.

de Villiers, S., G.T. Shen, and B.K. Nelson, 1994, The Sr/Ca-temperature relationship in coralline aragonite: Influence of variability in $(Sr/Ca)_{seawater}$ and skeletal growth parameters, *Geochim. Cosmochim. Acta, v. 58*, 197-208.

de Villiers, S., B.K. Nelson, and A.R. Chivas, 1995, Biological controls on coral Sr/Ca and $\delta^{18}O$ reconstructions of sea surface temperatures, *Science, v. 269*, 1247-1249.

Deser, C., and J.M. Wallace, 1990, Large-scale atmospheric circulation features of warm and cold episodes in the tropical Pacific, *Journal of Climate, v. 3*, 1254-1281.

Deutsch, C., J.L. Sarmiento, D. Sigman, N. Gruber, and J.P. Dunne, 2007, Spatial coupling of nitrogen inputs and losses in the ocean, *Nature, v. 445*, 163-167.

Drenzek, N.J., D.B. Montlucon, M.B. Yunker, R.W. Macdonald, and T.I. Eglinton, 2007, Constraints on the origin of sedimentary organic carbon in the Beaufort Sea from

coupled molecular 13C and 14C measurements, *Marine Chemistry, v. 103*, 146-162, doi: 10.1016/j.marchem.2006.06.017.

Elsdon, T.S., and B.M. Gillanders, 2005a, Alternative life history patterns of estuarine fish: barium in otoliths elucidates freshwater residency, *Canadian Journal of Fisheries and Aquatic Sciences*, *v. 62*, 1143-1152.

Elsdon, T.S., and B.M. Gillanders, 2005b, Strontium incorporation into calcified structures: separating the effects of ambient water concentration and exposure time, *Mar Ecol Prog Ser, v. 285*, 233-243.

Epstein, S., and T.K. Mayeda,1953, Variations of the 18O/16O ratio in natural waters, *Geochem.Cosmochim. Acta, v. 4*, doi:10.1016/0016-7037(53)90051-9.

Fabry, V.J., and W.G. Deuser, 1992, Seasonal changes in the isotopic compositions and sinking fluxes of euthecosomatous pteropod shells in the Sargasso Sea, *Paleoceanography, v. 7*, 195-213.

Fairbanks , R.G., 1989, A 17,000 year glacio-eustatic sea level record: influence of glacial melting rates on the Younger Dryas event and deep ocean circulation, *Nature, v. 342*, 637-642.

Fairbanks, R.G., M.N. Evans, J.L. Rubenstone, R.A. Mortlock, K. Broad, M.D. Moore, and C.D. Charles, 1997, Evaluating climate indices and their geochemical proxies measured in corals, *Coral Reefs, v. 16*, S93-S100.

Fairbanks, R.G., R.A. Mortlock, T.C. Chiu, L. Cao, A. Kaplan, T.P. Guilderson, T.W. Fairbanks, and A.L. Bloom, 2005, Marine Radiocarbon Calibration Curve Spanning 0 to 50,000 Years B.P. Based on Paired 230Th/234U/238U and 14C Dates on Pristine Corals, *Quaternary Science Reviews*, *v. 24*, 1781-1796.

Frische, A., and D. Quadfasel, 1990, Hydrography of the Sulu Sea, *Proceedings of the ODP, Initial Reports, 124, Ocean Drilling Program*, College Station, TX, 101-104.

Gamo, T., Y. Kato, H. Hasumoto, H. Kakiuchi, N. Momoshima, N. Takahata, and Y. Sano, 2007, Geochemical implications for the mechanism of deep convection in a semi-closed tropical marginal basin: Sulu Sea, *Deep-Sea Research II, v. 54*, 4-13.

Ganeshram, R.S., M.R. Fontugne, T.F. Pedersen, S.E. Calvert, and G.W. McNeil, 2000, Glacial-interglacial variability in denitrification in the world's oceans: Causes and consequences, *Paleoceanography, v. 15*, 361-376, doi: 10.1029/1999PA000422.

de Garidel-Thoron, T., L. Beaufort, B.K. Linsley, and S. Dannenmann, 2001, Millennial-scale Dynamics of the East Asian Winter Monsoon during the last 200,000 years, *Paleoceanography*, *v. 16*, 491-502.

Gordon, A.L., and Tessler, Z., Competing overflows into the deep Sulu Sea, unpublished.

Granger, J., D.M. Sigman, M.F. Lehmann, and P.D. Tortell, 2004a, Nitrogen and oxygen isotope effects associated with nitrate assimilation and denitrification by laboratory cutlures of marine plankton, *Eos Trans. AGU, v. 85*, Fall Meeting Supplement, Abstract H51E-O52.

Granger, J., D.M. Sigman, M.F. Lehmann, and P.D. Tortell, 2004b, Coupled nitrogen and oxygen isotope fractionation of nitrate during assimilation by cultures of marine

phytoplankton, *Limnology and Oceanography, v. 49*, 1763-1773.

Grossman, E.L., and T.L. Ku, 1986, Oxygen and carbon isotope fractionation in biogenic aragonite: temperature effects, *Chemical Geology, Isotope Geoscience Section, v. 39*, 59-74.

Haug, G.H., B. Nielsen, L.C. Peterson, T.F. Pedersen, D.M. Sigman, and S.E. Calvert, 1998, Glacial/interglacial variations in production and nitrogen fixation in the Cariaco Basin during the last 580kyr, *Paleoceanography, v. 13*, 427-432, doi: 10.1029/98PA01976.

Haug, G.H., U. Röhl, K.A. Hughen, D.M. Sigman, and L.C. Peterson, 2001, Southward migration of the intertropical convergence zone through the Holocene, *Science, v. 293*, 1304-1308.

Hemleben, Ch., M. Spindler, and O. R. Anderson, 1989, Modern Planktonic Foraminifera, *Springer Verlag, Berlin, 363 pp.*

Hodell, D.A., M. Brenner, and J.H. Curtis, 2005, Terminal Classic drought in the northern Maya lowlands inferred from multiple sediment cores in Lake Chichancanab (Mexico), *Quaternary Science Reviews, v. 24*, 1413-1427, doi: 10.1016/j.quascirev.2004.10.013.

Howell, P.J., N. Pisias, J. Ballance, J. Baughman, and L. Ochs, 2006, ARAND Time-Series Analysis Software, Brown University, Providence RI.

Hu, C., G.M. Henderson, J. Huang, S. Xie, Y. Sun, and K.R. Johnson, 2008, Quantification of Holocene Asian monsoon rainfall from spatially separated cave records, *Earth and Planetary Science Letters, v. 266*, 221-232.

Imbrie, J.D, A. McIntyre, 2006, 1984, SPECMAP time scale developed by Imbrie et al., based on normalized planktonic records (normalized O-18 vs time, specmap.017), doi:10.1594/PANGAEA.441706.

Juranek, L.W., A.D. Russell, and H.J. Spero, 2003, Seasonal oxygen and carbon isotope variability in euthecosomatous pteropods from the Sargasso Sea, *Deep Sea Research Part I: Oceanographic Research Papers, v. 50*, 231-245, doi:10.1016/S0967-0637(02)00164-4.

Kinsman, D.J.J., and H.D. Holland, 1969, The co-precipitation of cations with CaCO3-IV. The co-precipitation of Sr2 with aragonite between 16˚C and 96˚C, *Geochimica et Cosmochimica Acta v. 33*, 1-17.

Klein, S.A., B.J. Soden, and N.C. Lau, 1999, Remote sea surface temperature variations during ENSO: Evidence for a tropical atmospheric bridge, *J. of Climate, v. 12*, 917-932.

Koutavas, A., and J. Lynch-Stieglitz, 2005, Variability of the marine ITCZ over the eastern Pacific during the past 30,000 years: Regional perspective and global context, In *The Hadley Circulation: Present Past and Future*, R. Bradley and H. Diaz, Eds., Springer, 347-369.

Lachniet, M.S., S.J. Burns, D.R. Piperno, Y. Asmerom, V.J. Polyak, C.M. Moy, K. Christenson, 2004, A 1500-year El Niño/Southern Oscillation and rainfall history

for the Isthmus of Panama from speleothem calcite, *J. of Geophys. Res., v. 109*, doi:10.1029/2004JD004694.

Lambeck, K., T.M. Esat, and E.K. Potter, 2002, Links between climate and sea levels for the past three million years, *Nature, v. 419*, 199-206.

Langton, S.J., B.K. Linsley, R.S. Robinson, Y. Rosenthal, D.W. Oppo, T.I. Eglinton, S. Howe, Y.S. Djajadihardja, and F. Syamsudin, 2008, A 3,500 yaer record of centennial-scale El Niño variability from the Western Pacific Warm Pool, *Geology, v. 36*, 795-798, doi: 10.1130/G24926A.

Lea, D.W., T.A. Mashiotta, and H.J. Spero, 1999, Controls on magnesium and strontium uptake in planktonic foraminifera determined by live culturing, Geochimica et *Cosmochimica Acta, v. 63*, 2369-2397.

Lea, D.W., D.K. Pak, and H.J. Spero, 2000, Climate impact of late Quaternary equatorial Pacific sea surface temperature variations, *Science, v. 289*, 1719-1724.

Levitus, S., R. Burgett, and T.P. Boyer, 1994, World Ocean Atlas Salinity, NOAA Atlas NESDIS 3, US Gov. Print Off., Washington, D.C., 99 pp.

Lin, H.L., and H.Y. Hsieh, 2007, Seasonal variations of modern planktonic foraminifera in the South China Sea, *Deep-Sea Research II, v. 54*, 1634-1644.

Lin, H.L., D.D. Sheu, Y. Yang, W.C. Chou, and G.W. Hung, 2011, Stable isotopes in modern planktonic foraminifera: Sediment trap and plankton tow results from the South China Sea, *Marine Micropaleontology, v. 79*, 15-23.

Linsley, B.K., Thunell, R.C., Morgan, C., and Williams, D.F., 1985, Oxygen minimum expansion in the Sulu Sea, western equatorial Pacific, during the last glacial low stand of sea level, *Marine Micropaleontology*, *v. 9*, 395-418.

Linsley, B.K., and R.C. Thunell, 1990, The record of deglaciation in the Sulu Sea: Evidence for the Younger Dryas event in the tropical western Pacific, J.P. Kennett, ed., *Paleoceanography*, *Special Issue on the Younger Dryas, v. 5*, 1025-1039.

Linsley, B.K., and M.T. von Breymann, 1991, Stable isotopic and geochemical record in the Sulu Sea during the last 750 k.y.: assessment of surface water variability and paleoproductivity changes, In Silver, E.A., Rangin, C., von Breymann, M.T., et al., *Proc. ODP, Sci. Results, v. 124*, College Station, TX (Ocean Drilling Program), 379–396.

Linsley, B.K., and R.B. Dunbar, 1994, The late Pleistocene history of surface water δ13C in the Sulu Sea: Possible relationship to Pacific deepwater δ13C changes, *Paleoceanography, v. 9*, 317-340.

Linsley, B.K., R.B. Dunbar, G.M. Wellington, and D.A. Mucciarone, 1994, A coral based reconstruction of Intertropical Convergence Zone variability over Central America since 1707, *J. of Geophys. Res., v. 99*, p. 9977-9994.

Linsley, B.K., 1996, Oxygen isotope evidence of sea level and climatic variations in the Sulu Sea over the past 150,000 years, *Nature*, *v. 380*, 234-237.

Linsley, B.K, Y. Rosenthal, and D.W. Oppo, 2010, Holocene evolution of the Indonesian throughflow and the western Pacific warm pool, *Nature Geoscience, v. 3,* 578-583.

Liu, K.-K., and I.R. Kaplan, 1989, The eastern tropical Pacific as a source of ^{15}N-enriched nitrate in seawater off southern California, *Limnology and Oceanography, v. 34*, 820-830.

Lyle, M.W., F.G. Prahl, and M.A. Sparrow, 1992, Upwelling and productivity changes inferred from a temperature record in the central equatorial Pacific, *Nature v. 355*, 812-815.

Makou, M.C., S.P. Sylva, T.I. Eglinton, K.A. Hughen, and L. Xu, 2007, Isotopic records of tropical vegetation and climate change from terrestrial vascular plant biomarkers preserved in Cariaco Basin sediments, *Organic Geochemistry, v. 38,* 1680-1691.

Mariotti, A., J.C. Germon, P. Hubert, P. Kaiser, R. Letolle, A. Tardieux, and P. Tardieux, 1981, Experimental-Determination of Nitrogen Kinetic Isotope Fractionation - Some Principles - Illustration for the Denitrification and Nitrification Processes, *Plant and Soil, v. 62,* 413-430.

Masumoto, Y.; N. Hirose, T. Yamagata, T. Kagimoto, M. Yoshida, and M. Fukuda, 2001, Intraseasonal Eddies in the Sulawesi sea simulated in an ocean general circulation model, *Geophysical Research Letters, v. 28*, 1631-1634.

Meece, D.E. and L.K. Benninger, 1993, The coprecipitation of Pu and other radionuclides with CaCO3, *Geochim. Cosmochim. Acta, v. 57*, 1447-1458.

Merryfield, W.J., 2006, Changes to ENSO under CO2 Doubling in a Multimodel Ensemble, *J. of Climate*, *v. 19,* 4009-4027.

Middelburg, J.J., 1990, Early diagenesis and authigenic mineral formation in anoxic sediments of Kau Bay, Indonesia, *Geologica ultraiectina, v. 71*, 177pp.

Mitsuguchi, T., P.X. Dang, H. Kitagawa, T. Uchida, and Y. Shibata, 2008, Coral Sr/Ca and Mg/Ca records in Con Dao Island off the Mekong Delta: Assessment of their potential for monitoring ENSO and East Asian monsoon, *Global and Planetary Change, v. 63*, 341-352.

Moy, C.M., G.O. Seltzer, D.T. Rodbell, and D.M. Anderson, 2002, Variability of El Niño/Southern Oscillation activity at millennial timescales during the Holocene epoch, *Nature*, *v. 420*, 162-165.

Newton, A.; R. Thunell, L. Stott, 2006, Climate and hydrographic variability in the Indo-Pacific Warm Pool during the last millennium, *Geophys. Res. Letters*, *v. 33*, doi:10.1029/2006GL027234.

Ohkouchi, N., T.I. Eglinton, L. Xu, C.M. Reddy, and D. Montlucon, 2005, Radiocarbon dating of alkenones from marine sediments: I. Isolation protocol, *Radiocarbon, v. 47*, 401-412.

Oppo, D.W., B.K. Linsley, Y. Rosenthal, S. Dannenmann, and L. Beaufort, 2003, Orbital and suborbital climate variability in the Sulu Sea, western tropical Pacific, *Geophys. Geochem. Geosys., v. 4*, doi:10.1029/2001GC00260.

Oppo, D.W., Y. Rosenthal, and B.K. Linsley, 2009, 2,000-year-long temperature and hydrology reconstructions from the Indo-Pacific warm pool, *Nature*, *v. 460,* doi:10.1038/nature08233.

Pelejero, C., J.O. Grimalt, S. Heilig, M. Kienast, and L. Wang, 1999, High-resolution UK37 temperature reconstructions in the South China Sea over the past 220 kyr, *Paleoceanography v. 14*, 224-231.

Pflaumann, U., and Z. Jian, 1999, Modern distribution patterns of planktonic foraminifera in the South China Sea and western Pacific: A new transfer technique to estimate regional sea-surface temperatures, *Marine Geology v. 156*, 41–83.

Picaut, J., M. Ioualalen, C. Menkes, T. Delcroix, and M.J. McPhaden, 1996, Mechanism of the zonal displacements of the Pacific warm pool: Implications for ENSO, *Science, v. 274*, 1486-1489.

Qu, T., Y. Du, J. Strachan, G. Meyers, and J. Slingo, 2005, Sea surface temperature and its variability in the Indonesian region, In The Indonesian Seas, *Oceanography, v. 18*, 50-61.

Quadfasel, D., H. Kudrass, and A. Frische, 1990, Deep-water renewal by turbidity currents in the Sulu Sea, *Nature, v. 348*, 320-322.

Ravelo, A.C., R.G. Fairbanks, 1992, Oxygen isotopic composition of multiple species of planktonic foraminifera: Recorders of the modern photic zone temperature gradient, *Paleoceanography, v. 7*, 815-831.

Reimer, P.J., and R.W. Reimer, 2001, A marine reservoir correction database and on-line interface, *Radiocarbon, v. 43*, 461-463.

Rein, B., A. Lückge, and F. Sirocko, 2004, A major Holocene ENSO anomaly during the Medieval period, *Geophysical Research Letters, v. 31*, doi: 10.1029/2004GL020161.

Rein, B., A. Wolf, W.C. Dullo, A. Lückge, L. Reinhardt, and F. Sirocko, 2005, El Niño variability off Peru during the last 20,000 years, *Paleoceanography, v. 20*, doi: 10.1029/2004PA001099.

Reynolds, R.W.; and T.M. Smith, 1994, Improved global sea surface temperature analyses using optimum interpolation, *J. Clim*., *v. 7*, 929-948.

Rodbell, D.T., D.B. Enfield, J.H. Newman, G.O. Seltzer, D.M. Anderson, and M.B. Abbott, 1999, An ~15,000-year record of El Nino-driven alluviation in Southwestern Ecuador, *Science, v. 283*, 516-520.

Rodriguez, R., A. Mabres, B. Luckman, M. Evans, M. Masiokas, and T.M. Ektvedt, 2005, "El Niño" events recorded in dry-forest species of the lowlands of northwest Peru, *Dendrochronologia*, doi:10.1016/j.dendro.2005.05.002.

Ropelewski, C.F., and M.S. Halpert, 1987, Global and regional scale precipitation patterns associated with the El Niño/Southern Oscillation, *Monthly Weather Review, v. 115*, 1606-1626.

Rosenthal, Y., D.W. Oppo, B.K. Linsley, 2003, The amplitude and phasing of climate change during the last deglaciation in the Sulu Sea, western equatorial Pacific, *Geophys. Res. Letters, v. 30*, doi:10.1029/2002GL016612.

Rottman, M.L., 1979, Dissolution of planktonic foraminifera and pteropods in South China Sea sediments, *J. of Foraminiferal Res., v. 9,* 41-49.

Russell, A D; B. Hönish, H. Spero, and D.W. Lea, 2004, Effects of seawater carbonate ion concentration and temperature on shell U, Mg, and Sr in cultured planktonic foraminifera, *Geochim. Cosmoch. Acta*, v. *68*, 4347-4361, doi:10.1016/j.gca.2004.03.013.

Sachs, J.P., D. Sachse, R. H. Smittenberg, Z. Zhang, D.S. Battisti, and S. Golubic, 2009, Southward movement of the Pacific intertropical convergence zone AD 1400-1850, *Nature Geoscience*, doi: 10.1038/NGEO554.

Shintani, T., M. Yamamoto, and M.T. Chen, 2008, Slow warming of the northern South China Sea during the last deglaciation, *Terr. Atmos. Ocean. Sci., v. 19,* 341-346.

Sigman, D.M., K.L. Casciotti, M. Andreani, C. Barford, M. Galanter, and J.K. Bohlke, 2001, A bacterial method for the nitrogen isotopic analysis of nitrate in seawater and freshwater, *Analytical Chemistry, v. 73*, 4145-4153, doi: 10.1021/ac010088e.

Sigman, D.M., R. Robinson, A.N. Knapp, A. van Geen, D.C. McCorkle, J.A. Brandes, and R.C. Thunell, 2003, Distinguishing between water column and sedimentary denitrification in the Santa Barbara Basin using the stable isotopes of nitrate, *Geochem. Geophys. Geosys., v. 4,* doi:10.1029/2002GC000384.

Sigman, D.M., R. Ho, G. Cane, A. van Geen, J. Granger, P.J. DiFiore, and M.M. Lehmann, 2005, Coupled nitrogen and oxygen isotope measurements of nitrate along the eastern North Pacific margin, *Global Biogeochemical Cycles, v. 19*, doi:10.1029/2005GB002458.

Sijinkumar, A.V., B. Nagender Nath, M.V.S. Guptha, 2010, Late Quaternary record of pteropod preservation from the Andaman Sea, *Marine Geology, v. 275*, 221-229.

Smith, S.V., R.W. Buddemeier, R.C. Redalje, and J.E. Houck, 1979, Strontium-calcium thermometry in coral skeletons, *Science, v. 204*, 404-407.

Sosdian, S., D.K. Gentry, C.H. Lear, E.L. Grossman, D. Hicks, and Y. Rosenthal, 2006, Strontium to calcium ratios in the marine gastropod *Conus ermineus*: Growth rate effects and temperature calibration, *Geochem. Geophys. Geosys., v. 7,* doi:10.1029/2005GC001233.

Southon, J., W.W.S. Yim, M. Kashgarian, M. Fontugne, and B. Metivier, 2002, Marine reservoir corrections for the Indian Ocean and Southeast Asia, *Radiocarbon, v., 44*, 167-180.

Spero, H.J., J. Bijma, D.W. Lea, and B.E. Bemis, 1997, Effect of seawater carbonate concentration on foraminiferal carbon and oxygen isotopes, *Nature, v. 390*, 497-500.

Steinke, S., M. Mohtadi, J. Groeneveld, L. Lin, L. Lowemark, M. Chen, and R. Rendle-Buhring, 2010, Reconstructing the southern South China Sea upper water column structure since the Last Glacial Maximum: Implications for the East Asian winter monsoon development, *Paleoceanography, v. 25*, doi:10.1029/2009PA001850.

Stott, L., C. Poulsen, S. Lund, and R. Thunell, 2002, Super ENSO and global climate oscillations at millennial time scales, *Science, v. 297*, 222-226.

Sun, S., and E.H. James, 2003, Climate Simulations for 1951–2050 with a Coupled Atmosphere–Ocean Model, *American Met. Soc., v. 16*, 2807-2826.

Suparan, P., R.A.C. Dam, S. van der Kaars, and T.E. Wong, 2001, Late Quaternary tropical lowland environments on Halmahera, Indonesia, *Palaeogeography, Palaeoclimatology, Palaeoecology, v. 171*, 229-258.

Street-Perrott, F.A., P. Barker, L.B. Khelifa, D.D. Harkness, D.O. Olago, Y. Huang, R.A. Perrott, and G. Eglinton, 1997, Impact of lower atmospheric carbon dioxide on tropical mountain ecosystems, *Science, v. 278,* 1422-1426, doi:10.1126/science.278.5342.1422.

Tarutani, T., Clayton, R.N., Mayeda, T.K., 1969, The effect of polymorphism magnesium substituteion on oxygen isotope fractionation between calcium carbonate and water, *Geochim. Cosmochim. Acta, v. 33*, 987-996.

Thunell, R.C., R. Varela, D.M. Sigman, F. Muller-Karger, and Y. Aster, 2004, Nitrogen isotope dynamics of the Cariaco Basin, Venezuela, *Global Biogeochemical Cycles*, *v. 18*, doi:10.1029/2003GB002185.

Tian, J., P. Wang, R. Chen, and X. Cheng, 2005, Quaternary upper ocean thermal gradient variations in the South China Sea: Implications for east Asian monsoon climate, *Paleoceanography, v. 20*, doi:10.1029/2004PA001115.

Tierney, J.E., D.W. Oppo, Y. Rosenthal, J.M. Russell, and B.K. Linsley, 2010, Coordinated hydrological regimes in the Indo-Pacific region during the past two millennia, *Paleoceanography, v. 25,* doi:10.1029/2009PA001871.

Ueki, I., Y. Kashino, and Y. Kuroda, 2003, Observation of current variations off the New Guinea coast including the 1997-1998 El Niño period and their relationship with Sverdrup transport, *Journal of Geophysical Research C: Oceans*, *v. 108,* 36-1 - 36-17.

Van Aken, H.M., and H. Verbeek, 1988, The hydrography and ventilation of Kau Bay in Halmahera, *Netherlands Journal of Sea Research, v. 22,* 403-412.

van der Weijden, C.H., D. Hoede, S. Shofiya, G.F. de Lange, J.J. Middelburg, and H.A. van der Sloot, 1989, Geochemical characteristics of Kau Bay water, *Netherlands Journal of Sea Research, v. 24*, 583-589, doi:10.1016/0077-7579(89)90135-X.

van Riel, P.M., 1943, The Snellius Expedition in the eastern part of the Netherlands East Indies, 1929-1930, Vol. II, Oceanographic Results, Part V, The bottom water, Introductory remarks and oxygen content, Leiden, E.J. Brill.

Waliser, D.E., and C. Gautier, 1993, A satellite-derived climatology of the ITCZ, *Journal of Climate*, *v. 6,* 2162-2174.

Wang, L., M. Sarnthein, H. Erlenkeuser, J. Grimalt, P. Grootes, S. Heilig, E. Ivanova, M. Kienast, C. Pelejero, and U. Pflaumann, 1999, East Asian monsoon climate during the Late Pleistocene: high-resolution sediment records from the South China Sea, *Marine Geology, v. 156,* 245-284.

Wang, C., and D.B. Enfield, 2001, The tropical western Hemisphere warm pool, *Geophys. Res. Lett., v. 28*, 1635-1638, doi:10.1029/2000GL011763.

Wang, H., and R. Fu, 2000, Winter monthly mean atmospheric anomalies over the north Pacific and north America associated with El Nino SSTs, *J. of Climate, v. 13*, 3435-3447.

Wang, Y., H. Cheng, R. Lawrence Edwards, Y. He, X. Kong, Z. An, J. Wu, M. J. Kelly, C. A. Dykoski, and X. Li, 2005, The Holocene Asian monsoon: Links to solar changes and north Atlantic climate, *Science, v. 308*, doi:10.1126/science.1106296.

Wang, Y., H. Cheng, R. Lawrence Edwards, X. Kong, X. Shao, S. Chen, J. Wu, X. Jiang, X. Wang, and Z. An, 2008, Millennial- and orbital-scale changes in the East Asian monsoon over the past 224,00 years, *Nature, v. 451,* doi:10.1038/nature06692.

Winter, A., A. Almogi-Labin, Y. Erez, E. Halicz, B. Luz, and Z. Reiss, 1983, Salinity tolerance for marine organisms deduced from Red Sea Quaternary record, *Marine Geology, v. 53*, M17-M22.

Wyrtki, K., 1961, Physical oceanography of the Southeast Asian waters, *NAGA Report, v. 2,* 195pp.

Yan, X., C. Ho, Q. Zheng, and V. Klemas, 1992, Temperature and size variabilities of the western Pacific warm pool, *Science, v. 258,* 1643-1645.

Zacherl, D., G. Paradis, D.W. Lea, 2003, Barium and strontium uptake into larval protoconchs and statoliths of the marine neogastropod *Kelletia kelletii*, *Geochemica et Cosmochemica Acta, v. 67, 4091-4067.*

Zhang, C., 1996, Atmospheric intraseasonal variability at the surface in the tropical western Pacific ocean, *Journal of Atmospheric Science, v. 53,* 739-758.

APPENDIX A

Chapter 2 Data

Table A.1. Kau Bay 102GGC and 103MC-F $\delta^{15}N$ (top sample only). Age model calculated using a 300-yr reservoir correction and *Fairbanks et al. (2005)* calibration curve.

Depth, cm	Age, yrBP	$\delta^{15}N$, ‰
0-2 (103MC-F)	0	2.6
0	163.00	3.28
8	225.63	3.77
16	297.21	3.76
24	372.00	3.99
32	450.00	4.47
40	528.00	5.09
48	578.00	5.06
56	628.00	5.08
64	678.00	5.59
72	728.00	4.75
80	770.37	4.66
88	812.74	3.76
96	855.11	4.13
104	897.48	3.66
112	939.85	3.68
120	982.22	3.6
128	1024.59	4.08
136	1066.96	4.08
144	1109.33	4.65
152	1151.70	4.02
160	1189.02	3.97
168	1225.62	4.37
176	1262.21	4.24
184	1298.81	4.11
192	1335.40	4.06
200	1372.00	3.97
208	1419.50	3.69
216	1467.00	3.63
224	1514.50	3.61
232	1562.00	3.81
240	1609.50	3.74
248	1657.00	3.19

256	1704.50	2.74
264	1752.00	2.74
272	1806.00	2.56
280	1860.00	2.48
288	1914.00	2.68
296	1968.00	2.16
304	2022.00	2.72
312	2076.00	2.3
320	2118.12	2.65
328	2160.24	2.61
336	2202.37	2.45
344	2244.49	2.53
352	2286.61	2.5
360	2328.73	2.46
368	2450.78	2.37
376	2584.24	2.42
384	2717.70	2.68
392	2851.16	2.43
400	2984.62	2.84
408	3118.08	2.61
416	3251.54	2.89
424	3385.00	4.1

Table A.2. $\delta^{13}C$ of fatty acid methyl esters (FAMEs, even numbered chains) and alkanes (odd numbered chains), core BJ08-03 102GGC. C_n = carbon chain of *n* number of carbon atoms.

Depth, cm	**C_{34} $\delta^{13}C$ ‰**	**C_{32} $\delta^{13}C$ ‰**	**C_{30} $\delta^{13}C$ ‰**	**C_{28} $\delta^{13}C$ ‰**	**C_{26} $\delta^{13}C$ ‰**	**C_{29} $\delta^{13}C$ ‰**	**C_{31} $\delta^{13}C$ ‰**
1	-33.9	-33	-31.9	-31.7	-27.3	-33.58	-34.75
63	-35.2	-32.9	-32.6	-33.3	-27.2	-33.75	-36.06
87	-32.9	-32.6	-32.8	-34.6	-27.8	-32.38	-34.32
143	-33.3	-33.6	-32.2	-33.7	-25.5	-32.73	-34.21
298	-33.8	-32.6	-31.6	-33.7	-26.9	-31.41	-33.67

Table A.3. Ratio of terrestrial (C_{32}, long chain) to marine (C_{16}, short chain) FAMEs in Kau Bay core BJ08-03 102GGC.

Depth, cm	**$C_{32}/(C_{16}+C_{32})$**
1	0.20
3	0.27
5	0.89
7	0.63
31	0.47
63	0.55
73	0.67
87	0.40
99	0.67
103	0.56
121	0.90
143	0.67
155	0.51
167	0.53
179	0.80
191	0.53
209	0.62
231	0.66
259	0.69
279	0.56
298	0.69
321	0.83
353	0.70
393	0.90
417	0.47
419	0.88
421	0.68

Table A.4. Concentration of FAMEs (ppb) in core 102 GGC.

Depth, cm	C_{14}	C_{16}	C_{18}	C_{20}	C_{22}	C_{24}	C_{26}	C_{28}	C_{30}	C_{32}	C_{34}	C_{36}
1	0.00	0.28	0.00	0.00	0.00	0.74	0.22	0.33	0.19	0.07	0.00	0.33
3	0.28	1.48	0.28	0.06	0.19	0.93	0.76	0.71	0.59	0.54	0.21	0.00
5	0.00	0.07	0.03	0.00	0.09	0.59	0.59	0.60	0.48	0.58	0.35	0.00
7	0.00	0.35	0.07	0.03	0.12	0.68	0.61	0.64	0.45	0.60	0.38	0.00
9	0.00	0.00	0.00	0.00	0.00	0.68	0.35	0.40	0.16	0.05	0.00	0.21
31	0.22	0.53	0.05	0.04	0.11	0.63	0.67	1.11	0.54	0.48	0.24	0.00
47	0.00	0.00	0.00	0.00	0.00	0.94	0.48	1.26	0.43	0.39	2.80	0.42
63	0.08	0.42	0.04	0.00	0.07	0.43	0.51	1.04	0.50	0.51	0.30	0.19
73	0.03	0.41	0.06	0.00	0.11	0.69	0.81	1.00	0.75	0.83	0.46	0.28
87	0.07	1.52	0.06	0.06	0.22	0.95	1.12	1.31	0.91	1.01	0.59	0.37
99	0.00	0.98	0.07	0.03	0.10	0.38	0.52	0.96	1.38	1.95	1.14	0.17
103	0.00	0.31	0.04	0.00	0.16	0.75	0.80	0.92	0.55	0.39	0.16	0.23
121	0.00	0.33	0.04	0.03	0.15	0.92	1.35	2.13	2.22	2.93	1.67	0.00
143	0.04	0.31	0.03	0.02	0.06	0.45	0.56	0.62	0.54	0.63	0.35	0.14
155	0.10	0.37	0.02	0.02	0.06	0.66	0.54	0.58	0.37	0.39	0.23	0.11
167	0.10	0.48	0.07	0.00	0.11	0.79	0.73	0.71	0.49	0.54	0.30	0.22
179	0.10	0.47	0.06	0.06	0.24	1.06	0.98	1.13	1.41	1.94	1.06	0.42
191	0.09	0.32	0.02	0.00	0.05	0.33	0.44	0.55	0.34	0.35	0.19	0.15
209	0.19	0.33	0.02	0.02	0.06	0.37	0.55	0.70	0.48	0.55	0.33	0.16
231	0.00	0.00	0.00	0.00	0.00	0.00	0.00	0.00	0.00	0.00	0.00	0.00
239	0.03	0.13	0.00	0.00	0.03	0.14	0.28	0.39	0.23	0.26	0.13	0.09
259	0.10	0.57	0.06	0.04	0.13	0.77	1.14	1.94	1.15	1.28	0.75	0.31
279	0.00	0.45	0.00	0.00	0.04	0.32	0.57	0.99	0.59	0.58	0.26	0.00
298	0.04	0.29	0.02	0.02	0.06	0.22	0.42	0.63	0.54	0.64	0.43	0.22
321	0.06	0.35	0.03	0.04	0.16	0.47	0.98	1.24	1.30	1.69	1.11	0.48
353	0.12	0.35	0.05	0.03	0.11	0.35	0.49	0.55	0.62	0.83	0.40	0.20
393	0.06	0.35	0.05	0.03	0.09	0.33	0.76	1.23	1.90	3.16	2.01	0.25
417	0.08	0.19	0.02	0.01	0.04	0.23	0.24	0.40	0.19	0.17	0.09	0.21
419	0.01	0.10	0.02	0.01	0.03	0.19	0.31	0.43	0.50	0.74	0.41	0.11
421	0.14	0.70	0.06	0.07	0.24	1.28	1.13	1.27	1.25	1.50	0.93	0.50

Table A.5. Hydrocast Temperature and Salinity from BJ08-03 HC113, Kau Bay.

Water depth, m	Temperature, ˚C	Potential Temperature, ˚C	Salinity, p.s.u.
1	29.30	29.20	34.11
2	29.31	29.30	34.11
3	29.38	29.30	34.11
4	29.44	29.40	34.11
5	29.48	29.40	34.11
6	29.47	29.40	34.11
7	29.44	29.40	34.11
8	29.41	29.40	34.11
9	29.29	29.20	34.11
10	29.31	29.30	34.11
11	29.37	29.30	34.11
12	29.39	29.30	34.11
13	29.36	29.30	34.11
14	29.39	29.30	34.11
15	29.31	29.30	34.11
16	29.11	29.10	34.11
17	29.09	29.00	34.11
18	29.09	29.00	34.11
19	29.09	29.00	34.11
20	29.08	29.00	34.11
21	29.08	29.00	34.11
22	29.08	29.00	34.11
23	29.08	29.00	34.11
24	29.07	29.00	34.12
25	29.03	29.00	34.14
26	28.98	28.90	34.17
27	28.93	28.90	34.19
28	28.89	28.80	34.21
29	28.87	28.80	34.22
30	28.85	28.80	34.23
31	28.85	28.80	34.23
32	28.84	28.80	34.23
33	28.83	28.80	34.24
34	28.81	28.80	34.24
35	28.78	28.70	34.25
36	28.77	28.70	34.26
37	28.76	28.70	34.26
38	28.74	28.70	34.27
39	28.73	28.70	34.27
40	28.72	28.70	34.27

41	28.71	28.60	34.27
42	28.71	28.60	34.27
43	28.71	28.60	34.27
44	28.70	28.60	34.27
45	28.70	28.60	34.27
46	28.70	28.60	34.27
47	28.69	28.60	34.27
48	28.69	28.60	34.27
49	28.69	28.60	34.27
50	28.68	28.60	34.28
51	28.68	28.60	34.28
52	28.67	28.60	34.28
53	28.67	28.60	34.28
54	28.65	28.60	34.29
55	28.65	28.60	34.29
56	28.63	28.60	34.31
57	28.61	28.50	34.33
58	28.60	28.50	34.34
59	28.60	28.50	34.34
60	28.60	28.50	34.34
61	28.59	28.50	34.34
62	28.57	28.50	34.34
63	28.55	28.50	34.34
64	28.54	28.50	34.34
65	28.54	28.50	34.34
66	28.55	28.50	34.34
67	28.55	28.50	34.34
68	28.55	28.50	34.35
69	28.54	28.50	34.34
70	28.54	28.50	34.34
71	28.54	28.50	34.34
72	28.54	28.50	34.35
73	28.53	28.50	34.35
74	28.53	28.50	34.35
75	28.53	28.50	34.35
76	28.53	28.50	34.35
77	28.53	28.50	34.35
78	28.53	28.50	34.35
79	28.53	28.50	34.35
80	28.53	28.50	34.35
81	28.52	28.50	34.35
82	28.52	28.50	34.35
83	28.52	28.40	34.35
84	28.51	28.40	34.35
85	28.50	28.40	34.35

86	28.50	28.40	34.35
87	28.50	28.40	34.36
88	28.51	28.40	34.36
89	28.51	28.40	34.36
90	28.53	28.50	34.38
91	28.54	28.50	34.39
92	28.55	28.50	34.39
93	28.55	28.50	34.39
94	28.55	28.50	34.39
95	28.55	28.50	34.39
96	28.55	28.50	34.39
97	28.55	28.50	34.39
98	28.55	28.50	34.39
99	28.55	28.50	34.40
100	28.55	28.50	34.40
101	28.55	28.50	34.40
102	28.55	28.50	34.40
103	28.55	28.50	34.40
104	28.56	28.50	34.40
105	28.56	28.50	34.41
106	28.56	28.50	34.41
107	28.56	28.50	34.41
108	28.56	28.50	34.41
109	28.55	28.50	34.41
110	28.54	28.50	34.41
111	28.54	28.50	34.40
112	28.54	28.50	34.41
113	28.54	28.50	34.41
114	28.53	28.50	34.41
115	28.53	28.50	34.41
116	28.53	28.40	34.41
117	28.52	28.40	34.41
118	28.52	28.40	34.41
119	28.52	28.40	34.41
120	28.52	28.40	34.41
121	28.52	28.40	34.41
122	28.52	28.40	34.41
123	28.52	28.40	34.41
124	28.53	28.40	34.41
125	28.53	28.50	34.42
126	28.53	28.50	34.41
127	28.53	28.50	34.42
128	28.54	28.50	34.42
129	28.55	28.50	34.43
130	28.55	28.50	34.43

131	28.55	28.50	34.43
132	28.54	28.50	34.43
133	28.54	28.50	34.43
134	28.54	28.50	34.43
135	28.54	28.50	34.43
136	28.54	28.50	34.43
137	28.53	28.50	34.43
138	28.53	28.40	34.43
139	28.53	28.50	34.43
140	28.53	28.40	34.43
141	28.52	28.40	34.43
142	28.52	28.40	34.43
143	28.52	28.40	34.43
144	28.52	28.40	34.43
145	28.52	28.40	34.43
146	28.52	28.40	34.43
147	28.52	28.40	34.43
148	28.52	28.40	34.43
149	28.52	28.40	34.43
150	28.51	28.40	34.43
151	28.51	28.40	34.43
152	28.51	28.40	34.43
153	28.51	28.40	34.43
154	28.49	28.40	34.42
155	28.48	28.40	34.42
156	28.48	28.40	34.42
157	28.48	28.40	34.42
158	28.48	28.40	34.42
159	28.46	28.40	34.41
160	28.45	28.40	34.41
161	28.45	28.40	34.41
162	28.45	28.40	34.41
163	28.45	28.40	34.41
164	28.45	28.40	34.41
165	28.46	28.40	34.41
166	28.48	28.40	34.42
167	28.48	28.40	34.43
168	28.48	28.40	34.43
169	28.48	28.40	34.43
170	28.48	28.40	34.42
171	28.48	28.40	34.43
172	28.48	28.40	34.43
173	28.48	28.40	34.43
174	28.49	28.40	34.43
175	28.49	28.40	34.43

176	28.49	28.40	34.44
177	28.50	28.40	34.44
178	28.50	28.40	34.44
179	28.50	28.40	34.44
180	28.49	28.40	34.44
181	28.49	28.40	34.44
182	28.49	28.40	34.44
183	28.49	28.40	34.44
184	28.49	28.40	34.44
185	28.49	28.40	34.44
186	28.49	28.40	34.44
187	28.49	28.40	34.44
188	28.49	28.40	34.44
189	28.49	28.40	34.44
190	28.48	28.40	34.43
191	28.48	28.40	34.43
192	28.48	28.40	34.43
193	28.47	28.40	34.43
194	28.47	28.40	34.43
195	28.47	28.40	34.43
196	28.47	28.40	34.43
197	28.46	28.40	34.43
198	28.45	28.40	34.42
199	28.44	28.30	34.42
200	28.44	28.30	34.42
201	28.44	28.30	34.42
202	28.44	28.30	34.42
203	28.45	28.30	34.43
204	28.45	28.40	34.43
205	28.45	28.40	34.43
206	28.45	28.30	34.43
207	28.45	28.40	34.43
208	28.46	28.40	34.44
209	28.46	28.40	34.44
210	28.46	28.40	34.44
211	28.47	28.40	34.44
212	28.47	28.40	34.44
213	28.46	28.40	34.44
214	28.46	28.40	34.43
215	28.46	28.40	34.43
216	28.46	28.40	34.43
217	28.45	28.30	34.43
218	28.43	28.30	34.43
219	28.43	28.30	34.43
220	28.42	28.30	34.42

221	28.42	28.30	34.42
222	28.41	28.30	34.42
223	28.40	28.30	34.42
224	28.40	28.30	34.41
225	28.40	28.30	34.41
226	28.40	28.30	34.41
227	28.40	28.30	34.41
228	28.39	28.30	34.41
229	28.39	28.30	34.41
230	28.39	28.30	34.41
231	28.39	28.30	34.41
232	28.39	28.30	34.41
233	28.39	28.30	34.41
234	28.39	28.30	34.41
235	28.39	28.30	34.41
236	28.39	28.30	34.41
237	28.39	28.30	34.41
238	28.39	28.30	34.41
239	28.39	28.30	34.41
240	28.39	28.30	34.41
241	28.39	28.30	34.41
242	28.38	28.30	34.41
243	28.38	28.30	34.41
244	28.37	28.30	34.41
245	28.37	28.30	34.41
246	28.37	28.30	34.41
247	28.37	28.30	34.41
248	28.37	28.30	34.41
249	28.37	28.30	34.41
250	28.37	28.30	34.41
251	28.37	28.30	34.41
252	28.37	28.30	34.41
253	28.37	28.30	34.41
254	28.37	28.30	34.41
255	28.37	28.30	34.41
256	28.37	28.30	34.41
257	28.37	28.30	34.41
258	28.37	28.30	34.41
259	28.38	28.30	34.41
260	28.38	28.30	34.41
261	28.38	28.30	34.41
262	28.38	28.30	34.42
263	28.39	28.30	34.42
264	28.39	28.30	34.42
265	28.39	28.30	34.42

266	28.39	28.30	34.42
267	28.39	28.30	34.42
268	28.39	28.30	34.42
269	28.38	28.30	34.42
270	28.38	28.30	34.42
271	28.38	28.30	34.42
272	28.38	28.30	34.42
273	28.38	28.30	34.42
274	28.38	28.30	34.42
275	28.37	28.30	34.41
276	28.37	28.30	34.41
277	28.37	28.30	34.41
278	28.37	28.30	34.41
279	28.37	28.20	34.41
280	28.37	28.20	34.41
281	28.36	28.20	34.41
282	28.36	28.20	34.41
283	28.36	28.20	34.41
284	28.36	28.20	34.41
285	28.36	28.20	34.41
286	28.36	28.20	34.41
287	28.36	28.20	34.41
288	28.36	28.20	34.41
289	28.36	28.20	34.41
290	28.35	28.20	34.41
291	28.35	28.20	34.41
292	28.35	28.20	34.41
293	28.35	28.20	34.41
294	28.35	28.20	34.41
295	28.37	28.20	34.42
296	28.37	28.30	34.42
297	28.37	28.30	34.42
298	28.37	28.30	34.42
299	28.37	28.30	34.42
300	28.37	28.30	34.42
301	28.37	28.30	34.42
302	28.37	28.20	34.42
303	28.36	28.20	34.42
304	28.36	28.20	34.42
305	28.36	28.20	34.41
306	28.36	28.20	34.41
307	28.36	28.20	34.41
308	28.36	28.20	34.41
309	28.36	28.20	34.41
310	28.36	28.20	34.41

311	28.35	28.20	34.41
312	28.35	28.20	34.41
313	28.35	28.20	34.41
314	28.35	28.20	34.41
315	28.35	28.20	34.41
316	28.36	28.20	34.41
317	28.36	28.20	34.42
318	28.36	28.20	34.42
319	28.36	28.20	34.42
320	28.36	28.20	34.42
321	28.36	28.20	34.42
322	28.36	28.20	34.42
323	28.36	28.20	34.42
324	28.36	28.20	34.42
325	28.36	28.20	34.42
326	28.36	28.20	34.42
327	28.36	28.20	34.42
328	28.35	28.20	34.42
329	28.35	28.20	34.41
330	28.35	28.20	34.41
331	28.34	28.20	34.41
332	28.34	28.20	34.41
333	28.33	28.20	34.41
334	28.33	28.20	34.41
335	28.33	28.20	34.41
336	28.33	28.20	34.41
337	28.33	28.20	34.41
338	28.33	28.20	34.41
339	28.33	28.20	34.41
340	28.33	28.20	34.41
341	28.33	28.20	34.41
342	28.33	28.20	34.41
343	28.33	28.20	34.41
344	28.33	28.20	34.41
345	28.33	28.20	34.41
346	28.33	28.20	34.41
347	28.33	28.20	34.41
348	28.33	28.20	34.41
349	28.34	28.20	34.41
350	28.34	28.20	34.41
351	28.34	28.20	34.41
352	28.34	28.20	34.41
353	28.34	28.20	34.42
354	28.34	28.20	34.41
355	28.33	28.20	34.41

356	28.32	28.20	34.41
357	28.32	28.20	34.41
358	28.32	28.20	34.41
359	28.32	28.20	34.41
360	28.31	28.20	34.41
361	28.31	28.20	34.41
362	28.31	28.20	34.40
363	28.31	28.20	34.40
364	28.31	28.20	34.40
365	28.31	28.20	34.40
366	28.31	28.20	34.40
367	28.31	28.20	34.40
368	28.31	28.20	34.40
369	28.30	28.20	34.40
370	28.30	28.20	34.40
371	28.29	28.20	34.40
372	28.29	28.20	34.40
373	28.29	28.20	34.40
374	28.29	28.20	34.40
375	28.30	28.20	34.40
376	28.30	28.20	34.40
377	28.29	28.20	34.40
378	28.30	28.20	34.40
379	28.30	28.20	34.40
380	28.30	28.20	34.40
381	28.30	28.20	34.40
382	28.30	28.20	34.41
383	28.31	28.20	34.41
384	28.30	28.20	34.40
385	28.30	28.20	34.40
386	28.30	28.20	34.40
387	28.30	28.20	34.40
388	28.30	28.20	34.40
389	28.30	28.20	34.40
390	28.30	28.20	34.41
391	28.30	28.20	34.41
392	28.30	28.20	34.41
393	28.30	28.20	34.41
394	28.30	28.20	34.41
395	28.30	28.20	34.41
396	28.30	28.20	34.41
397	28.30	28.20	34.41
398	28.30	28.20	34.41
399	28.30	28.20	34.41
400	28.30	28.20	34.41

401	28.30	28.20	34.41
402	28.30	28.20	34.41
403	28.30	28.20	34.41
404	28.30	28.20	34.41
405	28.30	28.20	34.41
406	28.30	28.20	34.41
407	28.30	28.20	34.41
408	28.31	28.20	34.41
409	28.31	28.20	34.41
410	28.31	28.20	34.41
411	28.31	28.20	34.41
412	28.32	28.20	34.41
413	28.32	28.20	34.42
414	28.32	28.20	34.42
415	28.32	28.20	34.42
416	28.32	28.20	34.42
417	28.32	28.20	34.42
418	28.33	28.20	34.42
419	28.33	28.20	34.42
420	28.33	28.20	34.42
421	28.33	28.20	34.43
422	28.34	28.20	34.43
423	28.34	28.20	34.43
424	28.34	28.20	34.43
425	28.35	28.20	34.43
426	28.35	28.20	34.43
427	28.35	28.20	34.43
428	28.35	28.20	34.43
429	28.35	28.20	34.43
430	28.35	28.20	34.43
431	28.35	28.20	34.43
432	28.35	28.20	34.43
433	28.35	28.20	34.43
434	28.35	28.20	34.44
435	28.36	28.20	34.44
436	28.36	28.20	34.44
437	28.36	28.20	34.44
438	28.36	28.20	34.44
439	28.36	28.20	34.44
440	28.36	28.20	34.44
441	28.36	28.20	34.44
442	28.37	28.20	34.45
443	28.37	28.20	34.45
444	28.37	28.20	34.45
445	28.37	28.20	34.45

446	28.37	28.20	34.45
447	28.37	28.20	34.45
448	28.37	28.20	34.45
449	28.37	28.20	34.45
450	28.37	28.20	34.45
451	28.37	28.20	34.45
452	28.37	28.20	34.45
453	28.37	28.20	34.45
454	28.37	28.20	34.45
455	28.37	28.20	34.45
456	28.37	28.20	34.45
457	28.37	28.20	34.45
458	28.37	28.20	34.45
459	28.37	28.20	34.45
460	28.37	28.20	34.45
461	28.37	28.20	34.45
462	28.37	28.20	34.45
463	28.37	28.20	34.45
464	28.37	28.20	34.45
465	28.37	28.20	34.45
466	28.37	28.20	34.45

Table A.5. Oxygen concentration in Kau Bay from the BJ08-03 cruise in 2003.

Depth, m	**[O2] µM**
20	186
60	79
75	70
100	65
150	56
200	*26*
300	41
350	34
400	30
425	9
450	4
465	3
466	0

Table A.6. Kau Bay water column NO_3^- concentration, $\delta^{15}N\ NO_3^-$, and $\delta^{18}O\ NO_3^-$ from 2003, BJ08-03 cruise.

Depth (m)	$[NO_3^-]$ µM	$\delta^{15}N\ NO_3^-$	$\delta^{18}O\ NO_3^-$
444.05	2.7	8.39	
424.94	4.8	8.77	8.82
400.28	6.8	6.18	9.16
400.28		6.72	
350.36	7.9	6.26	2.70
300.00	8.6	5.82	4.29
200.22	9.0	5.82	2.74
150.25	9.1	5.59	3.41
99.67		5.65	0.94
99.67	9.5	5.33	
80.44	9.3	5.38	1.89
			2.44
59.55	9.1	5.06	0.72
14.67	0.6		

APPENDIX B
Chapter 3 data

Table B.1. $\delta^{13}C$ and $\delta^{18}O$ of *Creseis acicula* from core 102GGC. The age model includes a 200 year reservoir correction and Fairbanks0107 calibration (*Fairbanks et al., 2005*).

Depth, cm	Age, yrBP	$\delta^{13}C$‰	$\delta^{18}O$‰
2	451.50	0.81	-1.54
6	466.50	0.98	-1.06
8	474.00	0.33	-1.46
10	481.50	0.71	-1.34
12	489.00	0.97	-1.38
14	496.50	0.81	-1.32
16	504.00	0.67	-1.51
18	511.50	0.71	-1.52
20	519.00	0.79	-1.35
22	526.50	0.49	-1.27
23	530.25	0.58	-1.45
26	541.50	0.87	-1.38
28	549.00	0.32	-1.71
30	556.50	0.36	-1.76
32	564.00	0.80	-1.70
35	575.25	0.49	-1.09
38	586.50	0.38	-1.63
40	594.00	0.37	-1.68
44	624.38	0.71	-1.45
46	639.56	0.28	-1.73
48	654.75	0.23	-1.55
52	685.13	0.43	-1.01
54	700.31	0.23	-1.45
56	715.50	-0.06	-1.67
58	730.69	0.54	-1.09
60	745.88	0.32	-1.61
62	761.06	0.37	-1.37
64	776.25	0.03	-1.73
67	799.03	0.12	-1.41
68	806.63	0.11	-1.42
71	829.41	0.19	-1.37
72	837.00	-0.23	-1.69
76	858.19	-0.17	-1.61
78	868.78	0.42	-1.27
80	879.37	-0.06	-1.85
82	889.96	-0.42	-1.57
84	900.56	0.33	-1.47
86	911.15	0.41	-1.52

88	921.74	0.46	-1.52
92	942.93	0.37	-1.71
94	953.52	0.38	-1.65
96	964.11	0.46	-1.71
100	985.30	0.55	-1.40
104	1006.48	0.46	-1.45
106	1017.07	0.65	-1.41
108	1027.67	0.09	-1.97
110	1038.26	0.33	-1.81
112	1048.85	0.65	-1.62
114	1059.44	1.03	-1.51
116	1070.04	0.25	-1.15
118	1080.63	0.40	-1.61
120	1091.22	0.24	-1.44
122	1101.81	0.62	-1.55
124	1112.41	0.46	-0.91
126	1123.00	0.49	-1.04
128	1133.59	0.28	-1.67
130	1144.19	0.56	-1.13
132	1154.78	0.65	-1.42
134	1165.37	0.71	-1.60
136	1175.96	-0.34	-2.13
138	1186.56	-0.04	-1.60
140	1197.15	-0.16	-1.74
142	1207.74	0.41	-1.79
144	1218.33	0.09	-1.81
148	1239.52	0.73	-1.57
150	1250.11	0.46	-1.44
152	1260.70	0.86	-1.46
154	1270.49	0.16	-2.04
156	1279.47	0.44	-1.82
158	1288.45	0.65	-1.32
160	1297.43	0.26	-1.85
162	1306.40	0.61	-1.35
164	1315.38	0.55	-1.42
166	1324.36	0.55	-1.21
170	1342.32	0.48	-1.56
172	1351.30	0.37	-1.56
174	1360.28	0.86	-1.29
176	1369.26	0.12	-1.57
178	1378.23	0.53	-1.53
180	1387.21	0.14	-1.80
182	1396.19	0.35	-1.70
184	1405.17	0.19	-1.65
186	1414.15	0.16	-1.66

188	1423.13	0.30	-1.75
190	1432.11	0.45	-1.67
192	1441.09	0.18	-1.60
194	1450.06	0.55	-1.73
196	1459.04	0.19	-1.53
198	1468.02	0.61	-1.68
202	1489.09	0.72	-1.74
204	1501.19	0.61	-1.45
206	1513.28	0.30	-1.37
210	1537.47	0.20	-1.58
212	1549.56	0.28	-1.67
214	1561.66	0.02	-1.88
216	1573.75	-0.26	-1.86
218	1585.84	0.02	-1.97
220	1597.94	0.41	-1.67
222	1610.03	0.01	-1.29
224	1622.13	-0.39	-1.51
226	1634.22	-0.03	-1.39
228	1646.31	-0.11	-1.41
230	1658.41	0.06	-1.41
232	1670.50	-0.27	-1.54
234	1682.59	0.38	-1.23
236	1694.69	0.31	-1.48
238	1706.78	0.38	-1.22
240	1718.88	-0.01	-1.53
242	1730.97	0.55	-1.46
244	1743.06	0.24	-1.49
246	1755.16	0.06	-1.86
248	1767.25	0.05	-1.64
250	1779.34	0.08	-1.70
252	1791.44	-0.12	-1.31
254	1803.53	-0.16	-1.89
256	1815.63	-0.31	-1.83
258	1827.72	0.31	-1.69
260	1839.81	0.27	-1.56
262	1851.91	0.05	-1.72
264	1864.00	0.31	-1.54
266	1878.75	0.45	-1.57
268	1893.50	-0.15	-1.84
270	1908.25	-0.12	-1.92
272	1923.00	0.11	-1.80
274	1937.75	0.52	-1.44
276	1952.50	-0.03	-1.74
278	1967.25	-0.09	-1.81
280	1982.00	-0.29	-1.74

282	1996.75	0.31	-1.75
284	2011.50	0.25	-1.72
286	2026.25	0.37	-1.69
288	2041.00	0.05	-1.52
292	2070.50	0.22	-1.77
293	2077.88	0.45	-1.63
296	2100.00	-0.10	-1.91
299	2122.13	0.43	-2.11
300	2129.50	0.27	-1.83
302	2144.25	-0.17	-1.77
304	2159.00	0.07	-2.15
306	2173.75	0.39	-1.88
308	2188.50	0.10	-2.15
310	2203.25	0.21	-2.05
314	2225.31	0.50	-1.48
316	2232.61	0.36	-2.21
318	2239.92	0.23	-2.14
320	2247.22	-0.17	-2.40
322	2254.53	-0.34	-2.37
324	2261.84	-0.39	-2.24
326	2269.14	0.20	-2.54
328	2276.45	-0.23	-2.11
332	2291.06	-0.15	-1.79
334	2298.37	0.58	-1.72
336	2305.67	-0.13	-2.15
338	2312.98	-0.51	-2.10
340	2320.29	0.62	-2.20
344	2334.90	0.34	-2.06
346	2342.20	0.18	-2.18
348	2349.51	-0.03	-1.86
350	2356.82	0.03	-2.35
352	2364.12	0.08	-2.37
354	2371.43	0.10	-2.10
356	2378.73	-0.39	-1.77
358	2386.04	0.08	-1.89
360	2393.35	0.25	-2.45
362	2414.10	0.36	-2.18
364	2448.29	-0.02	-2.01
366	2482.48	-0.68	-2.29
368	2516.67	0.33	-2.46
370	2550.86	0.44	-2.27
374	2619.24	0.23	-1.85
376	2653.43	0.00	-2.30
378	2687.62	0.09	-2.01
380	2721.81	0.47	-1.86

382	2756.00	0.25	-2.09
384	2790.19	0.39	-1.73
388	2858.57	-0.47	-2.30
390	2892.76	0.17	-1.78
392	2926.95	0.21	-2.43
394	2961.14	-0.26	-1.64
396	2995.33	0.38	-1.76
398	3029.52	-0.36	-1.71
400	3063.71	0.15	-2.14
402	3097.90	0.13	-1.53
404	3132.10	-0.06	-2.09
408	3200.48	-0.55	-2.14
414	3303.05	1.02	-1.42
416	3337.24	0.13	-1.96
420	3405.62	0.64	-1.33
422	3439.81	0.55	-1.30

Table B.2. Sr/Ca of *Creseis acicula* from core 102GGC. The age model includes a 200 year reservoir correction and Fairbanks0107 calibration (*Fairbanks et al., 2005*).

Depth, cm	**Age, yrBP**	**Sr/Ca mmol/mol**
0	444.00	0.96
2	451.50	0.92
4	459.00	1.06
6	466.50	0.88
8	474.00	1.01
10	481.50	0.93
12	489.00	0.96
14	496.50	1.03
16	504.00	1.00
18	511.50	1.05
20	519.00	1.14
22	526.50	1.11
23	530.25	1.17
26	541.50	1.03
28	549.00	1.08
30	556.50	1.03
32	564.00	0.90
34	571.50	0.97
35	575.25	1.01
38	586.50	1.04
42	609.19	1.13

44	624.38	1.11
46	639.56	1.03
48	654.75	0.96
50	669.94	0.91
52	685.13	1.04
54	700.31	0.93
56	715.50	1.24
58	730.69	0.98
60	745.88	1.20
62	761.06	1.15
64	776.25	1.38
67	799.03	1.28
68	806.63	1.17
71	829.41	1.34
72	837.00	1.32
76	858.19	1.08
78	868.78	1.02
80	879.37	0.99
84	900.56	1.05
86	911.15	1.01
92	942.93	0.97
94	953.52	1.02
96	964.11	1.14
100	985.30	1.02
104	1006.48	1.12
106	1017.07	1.05
108	1027.67	0.93
110	1038.26	0.99
112	1048.85	0.98
114	1059.44	1.00
116	1070.04	0.95
118	1080.63	0.94
120	1091.22	1.06
122	1101.81	0.99
124	1112.41	0.94
126	1123.00	0.99
128	1133.59	1.01
130	1144.19	1.10
132	1154.78	1.06
134	1165.37	0.97
136	1175.96	1.25
138	1186.56	1.08
140	1197.15	1.04
142	1207.74	0.94
144	1218.33	0.94

148	1239.52	1.17
150	1250.11	0.92
152	1260.70	0.90
154	1270.49	0.86
156	1279.47	0.84
158	1288.45	0.93
160	1297.43	1.11
162	1306.40	0.91
164	1315.38	0.89
166	1324.36	0.84
170	1342.32	0.86
172	1351.30	1.00
174	1360.28	1.12
176	1369.26	0.96
178	1378.23	0.92
180	1387.21	0.90
182	1396.19	1.02
184	1405.17	0.96
186	1414.15	1.00
188	1423.13	0.89
190	1432.11	0.98
192	1441.09	0.97
194	1450.06	1.18
196	1459.04	0.95
198	1468.02	1.12
202	1489.09	1.07
204	1501.19	1.06
206	1513.28	1.13
208	1525.38	1.22
210	1537.47	1.15
212	1549.56	1.21
214	1561.66	1.16
216	1573.75	1.73
218	1585.84	1.21
220	1597.94	1.15
222	1610.03	1.16
224	1622.13	1.43
226	1634.22	1.20
228	1646.31	1.15
230	1658.41	1.28
232	1670.50	1.33
234	1682.59	1.16
236	1694.69	1.16
238	1706.78	1.23
240	1718.88	1.13

242	1730.97	1.03
244	1743.06	1.16
246	1755.16	1.07
248	1767.25	1.28
250	1779.34	1.04
252	1791.44	1.16
254	1803.53	1.19
256	1815.63	1.42
258	1827.72	1.01
260	1839.81	0.97
262	1851.91	1.04
266	1878.75	1.02
268	1893.50	1.00
270	1908.25	0.94
272	1923.00	1.32
274	1937.75	1.12
276	1952.50	1.00
278	1967.25	0.94
280	1982.00	1.32
282	1996.75	1.03
284	2011.50	1.09
286	2026.25	0.95
288	2041.00	1.02
292	2070.50	1.00
296	2100.00	0.92
299	2122.13	0.98
300	2129.50	1.06
302	2144.25	1.01
304	2159.00	1.09
306	2173.75	0.99
308	2188.50	0.90
310	2203.25	0.87
314	2225.31	1.00
316	2232.61	1.07
318	2239.92	1.06
320	2247.22	0.93
322	2254.53	0.95
324	2261.84	0.88
334	2298.37	0.91
336	2305.67	0.97
338	2312.98	0.94
340	2320.29	0.87
342	2327.59	0.95
344	2334.90	0.97
346	2342.20	0.95

348	2349.51	0.85
350	2356.82	0.94
352	2364.12	0.75
354	2371.43	0.92
356	2378.73	0.95
358	2386.04	0.90
360	2393.35	0.88
362	2414.10	0.99
364	2448.29	0.92
366	2482.48	0.91
368	2516.67	0.93
370	2550.86	0.84
372	2585.05	0.85
374	2619.24	0.93
376	2653.43	0.82
378	2687.62	1.01
380	2721.81	0.97
382	2756.00	0.99
384	2790.19	1.19
386	2824.38	0.88
388	2858.57	1.09
390	2892.76	1.12
392	2926.95	1.06
394	2961.14	0.97
396	2995.33	0.98
398	3029.52	0.95
402	3097.90	1.00
404	3132.10	0.90
420	3405.62	1.00
422	3439.81	1.20

Table B.3. Kau Bay multi-core 103MC-F $\delta^{13}C$ and $\delta^{18}O$. The age model includes a 200 year reservoir correction and Fairbanks0107 calibration (*Fairbanks et al., 2005*).

Depth, cm	Age, yrBP	$\delta^{13}C$ ‰	$\delta^{18}O$ ‰
2	21.59	-0.19	-1.61
8	86.37	-0.23	-1.70
12	129.55	0.40	-1.84
15	161.94	-0.04	-1.95
18	194.33	0.26	-1.77
21	226.71	0.59	-1.52
24	259.10	1.11	-0.93
27	291.49	0.77	-1.72
30	323.88	0.90	-1.34
33	356.27	0.66	-1.43
37	399.45	0.60	-0.96
40	431.84	0.59	-1.48
43	464.22	0.65	-1.41
49	529.00	0.60	-1.71
52	561.39	0.70	-1.65
56	604.57	0.87	-1.35

Table B.4. Kau Bay multi-core 103MC-F Sr/Ca. The age model includes a 200 year reservoir correction and Fairbanks0107 calibration (*Fairbanks et al., 2005*).

Depth, cm	Age, yrBP	Sr/Ca mmol/mol
2	21.59	0.92
8	86.37	0.96
12	129.55	0.98
15	161.94	0.99
18	194.33	1.03
21	226.71	0.99
24	259.10	1.18
27	291.49	1.04
30	323.88	1.12
33	356.27	1.15
37	399.45	1.16
40	431.84	1.11
43	464.22	0.98
46	496.61	1.31
49	529.00	1.03
52	561.39	
53	572.18	1.06
56	604.57	1.19

APPENDIX C
Chapter 4 Data

Table C.1. $\delta^{13}C$ and $\delta^{18}O$ of the foraminifera *Neogloboquadrina dutertrei* from Sulu Sea core ODP769A.

Depth, cm	Age, kyr	$\delta^{13}C$ ‰, *N. dutertrei*	$\delta^{13}C$ ‰, *N. dutertrei* replicate	$\delta^{18}O$ ‰, *N. dutertrei*	$\delta^{18}O$ ‰, *N. dutertrei* replicate
25	2.31	1.319	1.656	-1.513	-1.517
55	5.09	1.295		-1.336	
85	7.87	1.301		-1.215	
114	10.22	0.535		-0.480	
145	12.04				
175	13.93	1.301		-0.483	
205	15.81	1.707		-0.433	
235	17.69	1.161		-0.752	
265	21.54	1.517		-0.462	
295	26.37		1.200		-0.802
325	31.20	0.923		-0.806	
360	36.84	1.137		-0.539	
390	41.67	0.984		-0.963	
420	46.5	1.266		-0.826	
459	52.78	1.021		-1.303	
499	59	0.634		-0.970	
539	65	1.015		-0.524	
559	68	1.595	1.234	-0.641	-0.597
602	74.45	1.316		-1.192	
639	80	1.400		-1.272	
679	88	0.998		-1.230	
719	96	1.316		-0.845	
760	103.5	1.081		-1.051	
822	113.7	0.740	0.863	-1.149	-1.401
860	120	0.602		-1.496	
900	124.8	0.804		-1.370	
940	129.6	0.773		-1.019	
980	133.7	0.759		-0.661	
1010	136.3	1.044		-0.933	
1050	139.8	0.833		-0.857	
1090	143.2	0.823		-0.547	
1130	146.7	0.842	0.648	-0.648	-0.480
1160	149.3	0.592		-0.622	
1200	153.5	0.514		-0.545	
1240	158.6	0.360		-0.511	

1280	163.7	0.900		-0.815	
1310	167.5	0.701		-0.983	
1350	173.5	0.814		-0.933	
1390	180.5	0.985		-1.014	
1430	186.7	0.696	0.831	-1.188	-1.217
1460	190.7	0.243		-1.138	
1500	196	1.140		-1.097	
1540	199.6	0.861		-0.986	
1580	203.3	0.848		-1.174	
1610	206	1.237		-0.826	
1650	210.4	1.097		-1.195	
1690	214.8	1.138		-1.552	
1730	218.4	0.402		-1.201	
1760	220.6	0.683	0.543	-0.514	-0.865
1800	223.4	0.482		-0.921	
1837	226.0	0.627		-0.927	
1870	229.2	0.703		-1.089	
1910	233.7	0.736		-1.456	
1950	238.7	0.506		-0.884	
1989	243.9	0.707		-0.811	
2030	249.3	0.612		-0.810	
2070	254.7	0.288	0.917	-0.627	-0.662
2110	260	0.352		-1.248	
2150	265.3	0.496		-1.031	
2190	270.5	0.843		-0.850	
2250	278.5	0.769		-1.064	
2289	283.6	1.108		-1.054	
2330	289	0.952		-1.314	
2370	292.8	0.543		-1.163	
2410	296.6	0.696	0.733	-0.855	-1.089
2450	300.5	0.632		-1.256	
2490	304.3	0.629		-1.379	
2530	308.1	0.754		-1.151	
2570	312.5	0.548		-1.396	
2610	317.5	1.171		-0.900	
2650	322.5	0.775		-1.165	
2688	327.2	0.634		-1.586	
2730	332.2	0.423		-1.303	
2773	336.2	0.584		-0.480	
2800	341.3	0.712	0.551	-0.766	-0.512
2840	350.4	0.368		-0.623	
2880	355.5	0.608		-0.614	
2920	357.5	0.898		-0.479	
2958	359.4	0.890		-0.799	
3006	361.8	0.860		-0.939	

3039	363.4	1.027		-0.862	
3080	365.5	0.835		-1.031	
3120	367.5	1.170	1.161	-0.860	-0.694
3160	369.5	0.901		-1.276	
3200	371.5	1.085		-0.668	
3240	373.5	0.804		-1.427	
3280	376	1.018		-0.616	
3320	380	1.115		-1.523	
3360	384	1.045		-1.072	
3400	388	0.392		-0.833	
3440	392	0.132	0.279	-0.520	-0.807
3480	396	0.965		-1.097	
3520	400	0.237		-0.777	
3559	403.9	0.665		-0.363	
3600	419.5	0.578		-0.534	
3639	435.2	0.291		-0.491	
3680	441.2	0.569		-0.386	
3710	445.6	0.682		-0.316	
3750	451.4	0.811		-0.647	
3790	457.1	1.231		-0.825	
3830	462.9	0.946	1.036	-0.839	-0.911
3870	468.7	1.357		-0.829	
3910	474.5	0.608		-0.784	
3950	480.2	0.937		-1.212	
3989	485.9	0.623		-0.799	
4030	491.8	1.145		-1.096	
4070	497.6	0.758		-0.663	
4110	502.5	1.098	0.931	-0.710	-0.616
4150	504.6				
4230	508.8	0.879	1.168	-0.861	-0.885
4270	510.9	1.071		-0.731	
4310	513	1.085		-1.270	
4330	514	0.860		-1.068	
4390	517.1	1.146		-0.312	
4430	519.2	0.914		-1.030	
4470	521.3	0.804		-0.893	
4510	523.4	0.967	0.923	-0.998	-0.841
4550	526.4	1.100		-0.669	
4589	531.7	1.008		-1.299	
4630	537.5	1.006		-1.010	
4670	543.0	0.627		-0.862	
4710	548.6	0.528		-0.667	
4750	552.7	0.739		-0.761	
4789	556.165	0.611		-0.915	

4830	559.8	0.740		-0.940	
4870	563.3	1.095		-0.997	
4910	567	0.935	0.765	-1.619	-1.452
4950	570.5	0.760		-0.965	
4990	574.1	1.054		-0.951	
5030	577.8	0.711		-1.215	
5070	581.7	0.716		-1.388	
5110	585.5	0.710		-1.064	
5150	589.4	0.586		-1.098	
5190	593.2	0.862		-1.352	
5230	597.1	0.684	0.672	-1.664	-1.557
5270	600.8	0.991		-1.218	
5310	604.2	0.675		-0.998	
5410	612.7	0.206		-1.227	
5450	616.1	0.299		-0.580	
5490	619.7	0.346		-0.303	
5530	623.4	0.420		-0.403	
5570	627.1	0.797		-0.840	
5610	637.4	0.181	0.156	-0.258	-0.253
5641	647.2	0.469		-1.354	
5680	659.5	0.421		-0.652	
5723	670.1	0.635		-0.770	
5769	674.4	0.991		-0.917	
5800	677.2	1.057		-0.708	
5840	680.8	1.215		-1.134	
5870	683.5	0.919		-1.098	
5900	686.3	0.465		-1.022	
5941	690.0	0.407		-1.106	
5980	693.6	0.715	0.518	-0.569	-0.696
6023	697.5	0.824		-0.931	
6060	703.0	0.926		-0.968	
6100	714.4	1.162		-0.935	
6140	725.7	0.948		-1.089	
6180	737.0	0.956		-0.796	
6220	748.3	0.831		-1.430	
6280	765.3	0.467		-1.026	
6320	776.6	0.436	0.385	-0.431	-0.399
6360	787.9	0.855		-0.652	
6400	799.2	0.900		-0.409	
6440	810.5	0.886		-1.046	

Table C.2. $\delta^{13}C$ and $\delta^{18}O$ of the foraminifera *Pulleniatina obliquiloculata* from Sulu Sea core ODP769A.

Depth, cm	Age, kyr	$\delta^{13}C$ ‰, *P. obliquiloculata*	$\delta^{13}C$ ‰, *P. obliquiloculata* replicate	$\delta^{18}O$ ‰, *P. obliquiloculata*	$\delta^{18}O$ ‰, *P. obliquiloculata* replicate
25	2.31	1.082	1.027	-1.795	-1.909
55	5.09	1.121		-1.789	
85	7.87	0.809		-1.504	
114	10.22	0.573		-1.283	
145	12.04	0.504		-0.626	
175	13.93				
205	15.81	0.799		-0.391	
235	17.69	0.814		-0.362	
265	21.54	0.805		-0.861	
295	26.37	0.802	0.756	-0.568	-0.733
325	31.20	0.854		-0.802	
360	36.84	0.888		-0.798	
390	41.67	0.768		-0.901	
420	46.5	0.900		-0.843	
459	52.78	0.783		-0.865	
499	59	0.576		-1.014	
539	65	0.644		-0.733	
559	68	0.935	0.861	-0.482	-1.002
602	74.45	0.761		-0.965	
639	80	0.954		-1.432	
679	88	0.785		-1.376	
719	96	0.910		-1.125	
760	103.5	0.785		-1.400	
822	113.7	0.791	0.648	-1.339	-1.295
860	120	0.793		-1.786	
900	124.8	0.385		-1.569	
940	129.6	0.167		-1.008	
980	133.7	0.285		-0.777	
1010	136.3	0.382		-0.799	
1050	139.8	0.507		-0.490	
1090	143.2	0.567		-0.426	
1130	146.7	0.650	0.536	-0.200	-0.617
1160	149.3	0.580		-0.654	
1200	153.5	0.329		-0.655	
1240	158.6	0.478		-0.441	
1280	163.7	0.296		-0.878	
1310	167.5	0.559		-1.137	
1350	173.5	0.478		-0.731	
1390	180.5	0.557		-1.031	

1430	186.7	0.623	0.542	-0.848	-1.072
1460	190.7	0.799		-0.968	
1500	196	0.507		-1.114	
1540	199.6	1.018		-1.087	
1580	203.3	0.586		-1.144	
1610	206	0.796		-1.025	
1650	210.4	0.711		-1.217	
1690	214.8	0.850		-1.133	
1730	218.4	0.808		-1.148	
1760	220.6	0.247	0.398	-0.987	-1.107
1800	223.4	0.530		-1.491	
1837	226.0	0.281		-0.945	
1870	229.2	0.475		-1.435	
1910	233.7	0.804		-1.279	
1950	238.7	0.446		-1.478	
1989	243.9	0.429		-0.929	
2030	249.3	0.379		-0.882	
2070	254.7	0.508	0.588	-0.836	-0.480
2110	260	0.446		-0.823	
2150	265.3	0.392		-1.158	
2190	270.5	0.293		-0.912	
2250	278.5	0.736		-1.188	
2289	283.6	0.725		-1.061	
2330	289	0.675		-1.413	
2370	292.8	0.737		-1.228	
2410	296.6	0.917	0.826	-0.921	-1.260
2450	300.5	0.728		-1.141	
2490	304.3	0.640		-1.129	
2530	308.1	0.757		-0.770	
2570	312.5	0.766		-1.020	
2610	317.5	0.592		-1.202	
2650	322.5	0.776		-1.575	
2688	327.2	0.684		-1.665	
2730	332.2	0.435		-1.440	
2773	336.2	0.241		-0.408	
2800	341.3	0.538	0.786	-1.239	-1.307
2840	350.4	0.599		-0.897	
2880	355.5	0.396		-0.883	
2920	357.5	0.744		-1.178	
2958	359.4	0.711		-0.884	
3006	361.8	0.699		-0.942	
3039	363.4	0.718		-1.153	
3080	365.5	0.740		-1.399	
3120	367.5	0.817	0.656	-0.926	-0.960
3160	369.5	0.634		-0.990	

3200	371.5	0.853		-1.014	
3240	373.5	0.418		-1.502	
3280	376	1.049		-1.010	
3320	380	0.961		-1.530	
3360	384	0.815		-1.555	
3400	388	0.522		-1.277	
3440	392	0.742	0.520	-1.377	-1.256
3480	396	0.845		-1.149	
3520	400	0.127		-0.770	
3559	403.9	0.343		-0.379	
3600	419.5	0.629		-0.236	
3639	435.2	0.657		-0.582	
3680	441.2	0.630		-0.581	
3710	445.6	0.435		-0.590	
3750	451.4	0.645		-0.492	
3790	457.1	1.153		-0.671	
3830	462.9	0.882	1.015	-0.668	-0.985
3870	468.7	1.549		-0.883	
3910	474.5	1.355		-0.849	
3950	480.2	0.939		-0.839	
3989	485.9	1.236		-0.463	
4030	491.8	1.215		-0.979	
4070	497.6	0.922		-0.713	
4110	502.5	0.804		-0.706	
4150	504.6	1.042	1.119	-0.726	-0.709
4230	508.8	1.560		-0.861	
4270	510.9	1.287		-1.101	
4310	513	1.094		-0.945	
4330	514	1.029		-0.839	
4390	517.1	1.104		-0.809	
4430	519.2	1.015		-1.391	
4470	521.3	0.852		-1.156	
4510	523.4	1.077	0.971	-0.961	-0.746
4550	526.4	1.139		-0.858	
4589	531.7	0.964		-0.597	
4630	537.5	0.816		-0.771	
4670	543.0	0.625		-0.890	
4710	548.6	0.833		-0.621	
4750	552.7	0.937		-0.675	
4789	556.165	0.706		-0.934	
4830	559.8	0.825		-0.808	
4870	563.3	0.969		-0.964	
4910	567	0.630	0.771	-1.360	-1.085
4950	570.5	0.828		-1.064	
4990	574.1	1.042		-0.955	

5030	577.8	1.217		-1.043	
5070	581.7	0.825		-1.249	
5110	585.5	0.671		-1.048	
5150	589.4	0.619		-0.932	
5190	593.2	0.671		-1.222	
5230	597.1	0.510	0.761	-1.781	-1.310
5270	600.8	1.178		-1.208	
5310	604.2	0.658		-1.164	
5410	612.7	0.234		-1.144	
5450	616.1	0.122	0.013	-0.382	-0.214
5490	619.7				
5530	623.4	0.232		-0.724	
5570	627.1	0.469		-0.636	
5610	637.4	0.096	0.261	-0.459	-0.639
5641	647.2	0.669		-1.227	
5680	659.5	0.299		-0.797	
5723	670.1	0.511		-1.044	
5769	674.4	0.828		-0.817	
5800	677.2	0.855		-0.697	
5840	680.8	0.780		-0.894	
5870	683.5	0.635		-0.854	
5900	686.3	0.444		-1.081	
5941	690.0	0.203		-0.540	
5980	693.6	0.778	0.868	-0.605	-0.608
6023	697.5	0.893		-1.116	
6060	703.0	0.898		-0.958	
6100	714.4	0.815		-0.836	
6140	725.7	0.776		-1.042	
6180	737.0	0.797		-1.187	
6220	748.3	0.847		-1.344	
6280	765.3	0.124		-1.483	
6320	776.6	0.454	0.415	-0.395	-0.766
6360	787.9				
6400	799.2	0.409		-0.530	
6440	810.5	0.779		-0.974	

Table C.3. $\Delta\delta^{18}O$ (difference between $\delta^{18}O$ values) for *N. dutertrei* and *P. obliquiloculata* ($\Delta\delta^{18}O_{N\text{-}P}$), *G. ruber* and *P. obliquiloculata* ($\Delta\delta^{18}O_{N\text{-}P}$), and *G. ruber* and *N. dutertrei* ($\Delta\delta^{18}O_{N\text{-}P}$) from Sulu Sea core ODP769A.

Depth, cm	Age, kyr	$\Delta\delta^{18}O_{N\text{-}P}$	$\Delta\delta^{18}O_{G\text{-}P}$	$\Delta\delta^{18}O_{G\text{-}N}$
25	2.31	-0.337	-0.76	-1.10
55	5.09	-0.453	-0.79	-1.24
85	7.87	-0.289	-0.93	-1.22
114	10.22	-0.803	-0.71	-1.51
145	12.04		-1.29	
175	13.93			-1.02
205	15.81	0.042	-1.23	-1.19
235	17.69	0.39	-1.01	-0.62
265	21.54	-0.399	-0.87	-1.27
295	26.37	0.1515	-1.28	-1.13
325	31.20	0.004	-1.06	-1.06
360	36.84	-0.259	-1.00	-1.26
390	41.67	0.062	-1.11	-1.05
420	46.5	-0.017	-1.19	-1.20
459	52.78	0.438	-1.25	-0.81
499	59	-0.044	-0.99	-1.03
539	65	-0.209	-0.90	-1.11
559	68	-0.123	-1.05	-1.17
602	74.45	0.227	-1.04	-0.81
639	80	-0.16	-0.77	-0.93
679	88	-0.146	-0.59	-0.74
719	96	-0.28	-0.68	-0.96
760	103.5	-0.349	-0.68	-1.03
822	113.7	-0.042	-0.78	-0.83
860	120	-0.29	-0.82	-1.11
900	124.8	-0.199	-0.63	-0.83
940	129.6	0.011	-0.69	-0.68
980	133.7	-0.116	-0.65	-0.77
1010	136.3	0.134	-0.66	-0.53
1050	139.8	0.367	-0.91	-0.54
1090	143.2	0.121	-0.85	-0.73
1130	146.7	0.1555	-1.09	-0.94
1160	149.3	-0.032		
1200	153.5	-0.11	-0.90	-1.01
1240	158.6	0.07	-1.11	-1.04
1280	163.7	-0.063	-1.17	-1.24
1310	167.5	-0.154	-0.96	-1.12
1350	173.5	0.202	-1.13	-0.93
1390	180.5	-0.017	-0.61	-0.63

1430	186.7	0.2425	-1.17	-0.93
1460	190.7	0.17	-1.05	-0.88
1500	196	-0.017	-1.22	-1.23
1540	199.6	-0.101	-1.10	-1.20
1580	203.3	0.03	-1.03	-1.00
1610	206	-0.199	-0.86	-1.05
1650	210.4	-0.022	-0.89	-0.92
1690	214.8	0.419	-1.07	-0.65
1730	218.4	0.053	-0.98	-0.93
1760	220.6	-0.3575	-0.85	-1.21
1800	223.4	-0.57	-0.65	-1.22
1837	226.0	-0.018	-0.44	-0.45
1870	229.2	-0.346	-0.25	-0.59
1910	233.7	0.177	-0.83	-0.65
1950	238.7	-0.594	-0.60	-1.20
1989	243.9	-0.118	-0.64	-0.76
2030	249.3	-0.072	-0.64	-0.71
2070	254.7	-0.0135	-0.76	-0.78
2110	260	0.425	-1.06	-0.63
2150	265.3	-0.127	-0.67	-0.80
2190	270.5	-0.062	-0.83	-0.89
2250	278.5	-0.124	-0.19	-0.32
2289	283.6	-0.007	-0.86	-0.87
2330	289	-0.099	-0.88	-0.98
2370	292.8	-0.065	-0.76	-0.83
2410	296.6	-0.1185	-0.55	-0.67
2450	300.5	0.115	-0.73	-0.61
2490	304.3	0.25	-0.83	-0.58
2530	308.1	0.381	-1.06	-0.68
2570	312.5	0.376	-1.04	-0.66
2610	317.5	-0.302	-0.50	-0.80
2650	322.5	-0.41	-0.69	-1.10
2688	327.2	-0.079	-0.63	-0.70
2730	332.2	-0.137	-0.77	-0.91
2773	336.2	0.072	-0.96	-0.88
2800	341.3	-0.634	-0.04	-0.68
2840	350.4	-0.274	-0.56	-0.83
2880	355.5	-0.269	-0.87	-1.14
2920	357.5	-0.699	-0.63	-1.33
2958	359.4	-0.085	-1.10	-1.18
3006	361.8	-0.003	-0.72	-0.72
3039	363.4	-0.291	-0.39	-0.68
3080	365.5	-0.368	-0.37	-0.73
3120	367.5	-0.166	-1.01	-1.18
3160	369.5	0.286	-0.88	-0.59

3200	371.5	-0.346	-0.95	-1.29
3240	373.5	-0.075	-0.07	-0.15
3280	376	-0.394	-0.61	-1.00
3320	380	-0.007	-0.65	-0.65
3360	384	-0.483	-0.17	-0.65
3400	388	-0.444		
3440	392	-0.653		
3480	396	-0.052	-0.83	-0.88
3520	400	0.007	-1.17	-1.16
3559	403.9	-0.016	-1.69	-1.71
3600	419.5	0.298	-1.72	-1.42
3639	435.2	-0.091		
3680	441.2	-0.195	-0.69	-0.89
3710	445.6	-0.274	-0.75	-1.02
3750	451.4	0.155	-0.87	-0.71
3790	457.1	0.154	-0.79	-0.64
3830	462.9	0.0485	-0.75	-0.70
3870	468.7	-0.054	-0.99	-1.05
3910	474.5	-0.065	-0.79	-0.86
3950	480.2	0.373	-0.94	-0.57
3989	485.9	0.336	-1.69	-1.35
4030	491.8	0.117	-0.86	-0.74
4070	497.6	-0.05	-0.90	-0.95
4110	502.5	-0.043	-1.30	-1.34
4150	504.6		-0.91	
4230	508.8	0.012		
4270	510.9	-0.37		
4310	513	0.325		
4330	514	0.229	-1.09	-0.86
4390	517.1	-0.497	-1.05	-1.55
4430	519.2	-0.361	-0.34	-0.70
4470	521.3	-0.263	-0.81	-1.08
4510	523.4	0.066	-1.51	-1.45
4550	526.4	-0.189	-1.40	-1.59
4589	531.7	0.702	-1.49	-0.79
4630	537.5	0.239	-0.97	-0.73
4670	543.0	-0.028	-0.96	-0.98
4710	548.6	0.046	-1.57	-1.52
4750	552.7	0.086	-1.45	-1.36
4789	556.165	-0.019	-0.98	-1.00
4830	559.8	0.132	-1.03	-0.90
4870	563.3	0.033	-1.04	-1.00
4910	567	0.313	-0.69	-0.37
4950	570.5	-0.099	-1.07	-1.17

4990	574.1	-0.004	-1.32	-1.32
5030	577.8	0.172	-1.21	-1.04
5070	581.7	0.139	-0.69	-0.55
5110	585.5	0.016	-1.24	-1.23
5150	589.4	0.166	-1.30	-1.14
5190	593.2	0.13	-0.86	-0.73
5230	597.1	0.065	-0.70	-0.64
5270	600.8	0.01	-0.80	-0.79
5310	604.2	-0.166	-0.94	-1.10
5410	612.7	0.083	-1.03	-0.95
5450	616.1	0.282	-2.05	-1.77
5490	619.7			-2.00
5530	623.4	-0.321	-1.04	-1.36
5570	627.1	0.204	-0.53	-0.33
5610	637.4	-0.2935	-0.92	-1.21
5641	647.2	0.127	-0.53	-0.41
5680	659.5	-0.145	-1.16	-1.31
5723	670.1	-0.274	-1.37	-1.65
5769	674.4	0.1	-1.17	-1.07
5800	677.2	0.011	-1.16	-1.15
5840	680.8	0.24	-0.87	-0.63
5870	683.5	0.244	-0.77	-0.52
5900	686.3	-0.059	-0.38	-0.44
5941	690.0	0.566	-1.59	-1.02
5980	693.6	0.026	-1.35	-1.33
6023	697.5	-0.185	-0.71	-0.90
6060	703.0	0.01	-0.61	-0.60
6100	714.4	0.099	-0.88	-0.78
6140	725.7	0.047	-0.73	-0.68
6180	737.0	-0.391	-0.75	-1.14
6220	748.3	0.086	-0.50	-0.41
6280	765.3	-0.457	-0.43	-0.88
6320	776.6	-0.1655	-1.50	-1.67
6360	787.9			-1.54
6400	799.2	-0.121	-1.12	-1.24
6440	810.5	0.072	-0.38	-0.31

APPENDIX D
Additional Data

Table D.1. Kau Bay core 102GGC U/Ca and B/Ca.

Depth, cm	U/Ca mmol/mol	U/Ca Replicates mmol/mol	B/Ca mmol/mol	B/Ca replicates mmol/mol
0	110.4		41.804	
2	61.2		30.988	
4	83.6			
6	35.4		31.467	
8	43.6		28.829	
10	23.8		24.688	
12	25.3		25.195	
14	63.8		27.246	
16	93.7		22.095	
18	55.0	59.4	15.871	28.000
20	66.6		28.702	
22	71.9		24.683	
23	114.8		26.177	
26	69.4		24.926	
28	65.9	60.7	25.641	26.582
30	56.3		28.007	
32	27.0		25.113	
34	71.0		34.081	
35	56.2		24.000	
38	137.8		28.306	
42	58.0		24.823	
44	74.8		25.923	
46	120.0		22.897	
48	97.1	103.5	18.769	22.083
50	77.8		28.616	
52	56.7		18.819	
54	114.6		21.495	
56	107.9	118.8	26.989	36.601
58	71.4		21.773	
60	105.8		23.801	
62	82.9	99.4	24.510	20.815
64				
67	88.0		21.261	
68	99.3		18.478	
71	56.7		22.513	
72	60.0	61.8	19.286	27.986

76	48.7		15.524	
78	52.6		19.369	
80	29.6	27.0	19.080	19.999
84			20.534	
86			27.057	
92	110.5		15.994	
94	59.7		24.000	
96	67.4		21.375	
100	49.8		22.707	
104	13.1	35.1	21.463	20.803
106	90.2		14.726	
108	68.6		19.168	
110	52.8		19.047	
112	35.3	17.8	25.578	22.303
114	87.9		15.468	
116	72.0		18.074	
118	54.8		17.464	
120	36.2	42.1	21.989	23.950
122	90.8		18.195	
124	75.7		18.289	
126	29.7		18.384	
128	29.6	33.1	19.602	20.351
130	43.9		18.566	
132	82.3		17.795	
134	44.1		17.088	
136	26.2	55.1	21.862	21.853
138	34.2		21.406	
140			24.559	
142	71.3		17.669	
144	28.0	21.6	22.379	22.070
148	77.1		20.850	
150	122.1		21.908	
152	22.3	22.7	21.439	23.001
154	33.6		21.146	
156			14.266	
158	42.1		18.622	
160				
162	22.2		19.682	
164	65.4		16.670	
166	19.8		21.518	
170	43.4		20.563	
172	53.8		17.214	
174	64.4		22.200	
176				
178			25.103	

180	57.3	43.0	21.557	22.645
182	98.4		22.652	
184				
186	162.6		18.899	
188	33.4		18.029	
190	110.8	85.2	14.702	17.774
192				
194	125.4	110.2	19.940	21.921
196	47.8	54.6	17.053	16.498
198	95.2		17.985	
202	127.8		29.344	
204	64.9		21.216	
206	130.1	144.3	19.958	17.295
208				
210	94.5		20.892	
212	129.2		22.482	
214	81.4		22.885	
216				
218	69.4		21.330	
220	83.0		15.754	
222	122.3	49.7	17.269	17.040
224				
226	53.9	56.5	20.249	20.559
228	152.6		18.731	
230	86.1		19.724	
232				
234	63.1		22.844	
236	115.5		20.574	
238	104.5	62.4	18.658	18.645
240				
242	62.3		20.654	
244	110.1		19.694	
246	70.1		16.415	
248				
250	52.1		13.338	
252	42.5		9.551	
254	87.2		12.938	
256				
258	39.8	37.5	13.107	13.716
260	18.7		18.287	
262	63.6		15.092	
266	51.4		16.941	
268	58.9		16.125	
270	67.8	50.1	15.814	9.097
272				

274	35.6			
276	53.5		11.302	
278	28.9		17.825	
280				
282	40.3		13.478	
284	25.6		14.734	
286	71.0		14.253	
288				
292	30.6		7.143	
296				
299	82.3			
300	52.0		5.878	
302	20.3		19.906	
304				
306	22.5	23.5	6.733	9.975
308	41.4		11.745	
310	25.1	30.4	11.836	13.536
314	16.9		6.687	
316	31.1			
318	76.6		8.238	
320	88.1	94.6	5.064	10.580
322	80.7		9.610	
324	74.2		11.085	
334	15.0		13.164	
336	55.8	110.1	16.346	9.014
338	106.4		11.998	
340	75.7		8.324	
342	31.9		4.829	
344	24.8		13.977	
346			10.249	
348	87.8	91.5	4.227	6.001
350	60.8		16.240	
352	15.5		7.668	
354	55.8		14.801	
356	126.8			
358	40.8		11.937	
360	12.4		12.751	
362	6.8		17.991	
364	16.7	48.1	12.966	10.681
366	15.1		10.021	
368			22.008	
370	8.3		15.600	
372	8.4		11.391	
374	70.6	53.4	11.314	6.170
376	30.6			

Table D.2. Kau Bay core 102GGC Ba/Ca.

Depth, cm	Ba/Ca mmol/mol	Ba/Ca replicates mmol/mol
0		
2	0.499	
4		
6	0.607	
8	0.655	
10	0.314	
12	0.391	
14	0.510	
16	0.513	
18	0.314	0.661
20	0.606	
22	0.733	
23	0.535	
26	0.595	
28	0.550	0.521
30	0.561	
32	0.537	
34		
35	0.620	
38	0.938	
42	0.953	
44	0.666	
46	0.493	
48	0.878	
50	0.429	
52		
54	0.901	
56	0.689	
58	0.665	
60	0.807	
62	0.565	0.627
67	0.708	
68	0.818	
71	0.607	
72	0.587	0.571
76		
78	0.354	
80	0.591	0.497

84		
86		
92	0.509	
94	0.768	
96	0.648	
100	0.414	
104	0.569	
106	0.499	
108		
110	0.548	
112	0.527	0.568
114	0.617	
116	0.467	
118	0.745	
120	0.513	0.577
122	0.448	
124	0.543	
126	0.449	
128	0.518	0.481
130	0.724	
132	0.437	
134	0.362	
136	0.640	0.618
138		
140	0.686	
142	0.435	
144	0.466	0.396
148	0.732	
150	0.859	
152	0.374	0.400
154	0.280	
156	0.260	
158	0.312	
162	0.387	
164	0.366	
166	0.434	
170	0.451	
172		
174	0.384	
178	0.481	
180	0.291	0.370
182		

186		
188	0.374	
190	0.924	0.791
194	0.615	0.580
196	0.391	0.480
198	0.363	
202	0.594	
204	0.715	
206	0.610	0.532
210	0.465	
212	0.679	
214	0.666	
218	0.507	
220		
222	0.573	0.460
226	0.384	0.539
228	0.701	
230	0.783	
234	0.375	
236	0.493	
238	0.553	0.633
242	0.490	
244	0.769	
246	0.507	
250	0.507	
252	0.461	
254	0.511	
258	0.428	0.542
260	0.336	
262	0.468	
266	0.707	
268	0.748	
270	0.847	0.838
274	0.694	
276	0.621	
278	0.435	

282		
284	0.531	
286	0.330	
292	0.471	
299	0.801	
300	0.399	
302	0.469	
306	0.519	0.683
308	0.330	
310	0.328	0.341
314	0.454	
316	0.460	
318	0.679	
320		
322	0.757	
324	0.616	
334	0.533	
336	0.534	0.557
338		
340	0.803	
342		
344		
346		
348		
350		
352		
354		
356		
358	0.637	
360	0.657	
362		
364	0.965	
366	0.792	
368		
370	0.738	
372		
374	0.663	

Table D.3. Glycerol dialkyl glycerol tetraether (GDGT, as m/z) concentrations from Kau Bay core 102GGC. Quantities of each GDGT were derived through high performance liquid chromatograph peak integration.

Depth, cm	1298	1296	1292'	1300	1050	1036	1022
1	234,675	76,641	210,913	123,401		21,426	
3	273,106	87,945	244,792	145,508	14,037	21,738	36,120
5	169,587	55,198	148,748	89,515	8,135	12,169	20,254
7	237,936	80,090	217,108	125,959	15,475	23,842	37,570
9	155,976	53,464	145,471	80,667	11032	16,919	26967
31	338,788	121,336	346,161	171,737	30630	47,480	74212
47	131,000	47,900	135,000	69,500	11388	17,600	27500
63	302,302	109,424	309,838	161,924	23878	38,490	60354
73	216,941	74,920	211,522	112,973	14527	24,408	37550
87	181,523	65,373	159,939	106,086	12,583	21,255	30,584
99	513,824	187,244	461,223	294,933	33,216	54,962	81,177
103	325,795	113,117	277,241	185,639	16,213	25,359	40,036
121	625,776	211,362	577,371	339,865	52,393	40,030	61,912
143	876,160	306,348	863,185	458,072	62,767	92,130	138,524
155	309,256	106,358	275,641	169,946	14,254	22,752	35,719
167	660,385	231,538	582,097	353,273	38,062	57,934	89,252
179	426,118	151,505	397,091	226,592	26,039	39,469	61,021
191	278,209	96,147	259,851	150,380	17,659	26,445	39,828
209	129,867	44,471	115,037	71,947	8,911	13,464	21,016
231	483,491	169,463	490,679	256,741	32895	50,733	78,045
239	616,824	215,046	594,754	338,831	36,928	56,493	84,445
259	447,176	150,857	404,308	258,777	24,432	37,842	56,977
279	325,745	113,503	298,921	187,327	21,599	33,598	47,056
298	811,300	283,621	756,822	476,296	45,896	70,664	103,245
321	518,209	177,235	431,823	291,475	26,566	41,004	62,801
353	1,386,150	499,681	912,755	875,470	81,734	123,552	186,806
393	774,088	272,548	487,539	474,818	60,834	91,368	137,651
417	628,257	220,684	454,603	377,201	37,288	58,450	90,365
419	498,410	172,388	362,001	283,766	28,985	46,554	70,509
421	727,069	258,184	521,269	413,436	44,007	69,643	107,953

Table D.4. GDGT (as m/z in top row) concentrations from Kau Bay multi-core 103MC-F. Quantities of each GDGT were derived through high performance liquid chromatograph peak integration.

Depth, cm	1298	1296	1292'	1300	1050	1036	1022
2	350,124	125,816	316,387	169,817.00	22487	36,233	63,617
4	532,506	263,410	706,690	363,958	53,888	87,526	141,483
6	1,120,260	373,519	1,032,780	555,091	72,482	118,323	211,027
8	812,415	260,132	768,479	373,731	53,888	47,515	137,914
10	783,699	266,460	758,783	388,956	52,831	84,898	150,172
12	620,357	228,669	614,317	316,211	39,917	65,533	118,186
14	801,171	294,662	757,186	411,211	54,777	87,468	157,902
16	768,013	257,549	790,700	399,734	56,959	90,288	163,207
18	806,200	279,430	733,624	423,688	56,224	90,806	160,871
20	1,011,380	354,308	906,556	523,609	65,029	104,990	191,794
22	1,422,680	533,489	1,294,280	758,800	110,840	178,006	298,845
24	899,861	304,952	876,320	474,865	68,633	109,076	186,960
26	1,580,000	527,000	1,490,000	821,000	91,200	141,000	
28	956,859	345,074	1,011,100	498,232	87289	140,512	
32	910324	363314	867881	461857	73660.7	117216	
34	141,000	479,000	1,300,000	773,000	88200	140,000	217000
36	782,763	273,062	762,615	402,268	71711	122,837	183617
38	850,000	27,000	782,000	463,000	50822	82,200	124000
40	1,238,420	409,890	1,126,150	664,160	73,811	120,075	184,578

Table D.5. Kau Bay multi-core 103MC-F FAME concentrations, in ppb.

Depth, cm	C_{14}	C_{16}	C_{18}	C_{20}	C_{22}	C_{24}	C_{26}	C_{28}	C_{30}	C_{32}	C_{34}	C_{36}
2	0.02	0.14	0.03	0.03	5.16	0.21	0.21	0.29	0.19	0.20	0.09	0.21
6	0.07	0.66	0.14	0.20	0.48	1.50	1.48	1.85	1.68	1.99	1.29	1.25
10	0.08	0.74	0.16	0.20	0.52	1.76	1.71	2.23	2.58	3.85	2.39	0.00
14	0.00	0.12	0.12	0.07	0.18	0.64	0.63	0.80	0.77	1.02	0.59	0.00
18	0.05	0.35	0.08	0.09	0.24	1.01	0.93	0.99	0.88	0.99	0.59	0.45
22	0.09	0.61	0.11	0.13	0.43	2.02	1.95	2.20	2.09	2.70	1.60	0.83
36	0.07	0.51	0.08	0.08	0.29	1.33	1.03	0.97	0.91	0.86	0.55	0.50